UNIVERSIDAD DE SANTIAGO DE COMPOSTELA
Facultad de Química

Synthesis, Characterization and Properties of Copper Clusters

Noelia Vilar Vidal

PhD Dissertation
Santiago de Compostela
2012

Universidad de Santiago de Compostela
Facultad de Química
Departamento de Química Física

Synthesis, Characterization and Properties of Copper Clusters

Memoria presentada por Noelia Vilar Vidal
para optar al grado de Doctor en Quimica
por la Universidad de Santiago de Compostela
Santiago de Compostela, Septiembre 2012

D. M. Arturo López Quintela, Catedrático del Departamento de Química Física de la Universidad de Santiago de Compostela y **D. José Rivas Rey,** Catedrático de Física y director del International Iberian Nanotechnology Laboratory (INL), informan que:

La memoria adjunta titulada **"Synthesis, Characterization and Properties of Copper Clusters",** presentada por la Licenciada en Química Dª Noelia Vilar Vidal para optar al Grado de Doctor en Química, ha sido realizado bajo su dirección en el Departamento de Química Física de la Universidad de Santiago de Compostela.

Y para hacer constancia, firmamos la presente autorización:

Fdo. D. M .Arturo López Quintela

Fdo. D. José Rivas Rey

Santiago de Compostela, Septiembre 2012.

A mi familia

"Doubt is one of the names of intelligence".

Jorge Luis Borges.

CHAPTER 3:SYNTHESIS OF SMALL COPPER CLUSTERS

CHAPTER 4: THERMAL GROWTH OF SMALL COPPER CLUSTERS

CHAPTER 5: SYNTHESIS OF LARGE COPPER CLUSTERS

CHAPTER 6: PHOTOLUMINESCENCE STABILTY OF CuCLs

CHAPTER 7: CATALYTIC ACTIVITY OF CuCLs

List of abbreviatures:

AFM:	atomic force microscopy
AES:	Auger spectroscopy
AgNFs:	silver nanofibers
BE:	binding energy
CLs:	clusters
Cu:	copper
CuNPs:	copper nanoparticles
CV:	cyclic voltammetry
e^-:	electrons
E_{Fermi}:	Fermi energy
E_{gap}:	energy gap
ESI-TOF:	electrospray ionization-time of flight
EtOH:	ethanol
FWHM:	full width at half maximum
H_2O:	water
HOMO:	homo highest occupied molecular orbital
HPLC:	high-performance liquid chromatography
HRTEM:	high-resolution transmission electron microscopy
KE:	kinetic energy
LDI-TOF:	laser desporption ionization-time of flight
LUMO:	lowest unoccupied molecular orbital
MALDI-TOF:	matrix assisted laser desorption/ionization mass spectrometry-time of flight
MeCN:	acetonitrile
MS:	mass spectrometry
N_2:	nitrogen
nm:	nanometer
ORR:	oxygen electro-reduction
PA:	Auger parameter
PL:	photoluminescence
SPB:	surface plasmond band
T^a:	temperature
TBAAcO:	tetrabutylammonium acetate
$TBANO_3$	tetrabutylammonium nitrate
TBABr:	tetrabutylammonium bromide
TEM:	transmission electron microscopy
UV-Vis:	ultraviolet-visible
XPS:	X-ray photoelectron spectroscopy
λ_{exc}:	excitation wavelength
λ_{emi}:	emission wavelength

SUMMARY

Metal clusters are receiving a great interest nowadays due to their distinctive photoluminescence (PL) and catalytic properties owing their quantum confinement effect. The main purpose of this thesis has been the synthesis of copper clusters as an affordable alternative to the most studied clusters up to now: gold and silver clusters.

In this dissertation, firstly, we have explored the synthesis of different copper clusters (CuCLs) sizes and their subsequent purification. Various synthesis and post-treatments parameters were examined in order to improve the synthesis method. The as-synthesized CuCLs were thoroughly characterized by using different techniques, such as: UV-Vis spectroscopy, fluorescence, mass spectrometry, X-ray photoelectron spectroscopy, non-contact atomic force microscopy, transmission electron microscopy…in order to study the cluster size, their morphology and photoluminescent properties. Beside this, the great photoluminescent results obtained for our copper clusters lead us to a deep study on their photoluminescence stability and on their use as potential ion nanosensors. Finally, the catalytic activity of the copper clusters has been also investigated, focusing on their size dependent behavior. CuCLs were found to be useful as efficient and reusable catalyst in the redox reaction of the methylene blue and display good results working as photocatalyst on the silver nanofibers photodissolution reaction.

In summary, the simple electrochemical synthesis of copper clusters with excellent photoluminescent and catalytic properties will provide a wide range of potential applications in different fields: as nanosensors, catalyst and photocatalyst.

RESUMEN

Los clústeres metálicos despiertan un gran interés hoy en día por sus fantásticas propiedades fluorescentes y catalíticas que surgen debido al confinamiento cuántico. El principal objetivo de esta tesis se ha centrado en la síntesis de clústeres de cobre como una alternativa más asequible a aquellos clústeres más estudiados hasta ahora: los clústeres de oro y plata.

En primer lugar en esta tesis se ha desarrollado la síntesis de diferentes tamaños de clústeres de cobre (CuCLs) así como su posterior purificación. Se han examinado diferentes parámetros de síntesis y tratamientos posteriores con el objetivo de mejorar el método de síntesis. Los clústeres de cobre sintetizados fueron caracterizados por medio de diferentes técnicas, tales como: espectroscopía de absorción UV-Vis, fluorescencia, espectrometría de masas, espectroscopía fotoelectrónica de rayos X, microscopía de fuerzas atómicas en modo no contacto, microscopía de transmisión electrónica, etc. con el objetivo de determinar el tamaño del clúster, su morfología y estudiar sus propiedades fluorescentes. Además de esto, los excelentes resutados de fluorescencia dieron lugar a la realización de un estudio detallado en la estabilidad de fluorescencia así como en su posible aplicación como nanosensores de iones. Finalmente, se ha estudiado la actividad catalítica de los clústeres de cobre la cual muestra un comportamiento dependiente del tamaño. Los clústeres de cobre son eficientes y reciclables en la reacción redox del azul de metileno y presentan buenos resultados como fotocatalizadores en la reacción de fotodisolución de nanofibras de plata.

En resumen, mediante una síntesis electroquímica simple se obtienen clústeres de cobre con excelentes propiedades fluorescentes y catalíticas que serán muy útiles en un amplio rango de aplicaciones tales como nanosensores, catalizadores y fotocatalizadores.

OBJECTIVES

The main objective of this thesis is the electrochemical synthesis of different sized copper clusters with great photoluminescent properties. Besides, a thorough characterization process of the as-synthesized clusters and the study of different purification methods is needed to include in order to identify the copper cluster nature. Finally, the study of their fluorescent properties and their catalytic activity will be developed. Therefore, this work can be divided into four main parts:

A brief summary about metal clusters properties, different synthesis techniques of metal clusters and novel applications will be shown in Chapter 1. The different experimental techniques employed in this work will be summarized on Chapter 2.

Chapter 3, 4 and 5 will describe the synthesis, purification and characterization of different copper clusters sizes: small copper clusters (CuCLs) with 5 up to 13 copper atoms, medium CuCLs up to 20 copper atoms and larger CuCLs with 25 copper atoms, respectively. Different characterization techniques such as UV-Vis absorption, fluorescence, mass spectrometry, non-contact atomic force microscopy (NC-AFM) will be employed along the three chapters.

The fluorescence stability of the as-synthesized copper clusters (CuCLs) and their potential use as ion recyclable nanosensors will be shown on Chapter 6.

Catalytic and photocatalytic studies by using different CuCLs sizes will be described on Chapter 7, concluding on a size dependent catalytic behavior.

CHAPTER 1.

Introduction

1.1. OVERVIEW ON CLUSTERS.

Nanotechnology has received everyone's attention since the beginnings of XXI century although; it was Michael Faraday on the 1850s,[1] who started these studies on metal colloidal particles. Nanotechnology is focused on the synthesis, characterization, design, applications and manipulation of the matter at low levels, including: **"nanoparticles"** (aggregates of metal atoms where at least one dimension has a size from two to several tens of nanometers) and **"metal clusters"** (when particle size becomes comparable to the Fermi wavelength of an electron, <2nm) and **"sub-nanometer clusters"** (<1nm).

Due to their unique physical and chemical properties, metal clusters have become an interesting topic of research in recent years. This thesis will focus on the synthesis, characterization, study of the physical and optical properties and the potential applications of different sized copper clusters.

Clusters display intermediate properties between the isolated atom and the bulk metal and represent the most elemental building blocks in nature (after atoms). They will be characterized by their size, which establish a bridge between atomic and nanoparticle behaviors, with properties entirely different from these two size regimes. The percentage of atoms present on the surface of clusters increases with a decrease of the core size, which could strongly affect their properties. Bulk metal has a continuous band structure with free electrons oscillate, however when the size decreases to nanoparticles a splitting of the energies at the Fermi level is observed and therefore the valence density of states and the conduction band will be affected; changing from a continuous density of states (on the bulk metal) to discrete energy levels (Figure 1.1). As the size becomes smaller and approaches the nanoscale, the wave character becomes more important and quantum mechanics becomes necessary to explain its behavior. The metal clusters dramatically exhibit, unique electronic and optical properties smoothly size dependent, such as molecule-like energy gaps[2], strong photoluminescence [3] and high catalytic properties.[4]

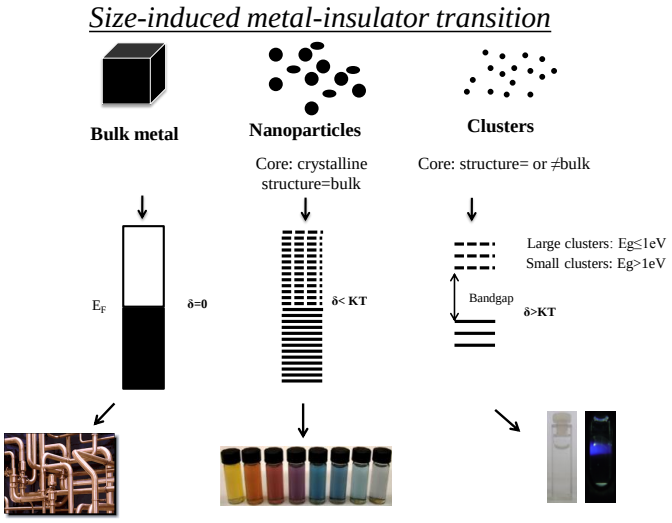

Figure 1. 1| *Evolution of the band gap as the number of atoms in a system increase (from right to left[5]). δ is the so-called Kubo gap.*

1.2. CLUSTERS STRUCTURE.

1.2.1. Electronic structure of metal clusters.

The calculation of the electronic structure of metal clusters is very difficult, particularly for smaller clusters in solution and protected by caping agents. The use of simple models as the *Jellium model* [6] (quantum mechanical model) gives a considerably good approximation, preserving many of the physicochemical characteristics of the clusters. The *Jellium model* was firstly developed for clusters in the gas phase and consists on the assumption that a metal cluster can be modeled by uniform, positively charged density spheres with the energy levels filled with free electrons in accordance with the Pauli principle. Hence, free valence electrons are assumed to move in a homogeneous spherical ionic background. Each time that filled electronic shells appear, the corresponding cluster exhibits enhanced stability.The total energies as a function of cluster size, calculated by this model agree with the position of the peaks obtained by mass spectrometry of the clusters, related with the abundance of most stable clusters.

Alkali metal clusters, Na_N, were studied by mass spectrometry by Knight et al. [7] showing unusual stability at specific cluster sizes N= 2, 8, 18, 34, 40…atoms. For instance, eight free electrons completely filled the 1s and 1p energy states forming a complete valence shell, thereby making Na_8 cluster very stable. Besides this, the intensity distributions show that clusters with an even number of atoms are more stable than those with an odd number of atoms. These specific cluster sizes will be known as ***"magic numbers".*** Most studied metal clusters as Au, Ag and Cu have an electronic configuration characterized by a closed d shell and a single s valence electron: [Cu: $Ar(3d)^{10}(4s)^1$], [Ag: $Kr(4d)^{10}(5s)^1$] and [Au: $Xe(5d)^{10}(6s)^1$] similar to the alkali metal clusters. Early experiments have established that Au_N, Ag_N, and Cu_N clusters (N= 2, 8, 20, 34, 58...) are all electronic magic-number clusters[8] (Figure 1.2) observing that clusters carrying a simple positive charge (cation) should exhibit magic numbers that are shifted by one, being sizes with 9, 21, 41 being those which contain 8, 20, 40 valence electrons. Experimental evidences for the inert electronic shell structure in some copper clusters have been given by Winter et al.[9] who studied the chemical stability of Cu_N clusters by a reduced reactivity towards O_2. Anomalously low intensities were observed for N=20, 34, 40, 58 and 92, concluding the reactivity of Cu_NCLs-O_2 is inhibited by electronic shell-closing effects at these sizes.

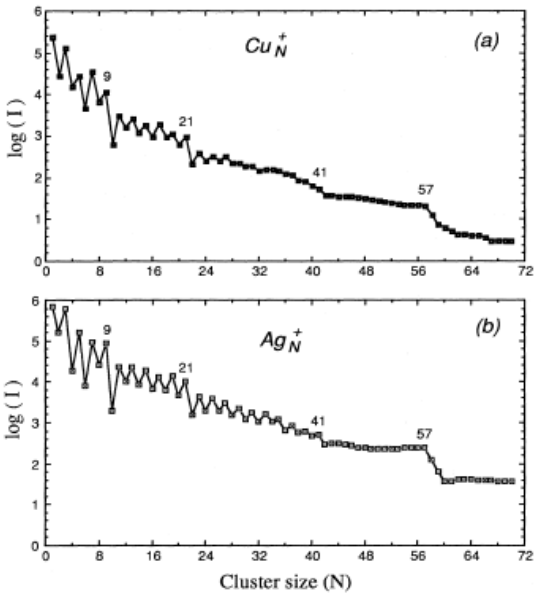

Figure 1. 2| *Logarithmic abundance spectra of (a) copper and (b) silver clusters ions produced in a sputtering source. Numbers correspond to spherical shell closings. Figure extracted from reference 8.*

1.2.2. Geometrical structure of metal clusters.

Besides the electronic factor, atomic packing and geometric symmetry is another important characteristic of highly stable copper clusters. Predictions of the geometrical structure of free copper clusters have been made by several ab initio studies. For sizes N < 10 first-principles based calculations have been developed[10], while Kabir et al. applied tight-binding methods[11] for sizes up to N = 55. Moreover, they calculated that most of the clusters in the size range 10 ≤ N ≤ 55 adopt an icosahedral geometry (Figure 1.3.B). Thus, highly symmetric clusters may be viewed as *geometric* magic-number clusters. Theoretical studies of the Cu_{13} clusters by the empirical potential method showed that the most stable structures were an icosahedron and cuboctahedron.[12] In both cases, the cluster consists on the central atoms surrounded by 12 neighbors, which form a close sphere.

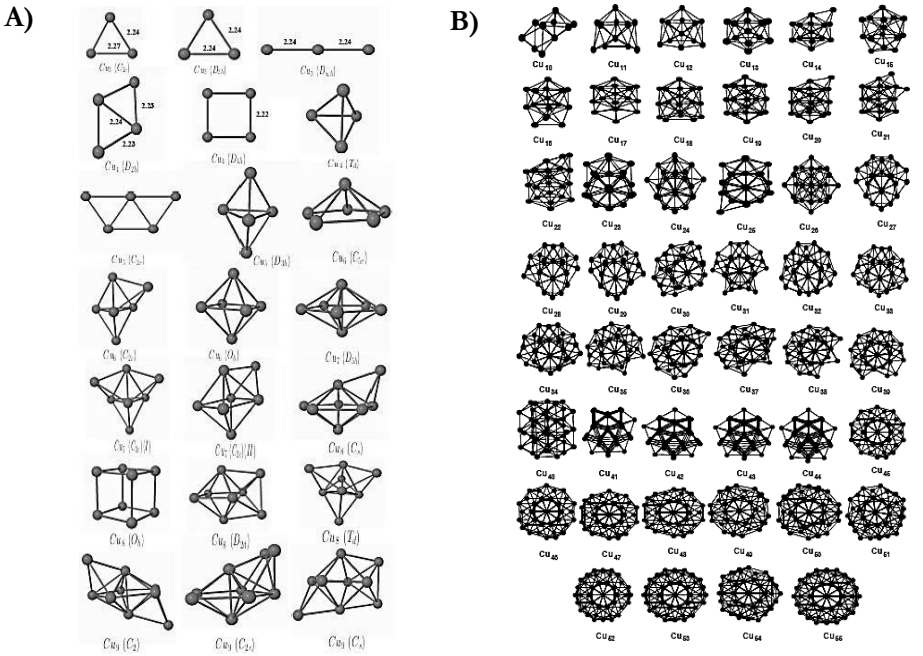

Figure 1. 3| *Ground state structure and isomers of Cu_N clusters for N=3-9. Point group symmetries are given in the parentheses (A) (Figure extracted from reference 13). Most stable structures for copper clusters with N =10-55 atoms. Most of the clusters adopt icosahedral structures except for N =40-44, where the structure are decahedral (B) (Figure extracted from reference 11).*

Different theoretical studies have concluded on the planar geometry of small clusters with a copper atom number N≤5 (Figure 1.3.A).[13] Kabir[11] also found relative stability at Cu_8, Cu_{18} and Cu_{20} (Figure 1.4) due to the electronic shell closing at N = 8, 18, and 20. This behavior corresponds to the magic number in electronic shell model besides a reversed even-odd alteration for N = 10−16 with maxima at odd sized clusters, Cu_{11}, Cu_{13} and Cu_{15}, which manifests the geometrical effect through icosahedral growth.

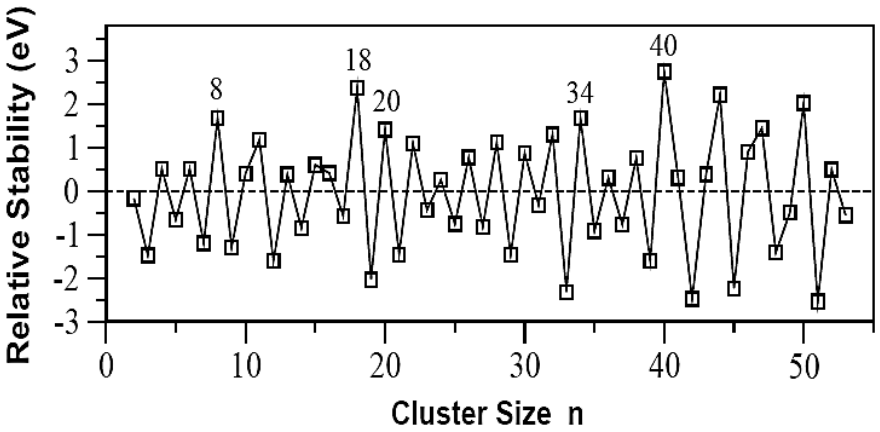

Figure 1. 4 | *Variation of relative stability Δ_2E with cluster size n, Shell closing effect at n=8, 18, 20, 34, 40 and even-odd alternation up to n~40 are found. However, due to geometrical effect this even-odd alternation is disturbed at 11, 13 and 15 atoms. Figure extracted from reference 13.*

Over the last few years, the study of prediction models for ligand-protected gold clusters has been very important. The calculation has to combine different aspects at the same time : (1) the magic numbers required for electronic stabilization of the cluster, (2) the requirements for an electronically closed shell,[14] formulated as $(L_S{\cdot}A_NX_M)^z$: $\boldsymbol{n^* = Nv_A - M - z}$, where $\boldsymbol{n^*}$ represents the number of electrons for shell-closing of the metallic core, which has to match one of the magic numbers corresponding to strong electron shell closures in an anharmonic mean-field potential giving rise to stable clusters; $\boldsymbol{N}$ stands for the number of core metal atoms (**A**); $\mathbf{v_A}$ is the atomic valence; **M** is the number of electron-localizing (or electron - withdrawing) ligands X, assuming a withdrawal of one electron per ligand molecule; and $\boldsymbol{z}$ represents the overall charge of the complex. The weak ligands represented by L_S may be needed for completing the steric surface protection of the cluster core and (3) the fact that solution-phase clusters require a sterically complete protective ligand shell compatible with a

compact atomic shell structure for the metallic core, the satisfying of all such conditions complicates the calculations of the structures enormously. Recently, research on the structure of metal clusters has mainly been focused on alkanethiolate-stabilized gold and silver clusters. However, due to the difficulty in synthesizing homogeneous and high-quality sub-nanometer sized crystals, only limited cluster systems have been investigated. For example: Jadzinsky et al.[15] reported the X-ray structure determination of a Au_{102}(p-MBA)$_{44}$ (p-MBA, p-mercaptobenzoic acid) single crystal. They found an Au_{49} core surrounded by two groups of 20 Au atoms face camping the Au_{49} and then 13 Au atoms dispersed without apparent symmetry. Zhu[16] and Heaven[17] proposed a similar Au combination for the $Au_{25}(SR)_{18}$ cluster: an icosahedral Au_{13} core plus the exterior 12 Au atoms in the form of six –RS–Au–RS–Au–RS– motifs. Besides this, Zhu et al. found that all the proposed $Au_{25}(SR)_{18}$ structure was independent of the employed ligands.

1.2.3. Clusters Band-Gap.

One of the consequences of the quantum-size regime (with the presence of discrete states in metal clusters) is the appearance of a sizable HOMO-LUMO band gap (similar to that of semiconductors). As can be seen on Figure 1.5, such a semiconductor like behavior is particular significant for smaller clusters with band gaps widely exceeding of 1 eV.

Zheng et al.[18] established a correlation of the emission energy with the number of atoms (N) for small gold clusters by observing that the energy emission (E_{gap}) decreases with the increasing number of cluster atoms. They quantitatively fitted this correlation by the expression: $\mathbf{E_{emission}=E_{gap}= E_{Fermi}/N^{1/3}}$, where $\mathbf{E_{Fermi}}$ is the Fermi energy of bulk gold (5.32 eV), as predicted by the Jellium model[6], this being a very good approximation for small metal clusters with N<20. However, for larger clusters, it was observed that a small anharmonic distortion term is required for N≥25.

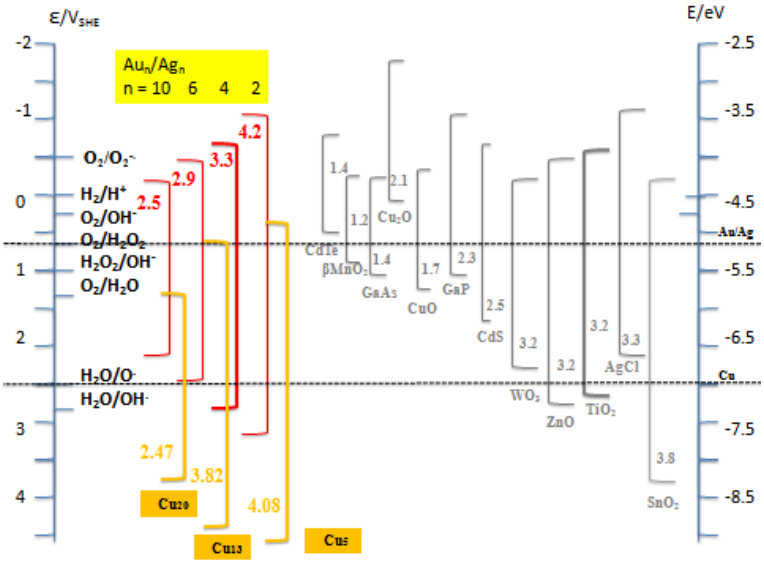

Figure 1. 5| *Schematic comparison between band-gaps of some silver, gold and copper clusters (M_N, M=metal and N= number of atoms) and those of well-known semiconductors. Bandgaps (E_g) were calculated from the spherical Jellium model ($E_g = E_F/N^{1/3}$; E_F = Fermi level) and the position of the conduction band, E_{CB}, was estimated by the formula $E_{CB} = \chi - E_F - ½ E_g$ (χ = electronegativity).*

Figure 1.5 shows characteristics band gaps of different metal clusters. It is known that, in general, bandgap decreases when the cluster size increases, having a nice agreement between the DFT calculated bandgap values and those predicted by the simple Jellium model, and also that ligands also play a minor role. Table 1.1 shows the change of the band gap with the cluster size and the ligands including the band gap calculated by Jellium for comparison (clusters sizes with N ≈ ≥ 25 atoms a correction of -0.4eV was used because of the anharmonicity observed in large clusters).[18]

Table 1. 1| *Comparison (adapted from reference 14) between: (1) experimentally determined band gaps for free gas-phase gold cluster anions from photoelectron spectroscopy, (2) theoretical (Density Functional Theory) values for HOMO-LUMO gaps of passivated gold cluster compounds that correspond to 8, 34, and 58 conduction-electron shell closings, and (3) band gaps calculated through the Jellium model for clusters with the same number of gold atoms; *for these clusters a correction of -0.4eV was used.*

	(1) Experiment		(2) Theory		(3) Jellium model
Shell closing	**Cluster**	**Gap/eV**	**Cluster compound**	**Gap/eV**	**$Eg=5.32/N^{1/3}$ /eV**
8e ($1S^21P^6$)			$Au_{11}(PH_3)_7(SMe)_3$	1.5	2.4
8e			$Au_{11}(PH_3)_7Cl_3$	2.1	2.4
8e			$Au_{13}(PH_3)_{10}Cl_2^{3+}$	1.8	2.3
8e			$Au_{25}(SMe)_{18}^-$	1.2	1.3*
34e($8e + 1D^{10}2S^21F^{14}$)	$Au34^-$	1.0	$Au_{39}Cl_6(PH_3)_{14}^-$	0.8	1.0*
58e ($34e + 2P^61G^{18}$)	$Au58^-$	0.6	$Au_{102}(p\text{-}MBA)_{44}$	0.5	0.6*
58e			$Au_{102}(SMe)_{44}$	0.5	0.6*

1.3. UNIQUE PROPERTIES OF METAL CLUSTERS.

1.3.1. Optical properties.

Significantly different from large nanoparticles, optical absorption spectra of clusters exhibit molecular like optical transitions (between the discrete energy levels corresponding to the last occupied orbital and the first unoccupied orbitals of the delocalized conduction electrons). [19,20] Bands at lower energies will appear with the increase of the cluster size. As it can be seen in Figure 1.6.A Cu nanoparticles show SPB around 580nm (interband transition $5d^{10} \rightarrow 6sp^{1}$)[21] according to the literature [22] and copper clusters show well-defined absorption bands indicating a *molecular-like* behavior (Figure 1.6.B) as a consequence of the energy level space increase and to their band structure separated at discrete levels.[23] The multiple absorptions could be attributed to the intraband (sp) HOMO-LUMO transmission, interband transition (d-sp), or mixed sp-sp intraband and d-sp interband transitions.

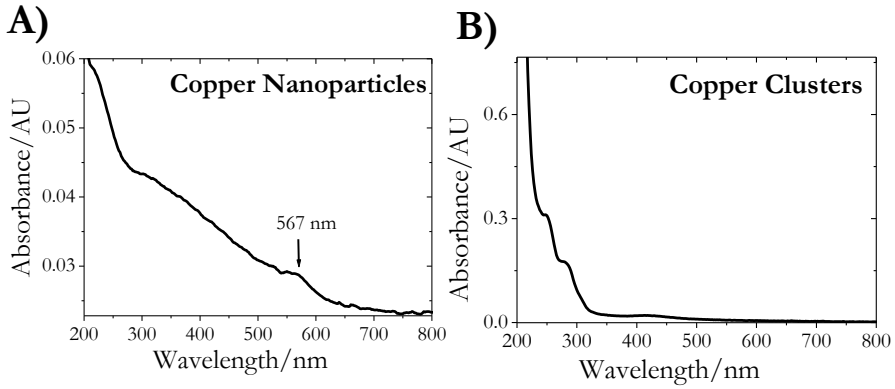

Figure 1.6| *UV-Vis absorption spectra of CuNPs displaying the typical plasmon band at ≈ 567nm (A) and large CuCLs with well-defined molecular-like absorption bands (B).*

1.3.2. Photoluminescence properties.

Luminescence is one of the major properties of metal clusters. Fluorescence of Au, Ag and Cu clusters has been extensively studied during the past decade. Several works have demonstrated that the photoluminescence could be assigned to the electronic transitions between the highest occupied orbital and

the lowest unoccupied orbital (HOMO-LUMO).[24] Photoluminescence was first observed in noble metal by Mooradian [25], who observed visible emission from copper and gold films with a quantum efficiency of ~10^{-10}. Size-dependent fluorescence properties of Au quantum dots were studied by the Dickson group.[18] They found that excitation and emission bands shift to smaller wavelengths with decreasing cluster size. The excitation and emission spectra of Au clusters composed of a different number of atoms is showed in Figure 1.7. The synthesized Au_5, Au_8, Au_{13}, Au_{23} and Au_{31} clusters show UV (385 nm), blue (455 nm), green (510 nm), red (760 nm) and near IR (866 nm) fluorescence, respectively. One can see that the excitation and emission bands shift to longer wavelengths (low energy) with increasing cluster size. Fluorescence properties of metal clusters are very sensitive to their chemical environments, including the cluster size, solvent and surface protecting ligands.[26,27] By increasing the charge transfer from the surface ligands to the metal core an enhancement of the fluorescence was observed.[27] This enhancement can be achieved by (1) increasing the electron donation capability of the ligands, (2) improving the electropositivity of the metal core and (3) using the protecting ligands with electron-rich atoms and groups.

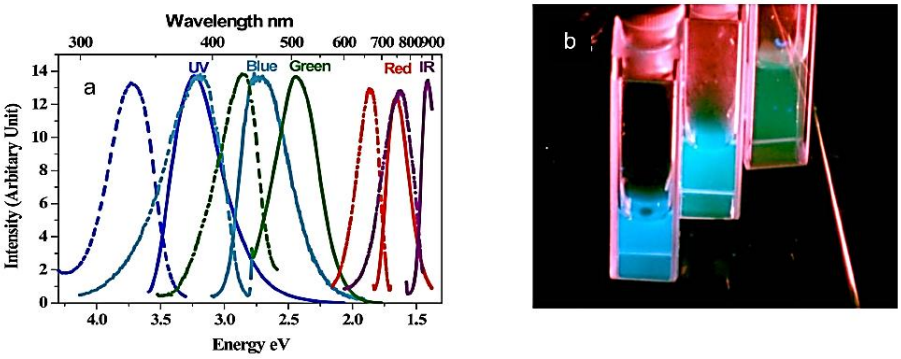

Figure 1. 7| *Excitation (dashed) and emission (solid) spectra of different gold clusters. Excitation and emission maxima shift to longer wavelengths with increasing the cluster size from Au_5 up to Au_{31} (a). Emission from the three shortest wavelengths emitting gold cluster solutions (from left to right) under long-wavelength UV lamp irradiation (366nm). (b) Figure extracted from reference 18.*

The discrete emission of these clusters open up new opportunities, which can be used as biological labels or light-emitting sources in nanoelectronics as an alternative to semiconductor quantum dots especially due to their biocompatibility and their reduced photobleaching.

1.3.3. Catalytic properties.

Metals including gold, silver and copper, are usually quite inert and show little activity for reactive molecules adsorption, but, when their dimensions are diminished to the nanoscale, the properties of the materials exhibit a dramatic deviation from those of the bulk. For instance, gold clusters were found to be reactive at room temperature with oxygen and other molecules. Quantum chemical calculations indicate that such high reactivity is due to under-coordination of the metal atoms forming the cluster.[28] In recent years, Au clusters have been extensively examined as active catalysts for CO oxidation and oxygen electro-reduction.[29] Although this is, a field not explored much so far, these electrocatalytic properties make metal clusters promising materials in fuel-cell applications. Oxygen electro-reduction (ORR) represents a critical cathodic reaction in fuel cells. Despite extensive research progress, wide-spread commercialization of fuel cells has been hindered partly because of the sluggish reaction dynamics for the ORR at the cathode and the high cost of Pt- based electrocatalyst. Therefore, numerous studies have focused on non-Pt catalyst like for example Au clusters. [29b, 30] Ag[31] and Cu [32] clusters.The results showed that the activity of clusters against ORR increases as the cluster core size decreases.

1.4. SYNTHESIS OF METAL CLUSTERS.

Due to the highly necessary control of experimental conditions and a suitable purification and isolation method for the synthesis of metal clusters, more accurate synthesis techniques will be required than for nanoparticles. Metal clusters can generally be prepared through "bottom-up" or "top-down" synthesis. The "bottom-up" approach involves metal precursors which are reduced to atoms with a reducing reagent forming the metal clusters by the nucleation of the zerovalent metal atoms. The "top-down" methods consist of a ligand etching process from nanoparticles to clusters. Here we will summarize some different synthesis techniques of metal clusters such as: electrochemical synthesis, photoreduction, microemulsion technique, chemical reduction, templating techniques and etching methods.

A) *Chemical reduction by modified Brust-Schiffrin method:* Here, metal precursors are first dissolved in an aqueous solution, subsequently, organic protecting ligands and reducing reagents are added into the solution to generate metal clusters and then they are transferred to an organic solvent by phase-transferring reagents such as tetraoctylammonium bromide. The core size and the surface properties of the metal clusters can be controlled effectively by adjusting the experimental parameters, such as the metal to ligand ratio, chemical structure of the protecting ligands, the nature of the reducing agent, reaction temperature and time, pH of the solution, etc. By using this method different metal clusters such as Au[33], Pt[34], Ag[35] and Cu[36] clusters have been successfully synthesized.

B) *Template-based synthesis.*- Template-based synthesis provides a predetermined environment for the clusters formation, which is favorable to produce clusters with well-controlled size and shape. Over the past few decades, template-based methods have proved to be efficient synthetic techniques for preparing fluorescent metal clusters, using polymers,[37] proteins,[38, 39, 40, 41] dendrimers[42, 43] or even DNA[44, 45, 46] as templates. Copper clusters have been synthesized by a modified poly(amidoamine) (PAMAM) dendrimer as a template.[47]

C) *Ligand induced etching of metal nanoparticles*.- The etching capability of some ligands (like thiols) is used to synthesized clusters by removing the surface atoms from metal nanoparticles leading to stable quantum clusters (shell-closing magic numbers).

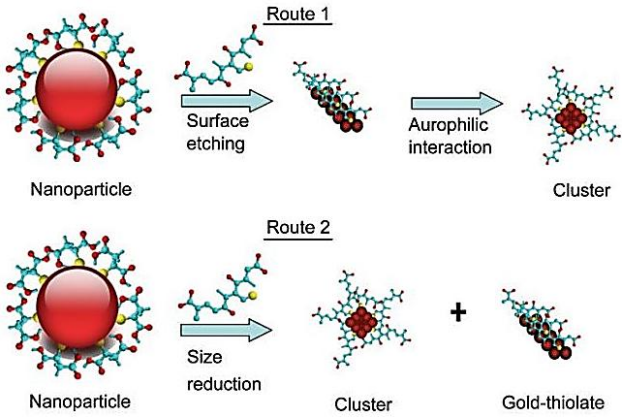

Scheme 1. 1| *Schematic representation of two possible routes for the formation of gold clusters by etching of mercaptosuccinic acid-capped gold nanoparticles. Figure extracted from reference 48.*

Examples of this technique are the synthesis of AuCLs (Au_8 or Au_{25}) from mercaptosuccinic acid (MSA)-protected Au nanoparticles (4-5nm core diameter) by etching with excess glutathione varying the etching pH (~7-8 to Au_8 and ~3 for Au_{25}).[48] Although the detailed mechanisms of the ligand- and precursor-induced nanocrystal etching have not yet been specified clearly (Scheme 1.1) this new synthetic strategy holds promise for preparing new types of sub-nanometer sized clusters containing only a few metal atoms.

D) Electrochemical synthesis.- Electrochemical synthesis, first developed by Reetz[49] in 1994, is a very promising technique to produce metal clusters because of their simplicity. Compared to chemical reduction, the electrochemical method exhibits many advantages in the preparation of metal clusters, such as the low reaction temperature, large-scale yield, low cost of the initial materials, and easy manipulation of cluster size by tuning current, voltage, electrolyte, concentration of stabilizers etc. For instance, Reetz et al. prepared 1–5 nm palladium nanoparticles just by changing the current density.[50] Based on this mechanism, this thesis will be focused on the use of this synthetic method in order to prepare photoluminescent copper clusters.

E) *Microemulsion method.*- Nanodroplets of water dispersed in oil using surfactants and/or amphiphilic blockcopolymers will be used as nanoreactors in order to obtain clusters with well-defined sizes. The cluster size can be tuned by

adjusting the liquid core dimensions of microemulsions. Silver clusters Ag_N ($N \leq 10$) were prepared in this way by Ledo et al.[51] achieving novel photoluminescent and magnetic properties. More recently, small copper clusters as Cu_N, with $N \leq 13$, showing UV photoluminescent properties have also been synthesized by this method.[52] As shown in Scheme 1.2, the core size of the copper clusters can be easily controlled by varying the amount of the reducing agent ($NaBH_4$).

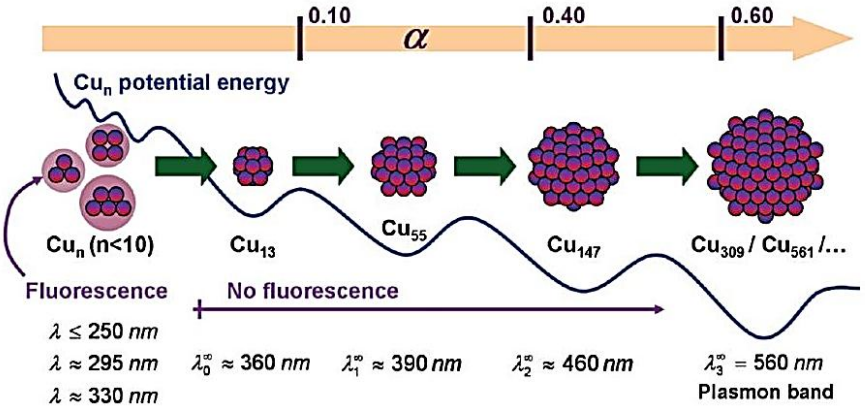

Scheme 1. 2| *Schematic picture of the evolution of the copper cluster size dependent on a (being a the used moles of $NaBH_4$ needed for the stoichiometric reduction of Cu(II) ions). Estimated wavelengths of the plasmon band for different sized copper clusters are shown at the bottom. Imagen extracted from reference 50.*

F) *Photoreduction synthesis*.- Photoreduction is a simple method where metal salts are reduced by irradiating the system by UV-light in presence of some capping agent. Since the first report of size-dependent fluorescent Ag and Au clusters prepared by Zheng and co-workers[53] photoreduction synthesis of metal clusters has received more and more attention and copper clusters are being to be studied.[54]

Copper clusters are being more studied nowadays, but their recent discovering has given us few references in the literature. Therefore, we summarize in the Table 1.2 the different types of CuCLs synthesis employed until now, the obtained cluster size and their PL range.

Table 1.2| *Literature summary of CuCLs synthesis.*

Synthesis	Reference	Cluster size/N (Cu_N)	PL (λ_{emi} /nm)	QY %
Dendrimer Template	43	-	-	-
	47	Cu_4-Cu_{65}	-	-
Microemulsions	52	Cu_N N≤13	330nm	-
Modified Brust	36	Cu_N N≤8	425-593nm	4.4
Polyol	55	Cu_9	460nm	0.65
BSA protein	41	Cu_{13}	410nm	0.15
DNA templated	46	-	593nm	
Photoreduction	54	Cu_5	600nm	2.2

1.5. APPLICATIONS OF METAL CLUSTERS.

Due to the unique physicochemical properties, metal clusters have already been applied in different fields, such as sensoring, catalysis, biological labeling, biomedicine and electronics. Here, we will briefly summarize several important applications of metal clusters in biodetection, biological imaging and catalysis, which are the main topic applications in this thesis.

1.5.1. Biodetection.

Recognition-based biosensing of metal ions by metal clusters is being extensively studied nowadays.[56] Many ions has been successfully detected by using fluorescence quenching of metal clusters as Pb, Cu, Co, Al, etc. Gold clusters can succesfully sense Hg^{2+} based on their fluorescence quenching through Hg (II)-induced aggregations of clusters (Figure 1.8).[57,58] Fluorescent silver clusters have also been demonstrated satisfactory to detect mercury ions even at subnanomolar concentrations.[59]

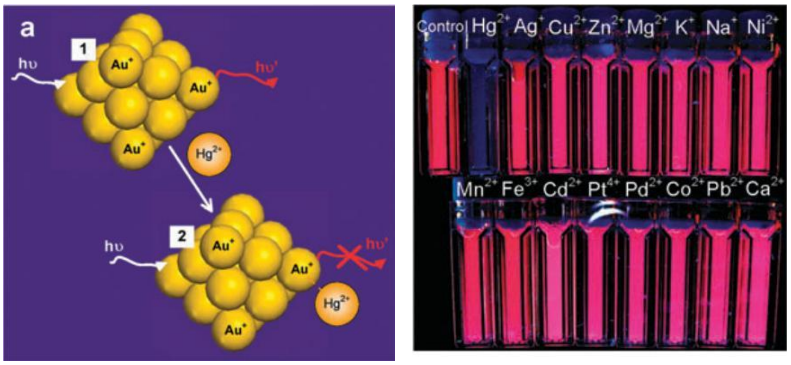

Figure 1. 8| *Schematic representation of Hg^{2+} sensing based on fluorescence quenching of Au CLs resulting from high-affinity metallophilic Hg^{2+}—Au^{+} bonds (left). Photographs of aqueous BSA-Au CLs solutions (20 μM) in the presence of 50 μM of various metal ions under UV light (right).Imagen extracted from reference 58.*

As well, small biomolecules, such as cysteine,[60] H_2O_2,[61]cyanide,[62]etc has been also detected using metal clusters.

1.5.2. Biological imaging and cellular labeling.

Metal clusters with their bright emission, good biocompatibility and photostability are becoming attractive alternatives to conventional fluorophores (organic dyes or quantum dots) for bioimaging. In a recent study, Jao et al[63] synthesized gold clusters (photobleaching resistant) with dendrimers templates (Au_8-dominating composition) which can act as bio-trackers for intracellular targeting and tracking. In vivo 1st study of fluorescence imaging have been presented by Wu et al.[64] by using ultrasmall BSA-stabilized Au clusters. As shown in Figure 1.9, fluorescence images of the subcutaneously injected mice exhibited bright emission from different locations depending on the injected Au clusters dose.

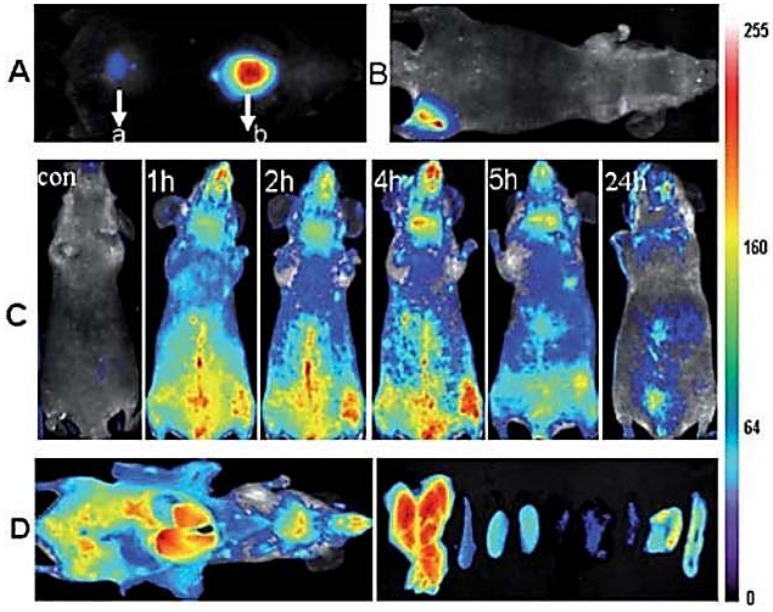

Figure 1. 9| *In vivo fluorescence image of 100 μL AuCLs injected (A) subcutaneously (a: 0.235 mg ml^{-1}, b: 2.35 mg ml^{-1}) and (B) intramuscularly (2.35 mg ml^{-1}) into the mice. (C) Real-time in vivo abdomen imaging upon intravenous injection of 200 μL AuCLs (2.35 mg ml^{-1}) at different time points, post injection.(D) Ex vivo optical imagen of anatomized mice with injection of 200 μL of AuCLs (2.35 mg ml^{-1}) and some dissected organs during necropsy at 5 h. The organs are liver, spleen, left kidney, right kidney, heart, lung, muscle, skin and intestine from left to right. Imagen extracted from reference 64.*

1.5.3. Catalysis.

The unusual catalytic activity of metal clusters has attracted more and more attention over the past years. Initially, clusters were dispersed on a solid support in order to prevent the clusters from aggregating during the catalysis reactions. Studies on supported metal clusters showed that in addition to the cluster size, the nature of the support materials also plays a key role for their catalysis performance. Harding et al. [65] studied the control and tunability of the catalytic oxidation of CO by Au_{20} clusters deposited on MgO surfaces. Catalysis of the oxidative dehydrogenation of propane by Pt clusters[66] or propene epoxidation catalysis[67] by gold clusters have been also studied. Another interesting example of the catalytic properties is the use of silver clusters to prevent pathologies, shuch as fetal alcohol syndrome.[68] It has been demonstrated that some silver clusters (AgCLs) are able to electrocatalyze the oxidation of alcohols and prevent its cytotoxicity under physiological conditions at very low potentials, like those found on live cells (Scheme 1.3).

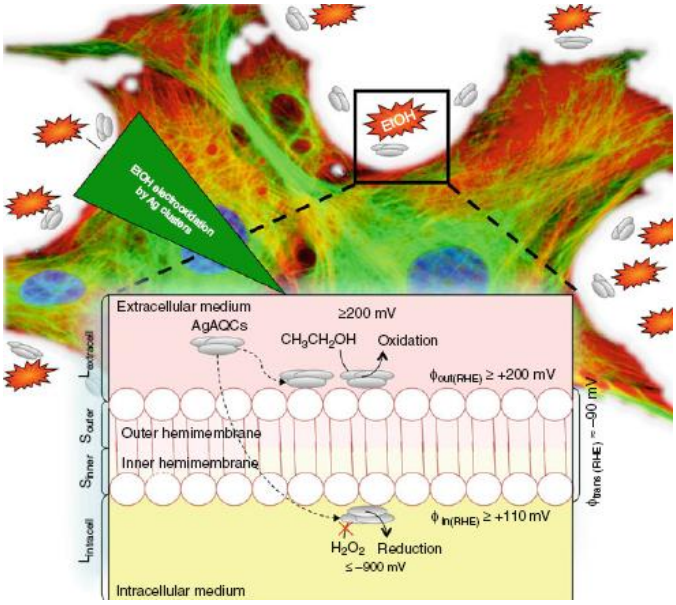

Scheme 1. 3| *Schematic representation of the ethanol oxidation electrocatalysis by AgCLs on the cellular membrane preventing the alcohol toxicity in living cells. Imagen extracted from reference 68.*

REFERENCES.

[1] Faraday M. *Philosophical transactions, 147*, 145 **(1857).**

[2] a) Murray R. W. *Chem. Rev. 108*, 2688 **(2008).** b) Quinn B. M.; Laaksonen T.; Ruiz V.; Liljeroth P. *Chem. Soc. Rev. 37*, 1836 **(2008).** c) Chen S. W. *J. Electroanal. Chem. 574*, 153 **(2004).**

[3] a) Xu H. X.; Suslick K. S. *Adv. Mater. 22*, 1078 **(2010).** b) Chang W. H.; Lin C. A. J.; Lee C. H.; Hsieh J. T.;. Wang H. H; Li J. K.; Shen J. L.; Chan W. H.; Yeh H. I. *J. Med. Biol. Eng. 29*, 276 **(2009).** c) Xu H.; Suslick K. S. *ACS Nano 4*, 3209 **(2010)**.

[4] a)Turner M.; Golovko V. B.; Vaughan O. P. H.; Abdulkin P.; Berenguer-Murcia A.; Tikhov M. S.; Johnson B. F. G.; Lambert R. M. *Nature 454*, 981 **(2008).** b) Chen W.; Chen S. W. *Angew. Chem. Int. Ed. 48*, 4386 **(2009).**

[5] Edwards P. P.; Johnston R. L.; Rao C. N. R. *On the Size- Induced Metal-Insulator Transition in Clusters and Small Particles, in Metal Clusters in Chemistry,* ed. P. Braunstein, L. A. Oro, P. R. Raithby, Vol. 3, Wiley, Weinheim **(1999).**

[6] Chou M.Y.; Cleland A.; Cohen M.L. *Solid State Commun. 52*, 645 **(1984).**

[7] Knight W. D.; Clemenger K.; de Heer W. A.; Saunders W.A.; Chou M. Y.; Cohen M.L. *Phys. Rev. Lett. 52,* 2141 **(1984).**

[8] Katakuse I.; Ichihara T.; Fujita Y.; Matsuo T.; Sakurai T.; Matsuda H. *Int. J. Mass Spectrom 67*, 229 **(1985).**

[9] Winter B. J.; Parks E. K.; Riley S. J. *J. Chem. Phys. 94*, 8618 **(1991).**

[10] Jug K.; Zimmermann B.; Calaminici P.; Köster A. M. *J. Chem. Phys. 116,* 4497 **(2002).**

[11] Kabir M.; Mookerjee A.; Bhattacharya A. K. *Phys. Rev. A 69,* 43203 **(2004).**

[12] Darby S.; Mortimer-Jones T. V.; Johnston R. L.; Roberts C. *J. Chem. Phys. 116,* 1536 **(2002).**

[13] Mukul K., PhD Dissertation, *"Electronic and magnetic properties of metal clusters"*. Jadavpur University, Kolkata **(2006).**

[14] Walter M.; Akola J.; Lopez-Acevedo O.; Jadzinsky P.D.; Calero G.; Ackerson C.J.; Whetten R.L.; Grönbeck H.; Häkkinen H. *PNAS* 105, 9157 **(2008).**

[15] Jadzinsky P. D.; Calero G.; Ackerson C. J.; Bushnell D. A.; Kornberg R. D.; *Science 318,* 430 **(2007).**

[16] Zhu M.; Aikens C. M.; Hollander F. J.; Schatz G. C.; Jin R. *J. Am. Chem. Soc. 130*, 5883 **(2008).**

[17] Heaven M. W.; Dass A.; White P. S.; Holt K. M.; Murray R. W. *J. Am. Chem. Soc. 130,* 3754 **(2008).**

[18] Zheng J.; Zhang C.; Dickson R.M. *Phys. Rev. Lett 93*, 077402 **(2004).**

[19] Schaaff T. G.; Shafigullin M. N.; Khoury J. T.; Vezmar I.; Whetten R. L.; Cullen W. G.; First P. N.; Gutierrez-Wing C.; Ascensio J.; Jose-Yacama M. J. *J. Phys. Chem. B 101*, 7885 **(1997).**

[20] Alvarez M.M.; Khoury J. T.; Schaaff T.G.; Shafigullin M.N.; Vezmer I.; Whetten R.L. *J. Phys. Chem. B 101,* 3706 **(1997).**

[21] Kreibig U.; Vollmer, M. *Optical Properties of Metal Clusters;* Springer: Berlin, **(1995).**

[22] Lisiecki I.; Pileni M. B. *J. Am. Chem. Soc. 115,* 3887 **(1993).**

[23] Kubo R. *J. Phys. Soc. Jpn. 17,* 975 **(1962).**

[24] a) Huang T.; Murray R. W. *J. Phys. Chem. B 105,* 12498 **(2001)** b) Bigioni T. P.; Whetten R. L.; Dag O. *J. Phys. Chem. B 104,* 6983 **(2000)**

[25] Mooradian A.; *Phys. Rev. Lett. 22,* 185 **(1969).**

[26] a) Diez I.; Pusa M.; Kulmala S.; Jiang H.; Walther A.; Goldmann A. S.; Muller A. H. E.; Ikkala O.; Ras R. H. A. *Angew. Chem., Int. Ed. 48,* 2122 **(2009).** b) Wu Z.; Jin R. *Nano Lett. 10,* 2568 **(2010).**

[27] Wu Z. K.; Jin R. C. *Nano Lett. 10,* 2568 **(2010).**

[28] Heiz U.; Landman U. *Nanocatalysis (Nanoscience and Technology).* Springer, Berlin **(2007).**

[29] a) Valden M.; Lai X.; Goodman D. W. *Science 281,* 1647 **(1998).** b) Chen W.; Chen S. W. *Angew. Chem., Int. Ed. 48*, 4386 **(2009)**

[30] Tang W.; Lin H. F.; Kleiman-Shwarsctein A.; Stucky G. D.; McFarland E. W. *J. Phys. Chem. C 112,* 10515 **(2008).**

[31] Lu Y.; Chen W. *J. Power Sources 197*, 107 **(2012).**

[32] Wei W.; Chen W. *International Journal of Smart and Nano Materials*, 1 **(2012).**

[33] a)Song Y.; Harper A. S.; Murray R. W. *Langmuir 21,* 5492 **(2005).** b) Rodríguez-Vázquez M.J.; Vázquez-Vázquez C.; Rivas J.; López-Quintela M.A. *Eur. Phys. J. D 52*, 23 **(2009).**

[34] Castro E. G.; Salvatierra R. V.; Schreiner W. H.; Oliveira M. M.; Zarbin A. J. G. *Chem. Mater. 22,* 360 **(2010).**

[35] Wu Z. K.; Lanni E.; Chen W. Q.; Bier M. E.; Ly D.; Jin R. C. *J. Am. Chem. Soc. 131,* 16672 **(2009).**

[36] Wei W. T.; Lu Y. Z.; Chen W.; Chen S. W. *J. Am. Chem. Soc. 133,* 2060 **(2011).**

[37] Shen Z.; Duan H. W.; Frey H. *Adv. Mater. 19,* 349 **(2007).**

[38] Xie J. P.; Zheng Y. G.; Ying J. Y. *J. Am. Chem. Soc. 131,* 888 **(2009).**

[39] Wei H.; Wang Z.; Yang L.; Tian S.; Hou C.; Lu Y. *Analyst 135,* 1406 **(2010).**

[40] Xavier P.L.; Chaudhari K.; Verma P.K.; Pal S.K.; Pradeep T. *Nanoscale 2* 2769. **(2010).**

[41] Goswami N.; Giri A.; Bootharaju M.S.; Xavier P.L.; Pradeep T.; Pal S.K. *Anal. Chem. 83*, 9676 **(2011).**

[42] Zheng J.; Petty J.T.; Dickson R.M. *J. Am. Chem. Soc. 125*, 7780 **(2003).**

[43] Zhao M.; Sun L.; Crooks R. M. *J. Am. Chem. Soc. 120,* 48777 **(1998).**

[44] Richards C. I.; Choi S.; Hsiang J. C.; Antoku Y.; Vosch T.; Bongiorno A.; Tzeng Y. L.; Dickson R. M. *J. Am. Chem. Soc. 130*, 5038 **(2008).**

[45] Petty J.T.; Zheng J.; Hud N.V.; Dickson R.M. *J. Am. Chem. Soc. 126,* 5207 **(2004).**

[46] Jia X.; Li J.; Han L.; Ren J.; Yang X.; Wang E. *ACS Nano 6* , 3311 **(2012).**

[47] Balogh L.; Tomalia D.A. *J. Am. Chem. Soc. 120,* 7355 **(1998).**

[48] Muhammed M.H.; Ramesh S.; Sinha S.; Pal S.; Pradeep T. *Nano Res. 1,* 333 **(2008).**

[49] Reetz M. T.; Helbig W. *J. Am. Chem. Soc. 116,* 7401 **(1994).**

[50] Reetz M.T.; Winter M.; Breinbauer R.; Thurn-Albrecht T.; Vogel W. *Chem. Eur. J. 7,* 1084 **(2001).**

[51] Ledo-Suárez A.; Rivas J; Rodríguez-Abreu C. F.; Rodríguez M. J.; Pastor E.; Hernández-Creus A.; Oseroff S. B.; López-Quintela M. A. *Angew. Chem., Int. Ed. 46,* 8823 **(2007).**

[52] Vázquez-Vázquez C.; Bañobre-López M.; Mitra A.; López-Quintela M.A., Rivas J. *Langmuir 25,* 8208 **(2009).**

[53] a) Zheng J.; Petty J. T.; Dickson R. M. *J. Am. Chem. Soc. 124,* 13982 **(2002**). b) Zheng J.; Petty J. T.; Dickson R. M. *J. Am. Chem. Soc. 125,* 7780 **(2003**).

[54] Zhang H.; Huang X.; Li L.; Zhang G.; Hussain I.; Li Z.; Tan B. *Chem. Commun. 48,* 567 **(2012).**

[55] Kawasaki H.; Hamaguchi K.; Osaka I.; Arakawa R. *Adv. Funct. Mater. 21*, 3508 **(2011).**

[56] Bootharaju M. S.; Pradeep T. *Langmuir 27*, 8134 **(2011).**

[57] Huang C. C.; Yang Z.; Lee K. H; Chang H. T. *Angew. Chem., Int. Ed. 46,* 6824 **(2007).**

[58] Xie J.; Zheng Y.; Ying J.Y. *Chem. Commun. 46,* 961 **(2010).**

[59] Adhikari B.; Banerjee A. *Chem. Mater. 22,* 4364 **(2010).**

[60] Shang L.; Dong S. *Biosens. Bioelectron. 24,* 1569 **(2009).**

[61] Shiang Y.-C.; Huang C.-C.; Chang H.-T. *Chem. Commun. 23,* 3437 **(2009).**

[62] Liu Y. L.; Ai K. L.; Cheng X. L.; Huo L. H.; Lu L. H. *Adv. Funct. Mater. 20*, 951 **(2010).**

[63] Jao Y.-C.; Chen M.-K.; Lin S.-Y. *Chem. Commun. 46,* 2626 **(2010).**

[64] Wu X.; He X.; Wang K.; Xie C.; Zhou B.; Qing Z. *Nanoscale 2,* 2244 **(2010).**

[65] Harding C.; Habibpour V.; Kunz S.; Farnbacher A.N-S.; Heiz U.; Yoon B.; Landman U. *J. Am. Chem. Soc 131,* 538 **(2009).**

[66] Vajda S.; Pellin M.J.; Greeley J.P.; Marshall C.L.; Curtiss L.A.; Ballentine G.A.; Elam J.W.; Catillon-Mucherie S.; Redfern P.C.; Mehmood F.; Zapol P. *Nature Mater. 8,* 213 **(2009).**

[67] Lee S.; Molina L.M.; López M.J.; Alonso J.A.; Hammer B.; Lee B.; Seifert S.; Winans R.E.; Elam J.W.; Pellin M.J.; Vajda S. *Angew. Chem. Int. Ed. 48,* 1 **(2009).**

[68] Selva J.; Martínez S.E.; Buceta D.; Rodríguez-Vázquez M.J.; Blanco M.C.; López-Quintela M.A.; Egea G. *J. Am. Chem. Soc. 132,* 6947 **(2010).**

CHAPTER 2.

Experimental Section

2.1. INTRODUCTION.

This chapter is focused on the description of the synthesis technique and the posterior characterization techniques of the as-synthesized copper clusters during my research. First of all, characteristics of the reactants will be explained. Secondly, details of the general synthetic procedure used throughout this thesis will be given and finally experimental characterization methods will be briefly summarized.

2.2. REACTANTS.

The different used reactants have been summarized in the Table 2.1. All the reactants were used without further purification.

Table 2. 1| *List of the used reactants.*

Name	Chemical Formula	Purity (%)	Brand
Copper electrode		99.99	GoodFellow
Platinum electrode		99.95	GoodFellow
Aluminium oxide	Al_2O_3	99.99	Alfa Aesar
Tetrabutylammonium nitrate	$(C_4H_9)_4NNO_3$	>97	Fluka
Tetrabutylammonium acetate	$(C_4H_9)_4NAcO$	99	Fluka
Tetrabutylammonium Bromide	$(C_4H_9)_4NBr$	99	Fluka
Acetone	C_3H_6O	100	Prolabo
Acetonitrile	C_2H_3N	99.9	Sigma-Aldrich
Sulfuric Acid	H2SO4	97	Merck
Pentane	C_5H_{12}	99	Sigma-Aldrich
Chloroform	$CHCl_3$	99	GPR-Rectapur
Ethanol	EtOH	99.9	GPR-Rectapur
Copper nitrate	$Cu(NO_3)_2$	98	Aldrich
Copper acetate	CuOAc	98	Aldrich
Toluene	C_7H_8	99.8	Aldrich
1-hexanethiol	$C_7H_{14}S$	95	Sigma-Aldrich
Hydrazine hydrate	$N_2H_4.H_2O$	98	Aldrich
Sodium hydroxide	NaOH		Prolabo
Dodecanethiol	$C_{12}H_{26}S$	98	Aldrich
Lead nitrate	$Pb(NO_3)_2$	99	Sigma-Aldrich
Aluminium nitrate	$Al(NO_3)_3.9H2O$	98	Aldrich
Potasium hydroxide	KOH		Sigma-Aldrich
Cobalt Sulphate	$Co(SO_4).7H_2O$	99	Sigma
Ferric nitrate	$Fe(NO_3)_3.9H2O$	98	Panreac
Nickel nitrate	$Ni(NO_3)2.6H_2O$		Aldrich
Zinc sulphate	$Zn(SO_4).7H_2O$	99	Aldrich
Sodium Nitrate	$Na(NO_3)$	99	Sigma-Aldrich
Methylene Blue	$C_{16}H_{18}ClN_3S \cdot 3H_2O$	82	Sigma-Aldrich
Heptane	C_7H_{16}		Sigma-Aldrich

2.3. ELECTROCHEMICAL SYNTHESIS AND PURIFICATION OF COPPER CLUSTERS.

2.3.1. Synthesis Procedure.

As we briefly explained in Chapter 1, electrochemical synthesis was first introduced by Reetz in 1994[1] and has been used by our group for many years in order to synthesize nanoparticles and clusters.[2] This synthesis displays different points:

(1) cluster size can be controlled by tuning the current density (high current densities give smaller particles). This relationship[3] between the current density and the particle size from the free energy formation of a metal cluster, $\Delta G(N)$, has two terms, as follows:

$$\Delta G(N) = -ze|\eta| + \Phi(N) \qquad [1]$$

where N is the number of ions in the cluster, η is the overpotential, z is the ion charge, e is the charge of the electron, and Φ isthe electrostatic potential. The first term is related to the number, N, of metal ions that move from the solution to the crystal phase on the surface of the cathode and the second term is related to the increase in the surface energy associated with the creation of the metal cluster surface. This increase in the surface energy equals the difference between the binding energies of the N bulk metal ions and those of the N metal ions arranged on the surface of the metal crystal. Both terms in Eq. 1 are functions of the size of the metal cluster, N. The size of the critical nucleus in two dimensions is given by:

$$N_c = bs\varepsilon^2/(zeN)^2 \qquad [2]$$

where N_c is the number of atoms in the cluster, b is the factor that relates the surface area S of the nucleus to its perimeter P ($b = P^2/4S$; $b = \Pi$ for a circular nucleus), s is the area occupied by one atom on the surface of the metal nucleus, and ε is the edge energy. Therefore, N_c strongly depends on the overpotential and is inversely proportional to η^2. The critical radius of the surface nucleus r_c is a function of the overpotential:

$$r_c = s\varepsilon/ze\,\eta \qquad [3]$$

Therefore, r_c is inversely proportional to the overpotential (**η**), and the electron transfer overpotential may be defined as the rate of change of electrode potential with the current associated with the limiting rate of electron transfer across the phase boundary between the electrically conducting electrode and the ionic conducting solution. The overpotential is directly related to the current density.

(2) the isolation of the clusters is simple—they precipitate out of the solution when formed; (3) tetralkyl ammonium salts were used as supporting electrolyte and also as a capping agent, therefore, the $R_4 N^+X^-$ stabilized the clusters (4) the reaction proceeds with high yields (>95%) and can be performed on a moderate scale.

The cluster formation mechanism consists of (1) dissolution of the sacrificial anode ($Cu^0 \rightarrow Cu^{2+}$), (2) transporting of the electroactive species (metal cations) to the cathode, (3) reductive metal adatom formation at the cathode interface, (4) aggregation of the metal adatoms, (5) stabilization by 'self organization' of the ammonium ions around the metal core (6) reaction product desorption from the cathode, (7) reaction product diffusion to the solution. A brief scheme of this mechanism can be observed in Scheme 2.1.

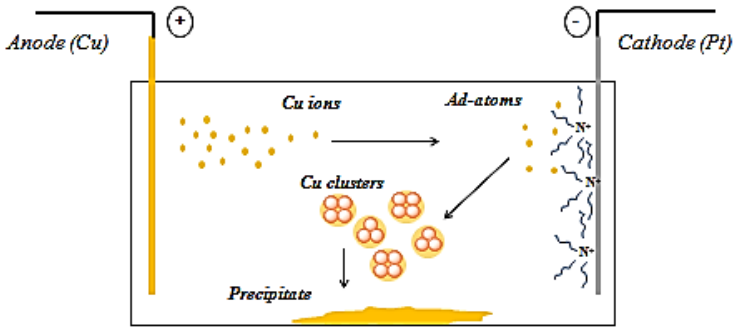

Scheme 2. 1| *Electrochemical mechanism formation of CuCLs stabilized by tetrabutylammonium salts.*

2.3.2. Clusters stabilization.

Metal clusters must be stabilized against the aggregation into larger particles. The stabilization of metal clusters can be classified as follows:

(1) *Electrostatic stabilization:* results from the adsorption of ions to the electrophilic metal surface creating a electrical double layer, which results in a coulombic repulsion force between particles (Figure 2.1.A).[4]

(2) *Steric stabilization*: achieved by surrounding the metal center by large organic molecules (such as poly (N-vinyl pyrrolidone) (PVP), which prevent close contact of the metal particle centers (Figure 2.1.B).

(3) *By ligands (P, N, S donors)*: phospines, thiols, etc have been very exploited throughout the years as suitable cluster ligands for the "metallic full shell clusters".

(4) *Electrosteric stabilization*: strong coordination of bulky molecules such as surfactants at the surface of the particles, which is achieved well using tetralkyl salts, where the negatively charged anion is binded to the metal surface and the alkyl chains shield the metallic core like an umbrella (Figure 2.1.C).

(5) *Solvent stabilization*: solvents as tetrahydrofurane (THF) or THF/MeOH can act as stabilizers.[5]

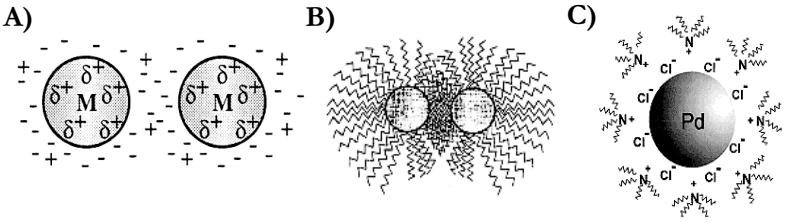

Figure 2. 1| *Schematic image of different stabilized nanoparticles. A) Ions adsorbed onto the particle surface, creating an electrical double layer which provides Coulombic repulsion and thus stabilization against aggregation. B) Two polymer-protected particles interacting. The region between the two particles becomes crowded as a high local concentration of polymer builds up. C) Electrosteric stabilization of a Pd particle by tetra(octyl) ammonium stabilizer.Imagen taken from reference 4.*

2.3.3. Synthesis Variables influence.

There are many variables which can affect to the cluster synthesis, such as: solvent, supporting electrolite, working electrode, synthesis time and of course, current density. As we have explained before, current density will directly affect the cluster size: bigger current densities will give smaller clusters sizes. Besides, the cathode would be carefully chosen by their structural characteristics, must have different lattice constant and atomic ratio from the copper (anode) in order to avoid the deposition onto the cathode.[2] In this work platinum has been chosen as the working electrode with a values of 3.92 Å and 1.380 Å for Pt and 3.61 Å and 1.280 Å for Cu, for lattice constant and atomic ratio. The supporting electrolyte must be inert (it cannot react with the generated species in the process), inactive in the used potential range and must have a high dielectric constant ($\geq$ 10). Tetraalkylammonium salts have been previously tested in our group for this purpose (and also by other authors) in aqueous and aprotic mediums[6,7] showing good stability under the synthesis potential conditions, which never exceeded -1.8 V (vs Ag/AgCl).[8,9] Here the tetraalkylammonium salts will act as the supporting electrolyte as well as a stabilizer of the synthesized clusters. Besides, an oxygen free solvent is carefully needed due to the possible passivation of the anode during the synthesis.[2] Therefore, the solution must be under an inert atmosphere. Time also has a big influence on the electrochemical, for instance, silver nanoparticles tends to deposite onto the cathode at long synthesis time. In the same way, a synthesis of PVP-protected gold clusters with gold nanoparticles happens when the synthesis time increases.[10] Therefore, time influence on the CuCLs synthesis has also been studied in a previous work.[11] The obtained results will be summarized here as a model of "optimization the synthesis".

2.3.4. Purification.

Purification of metal clusters is often required especially due to the polydispersity obtained from the synthesis methods of clusters. Size focusing and therefore properties focusing has been studied in order to obtain clusters with a high monodispersity. It was shown that monodispersed clusters can be obtained by separation processes, such as fractionated precipitation,[12,13] size exclusion column chromatography (SEC),[14] HPLC,[15] and gel electrophoresis.[16] These approaches might help to isolate the desired products. The purification methods for the copper clusters in this work involve: centrifugation, extraction and HPLC techniques. The centrifugue is often used to separate metal clusters from the

excess of capping agent, or, in our case, also in order to obtain the clusters as a precipitate and then washed with a different solvent excess. Extraction by an organic solvent can be used to isolate metal clusters soluble in the selected solvent. Besides the solubility of the protecting agents in different solvents is crucial in order to be able to the ligand exchange.

2.3.5. Overall strategy.

The synthesis of copper clusters here displayed, was based on a modification of Reetz's method. Copper ions produced during the electrolysis from the soluble anode were reduced in galvanostatic conditions in presence of a supporting electrolyte with an Autolab PGSTAT 20 potenciostat. The experiment was performed in all cases in a thermostatic three-electrode conventional electrochemical cell. Different tetrabutylammonium salts (tetrabutylammonium nitrate, acetate and bromide) were used as the supporting electrolyte. A copper sheet was used as an anode and the same size platinum as a cathode, and Ag/AgCl as a reference electrode. Both the working electrode and the counter electrode were carefully cleaned before synthesis; the Pt electrode was cleaned by polishing mirror-like with aluminium oxide and the copper electrode with sandpaper. Both were then washed with water in an ultrasonic bath. Further electrochemical polishing was carried out on the Pt electrode by repeated cyclic voltammetries in 1 M sulphuric acid. The cell (50mL) was maintained under a nitrogen atmosphere (to remove the oxygen and avoid the oxidation) and magnetic stirring, keeping the temperature at 25.0 ± 0.1 °C throughout the whole process. UV-Vis measurements were performed during the synthesis at different times by a pump system connected to the spectrophotometer. Purification through centrifugation was carried out in order to remove the excess of tetraalkylammonium salts or Cu ions present in the solution. The supernatant was removed and the solid redispersed in the selected solvent.Specific details of purification and different post-treatments will be explained in the each corresponding Chapter.

2.4. CHARACTERIZATION TECHNIQUES.

Characterization of metal clusters is essential to the deeply understand the structure–properties relationship. It should be noted that the tiny size of metal clusters make the characterization by some techniques difficult. For instance, the transmission electron microscopy (TEM) is a powerful tool in the studies of nanomaterials. However, due to the limited resolution, TEM is actually not a reliable method to obtain accurate core sizes (atom numbers) of sub-nanometre sized metal clusters. Here, we summarize the techniques commonly used for the characterization of our copper clusters: UV-Vis spectroscopy, transmission electron microscopy (TEM, HRTEM), mass spectrometry, fluorescence spectroscopy, lifetime measurements, X-ray photoelectron spectroscopy (XPS), cyclic voltammetry (CV), non contact atomic force microscopy (NC-AFM), etc.

2.4.1. Ultraviolet-Visible (UV-Vis) spectroscopy.

UV-Vis absorption spectroscopy has been used as a powerful qualitative and quantitative technique to study the electronic structures of metal clusters. The size dependence of the optical properties of noble metal nanoparticles has been reported theoretically and experimentally. As the size decreases, the localized surface plasmon band (SPB) for nanoparticles is blue-shifted and the band broadens. The SPB appears at 520nm for spherical AuNPs,[17] 400nm for AgCLs[2b] and 560-570 for CuNPs.[18] However, with particles with a diameter below 4 nm in diameter, a steady broadening of the plasmonic band was observed and more discrete optical features at smaller wavelengths with decreasing particle size appear, as it can be seen in Figure 2.2 for AuNPs[19]. The classical Mie theory cannot explain the size effects below diameters 2-5nm and quantum finite-size effects have to be considered.[20]

Therefore, metal clusters absorption show molecular-like optical transitions due to the quasi-continuous electronic energy band structure and the strong quantum confinement effects[21]. This may be translated as a significant blue-shift in the plasmon peak energy as the cluster size decreases. Absorption spectra of CuCLs (190-800 nm) were performed using a Hewlett-Packard HP8452A Diode Array Spectrophotometer in a 1 mm × 1 cm × 3 cm quartz cuvette at room temperature (unless otherwise noted) using the corresponding solvent as a blank.

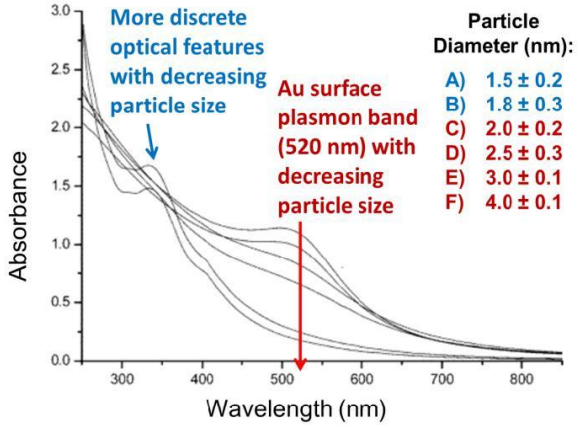

Figure 2. 2| *UV-Vis absorption spectrum for AuMPCs of varying core sizes. Figure extracted from reference 19b.*

2.4.2. Fluorescence spectroscopy measurements.

As we have explained before (Chapter 1) photoluminescence is an intrinsic property of metal clusters which can help us by using the Jellium model (Chapter 1) to approximate the cluster size. Fluorescence emission and excitation spectrum of copper clusters were obtained from 200 to 800nm at room temperature using a Cary Eclipse spectrophotometer from Varian (Xe pulse lamp 80 Hz, power 75kW). Samples were placed in a 10mm quartz cuvette, and the spectrometer slit was fixed to 5nm to obtain a spectra resolution of 1nm. All spectra were obtained at 6<pH<7 unless otherwise noted. Irradiation photostability studies were performed by using continuous irradiation at the desired wavelength for photobleaching. Quantum yield measurements of small CuCLs in water (Cu_{13}) (Chapter 6) were determined by the integrated luminescence intensity method by the comparison of the fluorescence emission with the standard reference sample of quinine in 0.1M H_2SO_4 (0.95) at room temperature. The slit width for the excitation and emission was set at 5nm. A series of copper solutions were prepared by diluting 2 to 20-fold and the fluorescence yield relative to absorbance was measured. The maximum fluorescence yield was obtained by extrapolating the curve to infinite dilution in order to avoid problems with self-quenching. A similar plot and extrapolation was obtained for quinine solutions prepared over the range of 0.001 to 0.01 in

concentration. The quantum yield (QY) can be calculated using the following equation:

$$\frac{Q_t}{Q_s} = \frac{\frac{I_t}{A_t} \cdot \eta_t^2}{\frac{I_s}{A_s} \cdot \eta_s^2}$$

where Q is the quantum yield, I the integral area under the PL spectrum, η the refractive index of the solvent, and A the absorption at the selected excitation wavelength. The subscripts "t" and "s" represent the test sample and the standard sample, respectively. Here, all luminescence signals were measured under 296nm excitation with the same experimental conditions, in the same system and with the absorption coefficients were set as 0.1.

Ion sensing by CuCLs was carried out by collecting the emission spectra of the CuCLs after 20 seconds reaction CuCLs+ion mixture and observing the emission fluorescence intensity quenching. Specific details will be shown on Chapter 6.

2.4.3. Mass spectrometry (MS) measurements.

It was in 1996, when Whetten and co-workers[22] realized that MS was an useful technique to determine the number of atoms of small gold nanocrystals by using laser-desorption/ionization (LDI) mass spectrometry. From then on, mass spectrometry has been widely used in almost all the structural studies of metal clusters. Until now, different MS techniques, such as laser desorption/ionization time-of-flight (LDI-TOF),[23] matrix-assisted laser desorption ionization time-of-flight (MALDI-TOF),[24] and electrospray ionization mass spectrometry (ESI) have been applied to the study of metal clusters. LDI-TOF MS has been checked[25,26] that can efficiently fragment the clusters causing the loss of metal atoms or ligands, MALDI-TOF is a much softer technique owing to the use of a matrix that absorbs the excess of energy irradiation preventing any fragmentation. Electrospray ionization mass spectrometry (ESI-TOF) is a much softer ionization technique but the disadvantage is the extremely necessary purification of the sample, which sometimes makes this technique difficult due to the existence of a high concentration of capping agents.

In this thesis the three mass spectrometry techniques were used. LDI-TOF and MALDI-TOF were performed using a Bruker Autoflex MALDI-TOF instrument with a pulsed nitrogen laser of 337 nm. Mass spectra were acquired in the reflectron mode (a linear mode was also studied but no successful results

were obtained). Experimental conditions for the mass spectra acquisition were optimized for two different m/z ranges: low mass range (m/z) 0-800 amu) and high m/z range (m/z) 750-2000 amu). Spectra were collected in both positive and negative ion mode and averaged from 300 spectra measured in each range. The general procedure to deposit the samples of copper clusters was spotted using 1μL of the clusters solution on the target plate directly and left to dry in room conditions. The assignment of the clusters was performed by comparing their experimental and theoretical isotopic patterns (isotopic distribution of copper (natural abundance ^{63}Cu 69.15% and ^{65}Cu 30.85%)). However, in order to obtain isotopic distribution high laser fluence is necessary as we will explain in posterior Chapters. ESI-TOF was performed using a Bruker Microtof instrument. The mass analysis of $TBANO_3$ was carried out in order to distinguish their peaks from those belonging to the CuCLs as it is shown in Figure 2.3. As we can clearly see the most abundant peak on positive ion mode is $TBAN^+$. Negative ion mode reveals NO_3^- as the major peak. Generally the TBA salts were observed to display m/z peaks smaller than 250 amu in both negative and positive modes.

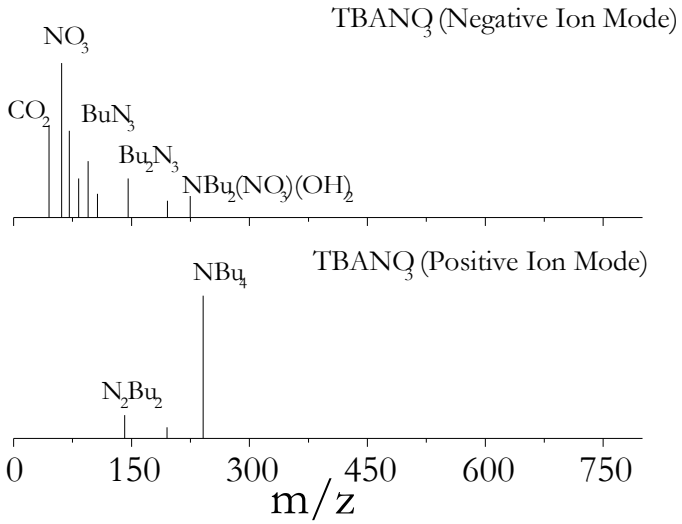

Figure 2. 3| *LDI-TOF mass spectrum of tetrabutylammonium nitrate used in this thesis as the supporting electrolyte.*

2.4.4. Transmission Electron Microscopy (TEM and HRTEM).

Transmission electron microscopy (TEM) has traditionally been used to obtain information about the nanoparticles size and shape. Although it should be noted that there is around a 0.2nm size uncertainty for TEM measurements and melting effects can occur under electron beam heating during the imaging.[27] Due to this, the size of sub-nanometer clusters cannot be obtained accurately from TEM measurements, but it can be useful for rejecting the presence of large nanoparticles. On the other hand, High resolution transmission electron microscopy (HRTEM) can provide us structural information (with a highest resolution of ~0.1 nm) in despite of more pronounced heating effects can occur during the measurement. Low-resolution TEM images of our CuCLs were obtained on a Philips CM20 electron microscope operating at an acceleration voltage of 120 kV, whereas HRTEM images were performed on a JEOL JEM-2010F electron microscope operating with an acceleration voltage of 200 kV. Samples were prepared on carbon-coated TEM grids by adding a drop of a diluted solution of CuCLs, onto the grid and evaporating the solvent in roomconditions. The measured lattice separations were compared against the standards for Cu, Cu_2O, and CuO (Table 2.2).

Table 2. 2| *Theoretical Lattice separations of the different Cu compounds.*

Compound	Cu	Cu_2O	CuO
Lattice separations/Å	1.81	3.02	2.51
	<200>	<110>	<002>

2.4.5. X-ray photoelectron spectroscopy (XPS).

Photoelectron spectroscopy is a powerful tool when investigating the composition and electronic state of metal cluster cores. The basis of XPS rely on the foton study by calculating the BE (atom binding energy or ionization energy for a certain level) of the inner atomic electron shells, which depends mainly of the atomic number. Atoms in a higher positive oxidation state will show higher binding energies due to the extra columbic interactions between the photo-emitted electron and the ion core. This ability to discriminate different oxidation states and chemical environments is one of the major strengths of XPS. Here, the average oxidation states of copper atoms in our samples were recorded using a VG Escalab 250iXL spectrometer (VG Scientific) equipped with a

hemispherical analyzer and Al KR X-ray monochromated source. An X-ray spot of 500 μm was used to generate photoelectrons, which were collected from a take-off angle of 90°. The argon partial pressure in the analysis chamber was maintained at 3×10^{-8} mbar during data acquisition by turbomolecular differential pumping. The measurement was performed in a constant analyzer energy mode (CAE) with 100 eV pass energy for survey spectra and 20 eV pass energy for the high resolution spectra. The intensities were estimated by calculating the area under each peak after subtraction of the S-shaped background. Binding energies (BEs) of Cu 2p could be determined by referencing to the adventitious C 1s peak at 285.0 eV. Atomic ratios were computed from peak intensity ratios and Schofield atomic sensitivity factors. Samples for XPS analysis were prepared, leaving a drop of solution containing CuCLs on a piece of mirror finish polished silicon wafer, evaporating the solvent quickly, and immediately introducing the sample into the XPS prechamber under high vacuum conditions. Ar^+ ions (1.5 keV, 60 s) were employed to remove adventitious carbon, which comes from the surface sample exposure to the atmosphere, and to remove also possible oxides at the sample surface. The amount of material removed is a function of the incident energy and sputtering time. Samples were kept rotating in order to avoid a shadow effect. The efficiency of the sputtering process was checked by the disappearance of the Si oxide native layer from the silicon wafer substrate. Bombardment was performed using an EXO5 ion gun incorporated into the equipment, provided with a scanning unit to raster the ion beam, operating at a voltage of 1.5 kV and a scan size of 2 mm, producing a sample current of 0.3 μA for 60 s of bombardment. The higher oxidation state of copper (II) can be identified by a shakeup satellite at ~10 eV from the Cu $2p_{3/2}$ main peak. This satellite peak is not present for other chemical species of copper, such as Cu(0) or Cu(I). Cu $2p_{3/2}$ binding energy and an Auger parameter in the copper clusters samples were investigated.

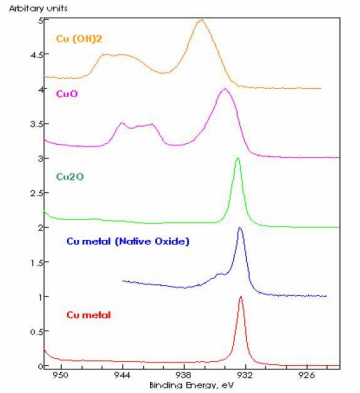

Figure 2. 4| *XPS database reference for Cu2p region of the different oxidation states of Cu.*

2.4.6. Cyclic Voltammetry (CV).

Cyclic voltammetry consists of cycling the potential of an electrode, which is immersed in an unstirred solution, and measuring the resulting current at the "working electrode" during the potential scan. The potential of the "working electrode" is controlled versus a reference electrode (Ag/AgCl). The important parameters of a cyclic voltammogram are the magnitudes of the anodic and cathodic peaks current and their position.

CV´s of different CuCLs sizes were performed by David Buceta Fernández. The experimental conditions consist on the deposition of the CuCLs solution onto glassy carbon (GC) electrodes and covered with one monolayer of Nafion (5μL of a 0.025% solution). The electrode surface was cleaned before each deposition by abrasion by polishing with alumina 0.5 μm average particle size. The final cleaning of the GC electrodes was performed in water in an ultrasonic bath. The counter electrode was a platinum wire while an Ag/AgCl electrode was used as the reference. The CuCLs were examined in 0.1M KOH by cyclic voltammetry (at sweep rate of 10mV/s) in the potential range between -0.5 V and +1.3V vs Ag/AgCl in a deaerated electrolyte solution under nitrogen at room temperature.

2.4.7. Atomic Force Microscope (AFM-NC).

An atomic force microscope can be used to investigate any surface, even poorly or non-conducting ones. The interaction force that dominates NC-AFM imaging is the short-range interaction force of the chemical bonding between the atoms of the AFM tip and the sample surface.[28] The resolution obtained by AFM is determined in large part by the size of the probe tip used for imaging. Attractive Van der Waals forces acting between the tip and the sample are detected, the tip scans above the surface and topographic images are created. The width of the particles depends on the probe shape; however, the particle height is independent of it. This fact is not a function of particle size but rather an intrinsic property of AFM. It is important to know if the probe is much smaller than the feature to be imaged; then the probe-generated artifacts will be minimal and the dimensional measurements will be accurate.

Here AFM tip Single Crystal Silicon, N-type, 0.01 -0.025Ω-cm, Antimony doped, was used. CuCLs samples were prepared by drying 5 μL of copper clusters on a mica substrate and using a XE-100 instrument (Park Systems Corporation) in noncontact mode.

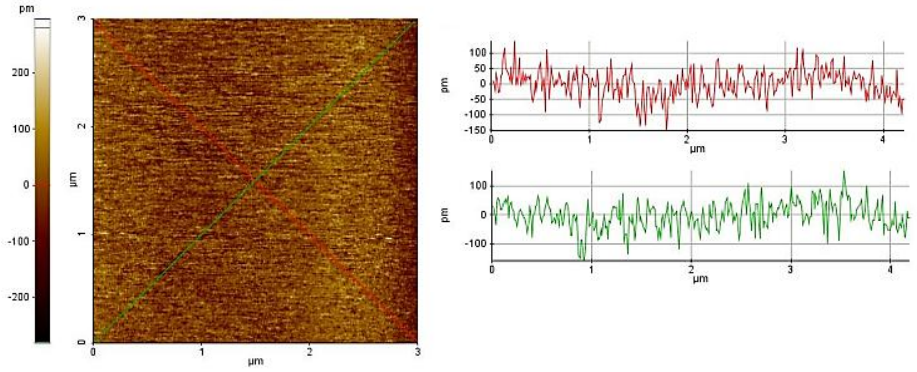

Figure 2. 5| *NC-AFM topography image of mica substrate with their corresponding cross-section.*

REFERENCES.

[1] Reetz M.T.; Helbig W. *J. Am. Chem. Soc. 116,* 1401 **(1994).**

[2] a) Rodríguez-Sánchez M.L.; Rodríguez M.J.; Blanco M.C.; Rivas J.; López-Quintela M.A. *J. Phys. Chem. B 109,* 1183 **(2005)**. b) Rodríguez-Sánchez M.L.; Blanco M.C.; López-Quintela M.A. *J. Phys. Chem. B 104*, 9683 **(2000).** c) Ledo A.; Martínez F.; López-Quintela M.A.; Rivas J.; *Physica B 398,* 273 **(2007).** d) Ledo-Suárez A.; Rivas J.; Rodríguez-Abreu C.F.; Rodríguez M.J.; Pastor E.; Hernández-Creus A.; Oseroff S.B.; López-Quintela M.A. *Angew. Chem. Int. Ed. 46,* 8823 **(2007).** e) Rodríguez-Vázquez M.J.; Blanco M.C.; Lourido R.; Vázquez-Vázquez C.; Pastor E.; Planes G.A.; Rivas J.; López-Quintela M.A. *Langmuir 24,* 12690 **(2008).** f) Ledo-Suárez A.; Rodríguez-Sánchez L.; Blanco M. C.; López-Quintela M. A. *Phys. stat. sol.* (a*) 203,* 1234 **(2006).**

[3] Reetz M.T. *Active Metals,* VCH, Weinheim, A. Fürstner Ed., 279 **(1996).**

[4] Aiken III J.D.; Finke R.G. *Journal of Molecular Catalysis A: Chemical 145*, 1 **(1999).**

[5] Franke R.; Rothe J.; Pollmann J.; Hormes J.; Bönnemann H.; Brijoux W.; Hindenburg T. *J. Am. Chem. Soc. 118,* 12090 **(1996).**

[6] Mayell J.S.; Bard A.J. *J. Am. Chem. Soc. 85,* 421 **(1963).**

[7] Littlehailes J.D.; Woodhall B.J. *Discuss. Faraday Soc., 45,* 187 **(1968).**

[8] Rodríguez-Sánchez L.; Blanco M. C., López-Quintela M. A. *J. Phys. Chem. B*, *104,* 9683 **(2000).**

[9] Fry A.J.; Krieger R.L. *J. Org. Chem. 41,* 54 **(1976).**

[10] Santiago González B.; Rodríguez M.J.; Blanco C.; Rivas J.; López-Quintela M.A.; Gaspar M. J.M. *Nano Lett. 10*, 4217 **(2010).**

[11] Vilar-Vidal, N. Master Thesis, "Synthesis, stabilization and characterization of atomic metal clusters", University of Santiago de Compostela **(2007).**

[12] Price R. C.; Whetten R. L. *J. Am. Chem. Soc. 127*, 13750 **(2005).**

[13] Whetten R. L.; Khoury J. T.; Alvarez M. M.; Murthy S.; Vezmar I.; Wang Z. L.; Stephens P. W.; Cleveland C. L.; Luedtke W. D.; Landmann U. *Adv. Mater. 8,* 428 **(1996).**

[14] (a) Siebrands T.; Giersig M.; Mulvaney P.; Fischer C.-H. *Langmuir 9,* 2297 **(1993).** b) Wilcoxon J. P.; Martin J. E.; Provencio P. *Langmuir 16,* 9912 **(2000).** c)Gautier C.; Taras R.; Gladiali S.; Beurgi T. *Chirality 20,* 483 **(2008).** d) Frein S.; Boudon J.; Vonlanthen M.; Scharf T.; Barber J.; Seuss-Fink G.; Beurgi T.; Dechenaux R. *Helv. Chim. Acta 91,* 2321 **(2008).**

[15] (a) Jiménez V. L.; Leopold M. C.; Mazzitelli C.; Jorgenson J. W.; Murray R. W. *Anal. Chem. 75*, 199 **(2003).** (b) Song Y.; Jiménez V.; McKinney C.; Donckers R.; Murray R. W. *Anal. Chem. 75,* 5088 **(2003).** (c) Choi M. M. F.; Douglas A. D.; Murray R. W. *Anal. Chem. 78,* 2779 **(2006).** (d) Zhang Y.; Shuang S.; Dong C.; Lo C. K.; Paau M. C.; Choi M. M. F. *Anal. Chem. 81,* 1676 **(2009).**

[16] Schaaff T. G.; Knight G.; Shafigullin M. N.; Borkman R. F.; Whetten R. L. *J. Phys. Chem. B 102*, 10643 **(1998).**

[17] Kreibig U.; Zacharias P. *Z. Phys A-Hadron Nucl. 231,* 128 **(1970).**

[18] Lisiecki I.; Pileni M.B. *J. Am. Chem. Soc. 115,* 3887 **(1993).**

[19] a) Hussain I.; Graham S.; Wang Z.; Tan B.; Sherrington D. C.; Rannard S. P.; Cooper A. I.; Brust M. *J. Am. Chem. Soc. 127*, 16398 **(2005).** b) Robinson III, D.A., PhD Dissertation, *"Synthesis and characterization of metal nanoclusters stabilizaed by dithiolates"*. Georgia State University **(2011).**

[20] Cottancinm E.; Celep G.; Lemé J.; Pellarin M.; Huntzinger J.R.; Vialle J.L.; Broyer M. *Theor. Chem. Acc. 116,* 514 **(2006).**

[21] a) Kelly K. L.; Coronado E.; Zhao L. L.; Schatz G. C. *J. Phys. Chem. B 107*, 668 **(2003).** b) Rao T. U. B.; Pradeep T. *Angew. Chem. Int. Ed. 49,* 3925 **(2010).**

[22] Whetten R. L.; Khoury J. T.; Alvarez M. M.; Murthy S.; Vezmar I.; Wang Z. L.; Stephens P. W.; Cleveland C. L.; Luedtke W. D.; Landman U. *Adv. Mater. 8,* 428 **(1996).**

[23] Waters C. A.; Mills A. J.; Johnson K. A.; Schiffrin D. J. *Chem. Commun. 4,* 540 **(2003).**

[24] Dass A.; Stevenson A.; Dubay G. R.; Tracy J. B.; Murray R. W. *J. Am. Chem. Soc. 130,* 5940 **(2008).**

[25] Arnold R. J.; Reilly J. P. *J. Am. Chem. Soc. 120,* 1528 **(1998).**

[26] Schaaff T. G. *Anal. Chem. 76,* 6187 **(2004).**

[27] a) Zhang W.J.; Miser D.E. *Journal of Nanoparticle Research 8*, 1027 **(2006).** b) Ramasamy P.; Guha S.; Shibu E. S.; Sreeprasad T. S.; Bag S.; Banerjee A.; Pradeep T. *J. Mater. Chem. 19,* 8456 **(2009).** c) Rao T. U. B.; Pradeep T. *Angew. Chem. 122,* 4017**(2010)** *Angew. Chem. Int. Ed. 49*, 3925 **(2010).**

[28] Perez R.; Payne M. C.; Stich I.; Terakura K. *Phys. Rev. Lett. 78,* 678 **(1997).**

CHAPTER 3.

Synthesis of Small Copper Clusters

3.1. INTRODUCTION.

Fluorescent metal clusters have been generating significant interest nowadays; their syntheses have been optimized and their properties studied mostly due to their possible application as proteins or cellular labels (in biological imaging applications). Ideally, for biomedical applications, non-toxic aqueous-soluble clusters with a strong emission and good photostability are desirable. Besides, small metal clusters consisting of only in a few atoms are of considerable interest due to their greater stability. Several approaches have been reported for the synthesis of metal clusters in aqueous solution,[1] being Cu clusters less studied. In this research work, we first developed a new aqueous electrochemical synthesis of small copper clusters. The optimization of the synthesis has been studied by studying the different parameters which had an influence on the product. Purification of the obtained CuCLs by centrifugation was studied resulting in a control-size selective method. CuCLs should be optical, structural and morphological characterized by using UV-Vis, TEM/HRTEM, LDI-TOF and ESI-TOF, NC-AFM, Fluorescence, CV, XPS.

3.2. EXPERIMENTAL SECTION.

A typical synthesis procedure was carried out as the protocol explained on Chapter 2. Different synthesis parameters such as synthesis time, solvent and supporting electrolyte were studied (details summarized on Table 3.1) in order to optimizate the synthesis method. Immediately, after the synthesis the purification process was developed, in order to eliminate the possible remaining copper ions and the tetrabutylammonium salt excess. The purification method was been carried out in different steps (Scheme 3.1). 1) Centrifugation at 8000rpm for 15min of the whole sample (supernatant and precipitate). 2) The supernatant was removed. 3) The solid copper clusters were centrifuged three times with water (8000rpm, 10min) or twice with ethanol (8000rpm, 30min). 4) Finally, the obtained precipitate was redispersed in water (50mL) or in ethanol (50mL) respectively.

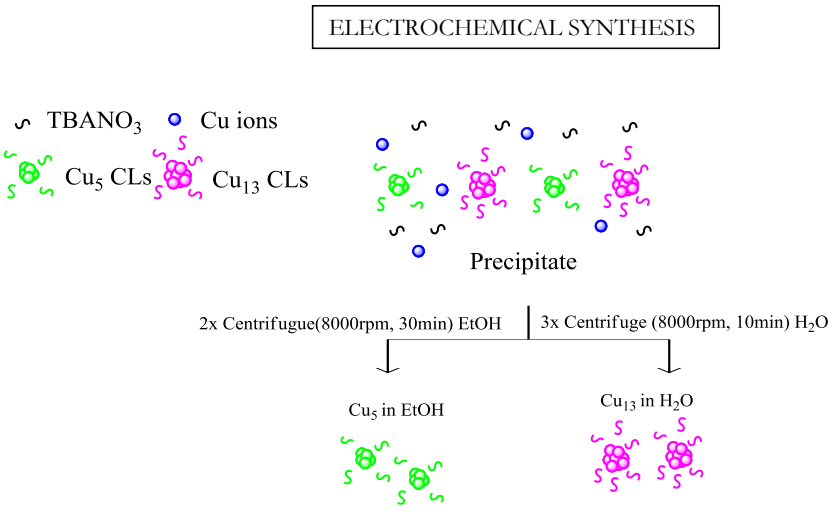

Scheme 3. 1| *Visual scheme of small CuCLs purification after synthesis.*

3.3. RESULTS AND DISCUSSION.

3.3.1. Synthesis of small CuCLs: optimization method.

The effects of several processing variables, including synthesis time, solvent and supporting electrolyte on the PL properties of the obtained aqueous CuCLs were examined. As it has been explained on Chapter 2 particle size can be increased with synthesis time, solvent effects can induce the particle aggregation and the supporting electrolyte can display undesirable secondary reactions under the chosen current density. Taking into account all of these variables five experiments were carried out in order to obtain the best synthesis conditions for small copper clusters. Conditions of the experiments are showed in Table 3.1. The variation of the potential during the copper clusters synthesis was monitored (Figure 3.1). It is clearly observed that the potential increases (becomes more negative) very fast attaining higher overpotential values in the range 0.2-0.4 V depending on the conditions, this can be associated to the increase of the $[Cu^{+2}]$, because at the beginning of the electrolysis $[Cu^{+2}] = 0$, and after a certain time (~60s) it reaches a stationary state. When this occurs, the electrochemical potential remains approximately constant. After that, the potential remained approximately constant except for E38, where we saw a potential decrease, related to a competing process: the deposition onto the cathode electrode. When the Pt electrode was completely covered with Cu, the electrodeposition was more favourable than the formation of the clusters and the cluster formation stopped. CuCLs were obtained in solution with a solid precipitate for all the synthesis excluding E2.

Table 3. 1| *Synthesis conditions of the different CuCLs samples.*

Sample	ϱ/(mA/cm^2)	T^a/^{o}C	t/s	Solvent	Supporting electrolyte	Cathode	PL
E2	*10*	*25*	*200*	*H_2O*	*$TBANO_3$*	*Pt*	*NO*
E31	*10*	*25*	*800*	*H_2O*	*$TBANO_3$*	*Pt*	*YES*
E3	*10*	*25*	*1200*	*H_2O*	*$TBANO_3$*	*Pt*	*NO*
E39	*10*	*25*	*800*	*MeCN*	*$TBANO_3$*	*Pt*	*YES*
E20	*10*	*25*	*800*	*H_2O*	*TBABr*	*Pt*	*YES*

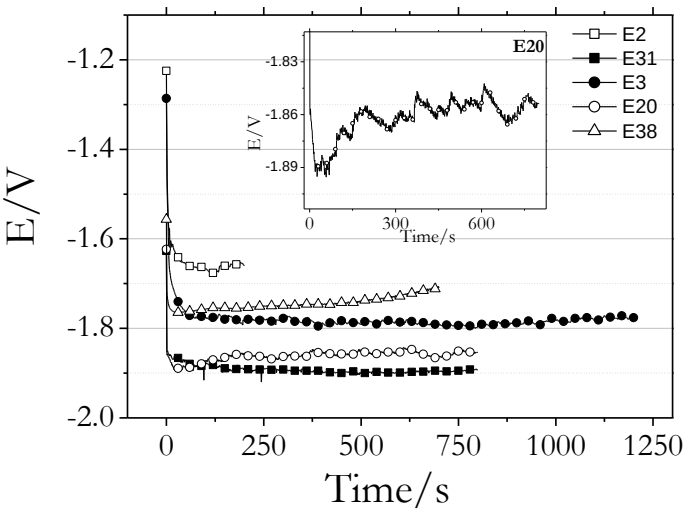

Figure 3. 1| *Change of the electrode potential during the CuCLs synthesis under different conditions.*

The TEM image of **E2** showed a lamellar association of small particles (1.64±0.69nm) (Figure 3.2.A), **E3** showed a mixture between lamellar structures and large spherical particles (4.0±1.91nm) (Figure 3.2.C). No emission was detected for both samples. **E31** gave a monodisperse solution of spheres with an average diameter less than 1nm (0.98±0.45nm) (Figure 3.2.B) and good PL results (Figure 3.3.B). The synthesis of CuCLs in an aprotic solvent like acetonitrile (E39) was observed to be monodisperse by the TEM image (Figure 3.2.D) (1.23±0.32nm) and different emission results were obtained on the supernatant and the redispersed precipitate in water (Figure 3.3.C-D). As a final point, the supporting electrolyte effect was also studied by using a different counterion: Br^-. A different behavior of this synthesis was obtained even on the potenciogram. Small oscillations on the potenciogram appear possibly attributed to the existence of a competitive process (Inset Figure 3.1). Previous studies by our group[2] have demonstrated that TBABr salt is electrochemically inert in the range 0.8-1.8V, but at higher potentials Br^- can be oxidized (onto the anode) forming Br_2 :

$$Br^- \rightarrow Br^{\cdot} + 1\ e^-$$
$$2\ Br^{\cdot} \rightarrow Br_2$$

Our synthesis underwent to E>1.8V (E_{E20}~1.89V), therefore these oscillations can be due to the diffusion of Br_2 from the solution. Beside this, Cu was deposited onto the cathode since t=100s, giving a less yield of the product. In addition, corrosion of the anode was obtained after the synthesis. TEM image showed large amorphous aggregates but PL properties were found on the supernatant (Figure 3.3.A). The new emission at smaller wavelengths (related with smaller clusters by the Jellium model) can be explained by the corrosion of the anode (Cu). During the synthesis the anode begins to be covered, therefore less Cu^{+2} ions will be produced and less Cu^{+2} ions will be able to achieve the cathode to reduce in and create clusters. Meanwhile, when less Cu^{+2} ions are produced small nuclei are formed, so small clusters will be formed.

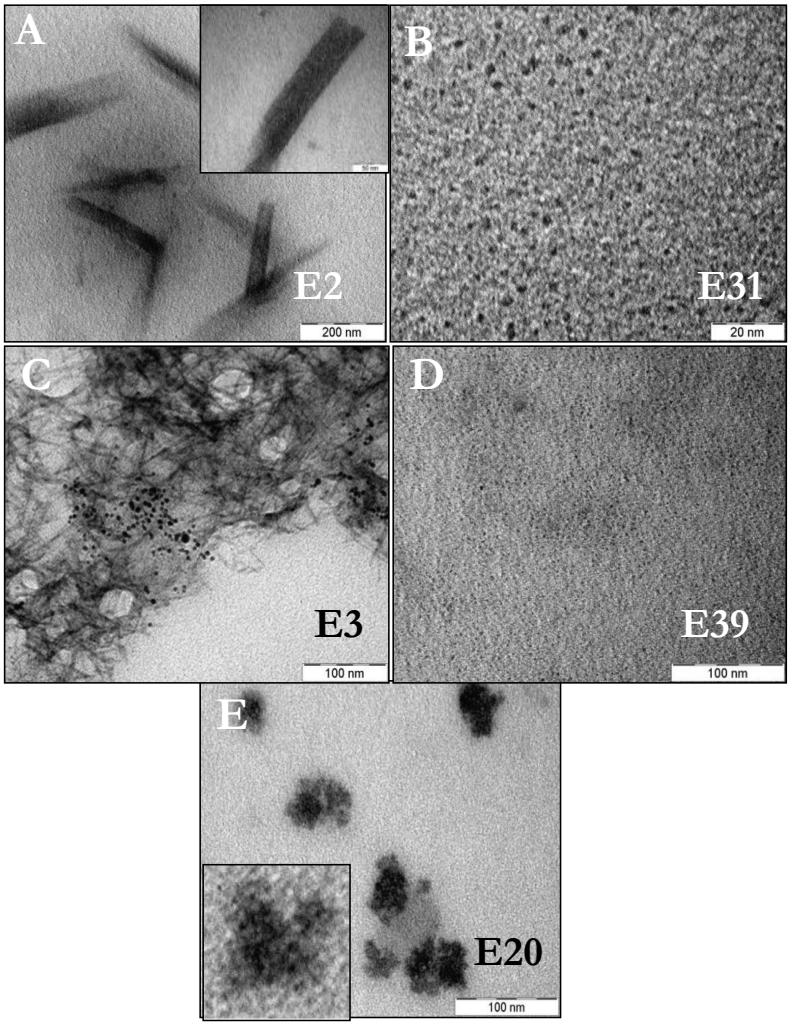

Figure 3. 2| *TEM images of the different synthesized CuCLs corresponding to E2 (A), E31 (B) , E3 (C), E39 (D) and E20 (E).*

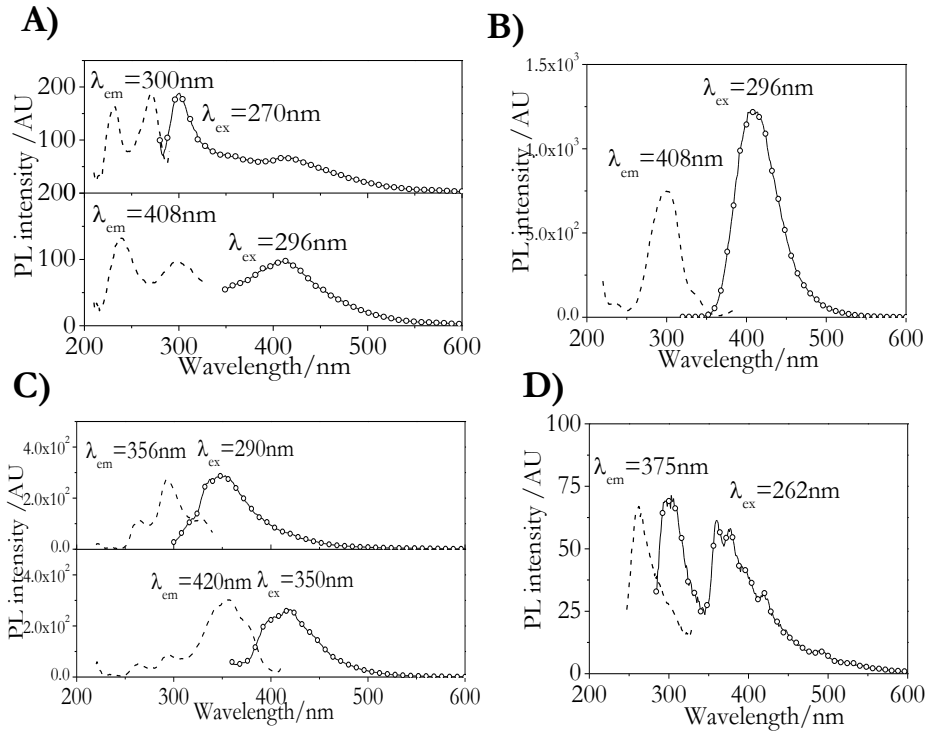

Figure 3. 3| *PL spectra of CuCLs. Sample E20 (A), E31 (B), E39 (C and D).*

In order to study the non-influence of undesired effects of the tetrabutylammonium salts on the PL properties of the clusters, a photoreductive study of metal precursor salts was made (Annex C3). The obtained results conclude that the emission came from the metal core and not from the surrounding environment. Besides, a cheap alternative to the high expensive cathode has been studied by using instead Pt an aluminium (Al) cathode. The results (under E31 conditions) were successful (Annex C3), but with a small yield. Therefore, taking into account the emissive properties, yield and the possible biocompatibility CuCLs of **E31** has been chosen as model synthesis of ***photoluminescent aqueous-soluble small CuCLs.***

3.3.2. Kinetic evolution during the synthesis.

UV-Vis absortption spectrum (Figure 3.4.A) changes in the course of the synthesis at different synthesis times.The UV-Vis absorption at the beginning (t=40s) shows the first absorption band centered at 250nm. When the time is around 100s another two bands centered at 275 and 300nm appears, which will increase their intensity with the time. Surface plasmon band of copper $\mathbf{Cu_{SPB}}$ ≈560-570nm[3] is not observed nor 800 nm absorption band attributed to the aqueous Cu cations $[Cu(H_2O)_6]^{+2}$ *d-d* transition in a tetragonally distorted octahedral or square-planar ligand field. The band at 250 nm was considered by Zhao et al.[4] as a ligand-to-metal charge transfer transition. But, studies by Ozin et al. [5] revealed CuCLs absorption at 247-256 nm (in solid Xenon) related with a Cu_2 cluster and 272 nm with a Cu_3. Therefore, these bands (250 and 275 nm) can be associated to the first "*stable*" copper clusters. De Waele et al. [6] and Vazquez-Vazquez et al.[7] obtained similar results by radiolytic and microemulsions synthesis showing absorptions at 264 nm and 250 nm respectively on the earliest stages of the synthesis.

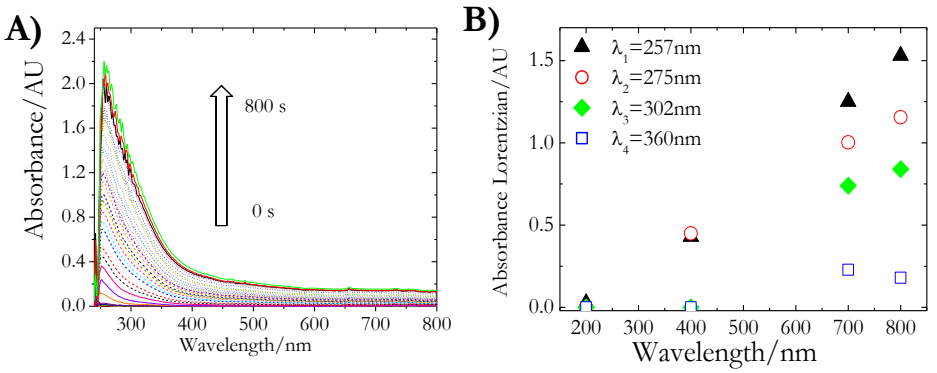

Figure 3. 4| *Absorbance versus time during the electrochemical synthesis of small copper clusters E31. Time between successive spectra is ⊿t =20 s.(A) Absorbance versus time obtained by fitting to Lorentzians for the peaks centered at 257, 275,302 and 360 nm during the synthesis.(B)*

In addition, for a more systematic study, we have fitted each absorption band to Lorentzians. In this way, one can see the increase of the different absorption intensity for each peak at different times (Figure 3.4.B). It can be seen that the absorbance at 275 and 300 nm began at 400s, which evolve more slowly than the 257 nm band; therefore, it can be ascribed to intermediate larger

clusters. The broad band located at 360 nm could be attributed to the aggregation of the particles at the end of the synthesis. These results agree with the literature.[8]

3.3.3. Purification and PL characterization of small CuCLs.

According to the Experimental Section, two different purification processes of the precipitated obtained in **E31** have been done. We have obtained two different samples: CuCLs in water and CuCLs in EtOH. UV-Vis results showed on Figure 3.5.A display three main absorption bands located at (1) 5.85 eV (212 nm), (2) 5.36 eV (231 nm), and (3) 4.19 eV (296 nm) for CuCLs/H_2O and Figure 3.5.B two main bands at (1) 5.99 eV(207 nm) and (2) 4.54 eV (273 nm) for CuCLs/EtOH.

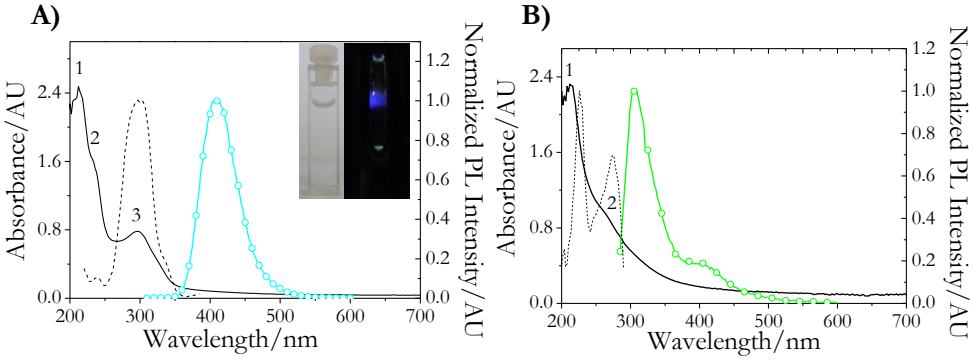

Figure 3. 5| *UV-visible and fluorescence spectra of CuCLs/H_2O . Excitation wavelength=296nm, emission wavelength = 408nm. Inset: Blue emission observed for an aqueous solution of CuCLs irradiating at λexcitation=296nm. (A) UV-Vis and emission and excitation spectra of CuCLs/EtOH. Excitation wavelength =275nm, emission wavelength=300nm.*(B)

The maximum emission peak of the as-purified CuCLs was located at 3.04 eV (408 nm) for CuCLs/H_2O and at 4.13 eV (300 nm) for CuCLs/EtOH. It has to be noted that CuCLs/EtOH displays also some emission at 408 nm. The maximum excitation peak appears of both samples agree with the last absorption bands found in their UV-Vis spectra. Samples are colorless under day light, but are highly blue when irradiated with UV light (300nm) as it is shown in the inset of Figure 3.5.A.

It has been shown that the simple spherical Jellium model seems to describe sufficiently well the emission energy in Au clusters[1c] through the expression:

$$\mathbf{E_g = E_{fermi}/N^{1/3}}, \qquad \textbf{Eq. 1}$$

where $\mathbf{E_{fermi}}$ is the Fermi energy of bulk material[9] and **N** is the number of atoms per cluster. Assuming that a similar model can be applied to Cu clusters, one can get the number of atoms per cluster from the position of the emission band. The double emission peaks displayed by CuCLs/EtOH sample indicates the existence of two different size populations. Table 3.2 shows the energy emission values of the different samples and their metal core obtained by Eq.1.

Table 3.2| *Summary of the emission properties of the different as-purified CuCLs.*

Sample	E_{emi1}/eV	E_{emi2}/eV	N_1	N_2
CuCLs/H_2O	*3.04*	-	*12*	-
CuCLs/EtOH	*4.08*	*3.04*	*5*	*12*

In order to check that the PL properties of the CuCLs are inherent of metal core and are not due to a possible solvatochromic effect, CuCLs/H_2O was dried and redispersed in ethanol showing (Figure 3.6) the same emission band, which corroborates the assumption that the fluorescence come from the metal core. Although there are only a few reports about fluorescent CuCLs (Table 1.2-Chapter 1), our results are consistent with other works. Vázquez-Vázquez et al.[7] observed emission of CuCLs at 333nm at first stages of their synthesis, assigned to small Cu_NCLs with N<10. Emission at 408nm has also observed by Goswami et al.[10] assigned the emission to a Cu_{13} center. Thiol protected CuCLs studied by Wei et al.[11] display emission at 425 nm and they assigned to a Cu_8 cluster. Therefore, different characterization techniques will be necessary in order to check the first approximation cluster size by the Jellium model.

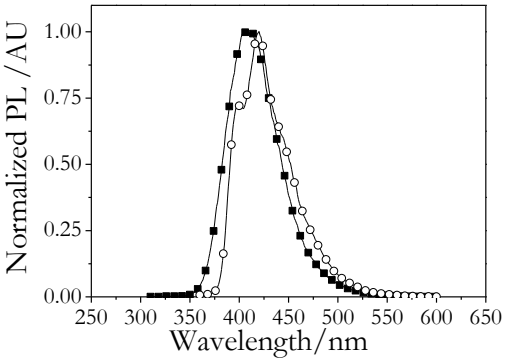

Figure 3. 6| *PL emission spectrum of CuCLs/H_2O (black squares) initially ($\lambda_{excitation}$=296 nm) and after being redispersed in EtOH (red open circles) ($\lambda_{excitation}$=350 nm). Almost no emission maximum shift (408 nm) is observed.*

3.3.4. Further characterization of small CuCLs.

(A) Tauc approach.

It is known that small metal clusters display a semiconductor-like behavior because of the appearance of a band gap at the Fermi level. For this reason, we have tried to determine the band gap by the traditional Tauc approach used for semiconductors, using the equation:

$$(\alpha h\upsilon) = A\,(h\nu - Eg)^n, \qquad \text{Eq.2}$$

where $h\upsilon$ is the photo energy (h is Plank constant and υ is the frequency radiation), a is the absorption coefficient, A is a constant, E_g is the band gap value and n equals ½ for a direct transition and 2 for an indirect transition. One can see (Figure 3.7) that it is difficult to fit the spectral data by this equation, which indicates that clusters display a molecule-like behavior rather than a classical semiconductor behavior. Nevertheless, the approximate band gap, which can be deduced by the Tauc approach. CuCLs/H_2O would display 3.7eV for a direct transition, which are larger than the direct band gap of bulk Cu_2O (2.17eV) and CuO (1.4eV)[12], and also larger than other reported copper oxides nanostructures showing values in the range 2.24eV to 2.75eV.[13] CuCLs/EtOH direct transition would give us a mixture of band gaps between 5.29-4.15eV. The

results here obtained agree with the Jellium model: E_{Tauc} (CuCLs/H_2O) ≈ 3.7 eV (Jellium E_g≈ 3.04 eV) and E_{Tauc} (CuCLs/EtOH) ≈4.15 eV (Jellium E_g ≈ 4.15 eV). In conclusion, bigger energy gaps are obtained for CuCLs/EtOH indicating the presence of smaller clusters sizes.

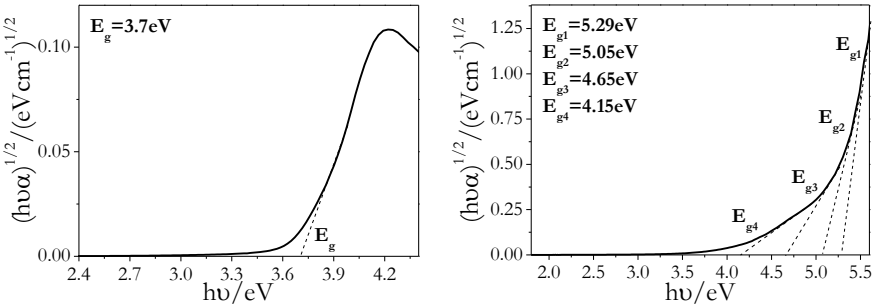

Figure 3.7| *Tauc plots derived from the absorption spectra of CuCLs/H_2O for a direct bandgap fitting (Eg = 3.7eV) (left) and for CuCLs/EtOH (5.29eV≤Eg≤ 4.15eV) (right).*

(B)TEM/HRTEM:

TEM and HRTEM studies of CuCLs/H_2O have been carried out. Small clusters are sensitive to electron beam irradiation and can produce larger nanoparticles upon irradiation for a prolonged time. [14] The isolated clusters of sub-nanometer dimensions are not expected to be seen clearly. Figure 3.8 shows the presence of small CuCLs forming aggregates of different sizes. The average size of the clusters inside the aggregates (Figure 3.8.C) is 0.61±0.13nm. This size is comparable to the size expected for the smallest 3D more stable closed-shell geometrical cluster, Cu_{13}, (0.77nm). Therefore, one can conclude that the number of atoms per cluster is N ≈ < 13 atoms, which again agrees with previous estimations. Figure 3.9.A shows the HRTEM image of the sample after some time of irradiation with the strong electron beam. Crystal planes are now observed with a *d* space distance of 2.02±0.23Å (corresponding to the (111) plane of the *fcc* phase of metal copper) indicating that clusters fuse to form crystal nanoparticles under the strong electron irradiation beam.[15]

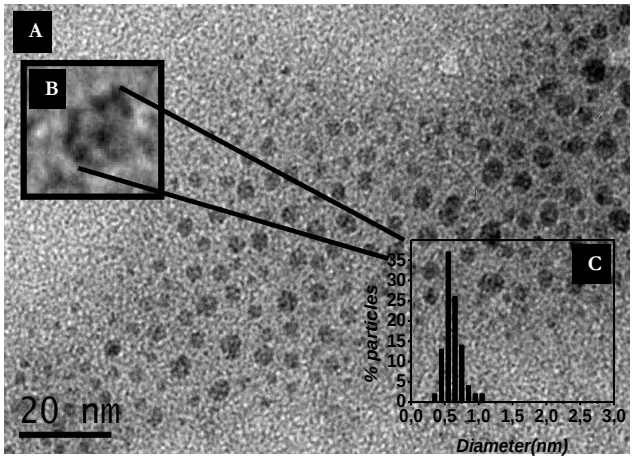

Figure 3. 8| *TEM image of Cu samples showing CuCLs forming aggregates of different sizes (A). Enlargement of one aggregate of CuCLs (B). Size histogram of individual clusters inside of the aggregates shown in A (100 counts). Average cluster size: 0.61±0.13nm(C).*

On Figure 3.9.B the same area was examined during upon five minutes. As the irradiation time increase big particles started to appear on the grid. It is believed to be due to the coalescence of small CuCLs leading to the formation of large particles.

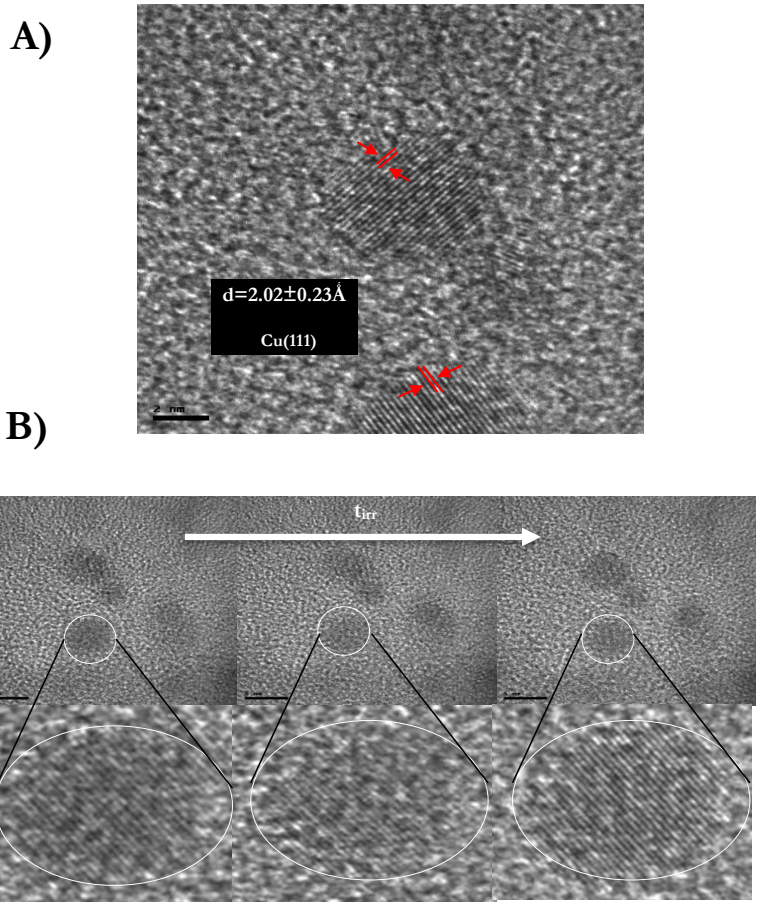

Figure 3. 9| *HRTEM of Cu samples after being exposed to the electron beam. HRTEM image of the cluster's evolution under the irradiation beam with time. HRTEM showing lattice spacing of 2.02±0.23Á (average from 100 measurements) corresponding to the Cu (111) plane (A). TEM image of small copper clusters showing their conversion into bigger nanocrystals upon the irradiation of the electron beam, when a grid with clusters was irradiated during 5minutes (B).*

(C) NC-AFM:

To further investigate the size of the copper clusters, non-contact atomic force microscopy (AFM-NC) studies were carried out (Experimental details on Chapter 2) deposited on mica substrates (with a rms ≈ 150pm). Small clusters (CuCLs/EtOH) NC-AFM image is displayed on Figure 3.10.A (average size 0.42±0.21 nm). Figure 3.10.A shows CuCLS/H_2O with an average size (0.6±0.27 nm). It has to be noticed that the calculated size for the CuCLs/H_2O clusters agrees with TEM results and also with the size estimated for a closed-shell cuboctahedra or icosahedra structure Cu_{13}, (0.77nm). From theoretical studies,[16] it is known that small copper clusters Cu_NCLs (N≤6) have a tendency to be planar. Thus, the AFM images suggest than mainly planar Cu_N clusters with N≤6 are obtained in the CuCLs/EtOH sample and 3D clusters with N≈13 atoms are seen for CuCLs/H_2O. The presence of a small amount of larger CuCLs on the Figure 3.10.B could be explained by the aggregation of smaller clusters when drying the drop deposited on the mica surface (e.g., sizes above 1.4 nm).

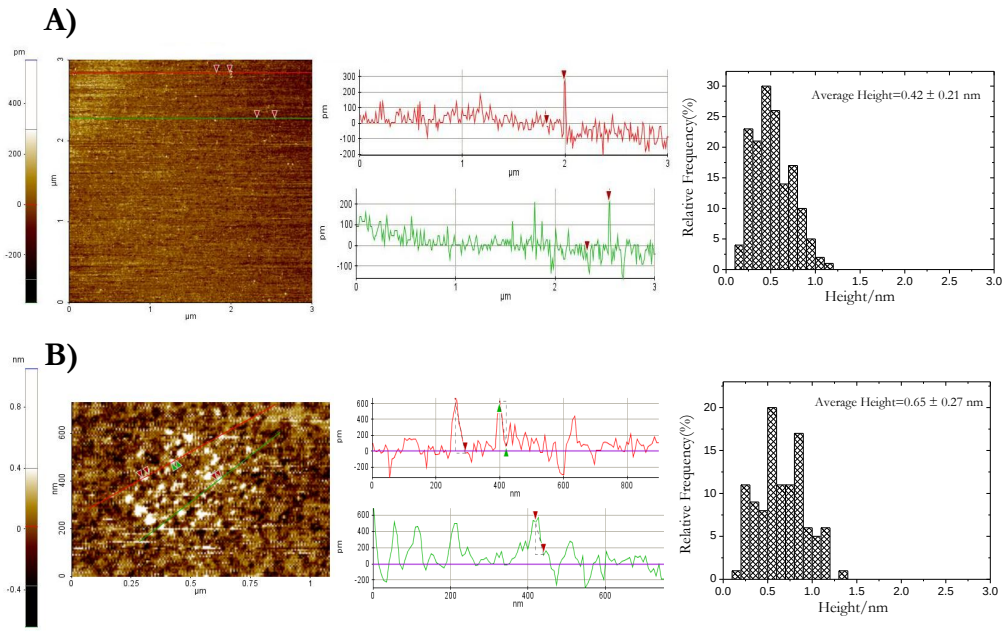

Figure 3. 10| *NC-AFM topography images of CuCLs/EtOH (A) and CuCLs/H_2O (B) deposited on mica substrates (rms ≈150 pm) (left). Section analysis of the solid lines of AFM images (middle) and their corresponding histogram distribution heights (right).*

(D) Mass spectrometry Study:

Mass spectrometry analysis was performed in order to determine the number of atoms of the clusters here studied. Two different techniques were used: laser desorption ionization time of flight (LDI-TOF) and electrospray ionization time of flight (ESI-TOF).

(D.1) LDI-TOF results:

The clusters will be identified by a comparison between the theoretical and the experimental mass spectra. Two different LDI analyses were carried out: one at low mass range from 100 to 600 amu (Figure 3.11) and high mass range from 900 to 2000 amu (Figure 3.12). For simplicity, assignments of CuCLs in the mass spectra are named as [N:X:Y] being N the number of copper atoms, X, buthyl groups and Y nitrogen atoms in the identified clusters. Eight different species Cu_N were found with N=2-5 in the low-mass range and N= 11-14 in the high-mass range. Peaks found in the low-mass range marked with *, corresponding to Cu_1 species, were not considered as clusters because of the associated difficulty to assign them either as clusters of Cu(0) or complexes of Cu(I), and will not be further discussed. Experimental and predicted isotopic patterns, as well as a summary of the ligands associated with different clusters are shown in the Annex C3. A summary of the main mass peaks will be showed in Tables 3.3 and 3.4 with their calculated theoretical m/z value. We should point out that the found divergence (1-2 m/z units) between theoretical and experimental data for some clusters could be attributed to the presence of adsorbed H^+ ions. Besides no clusters peaks were found in the positive ion mode. The main conclusion we can derive from this mass spectra analysis is the presence of Cu_N clusters formed by $N \approx < 14$ atoms which nicely agrees with the previous estimations made from the photoluminescent properties.

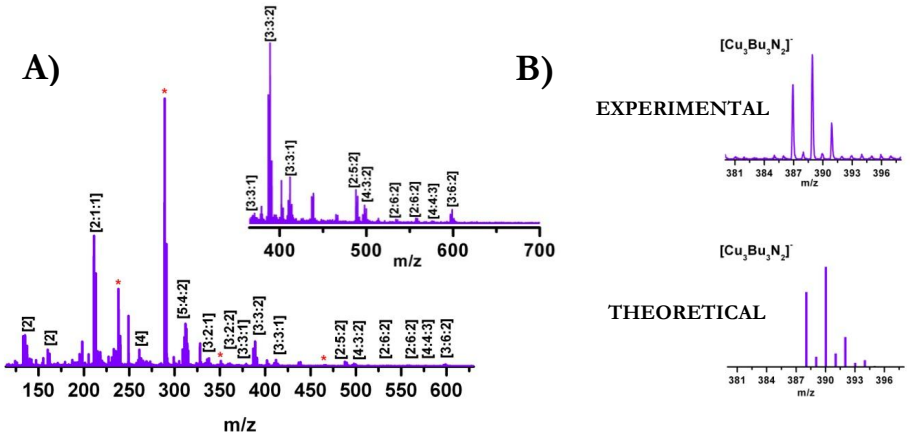

Figure 3. 11| *Low m/z range LDI-TOF mass spectrum of copper clusters samples in water detected in negative ion mode. (A). Inset: Magnification of 350-700 amu range. Magnification showing one of the identified CuCLs together with its theoretical isotopic pattern: $[Cu_3Bu_3N_2]^-$ (B).*

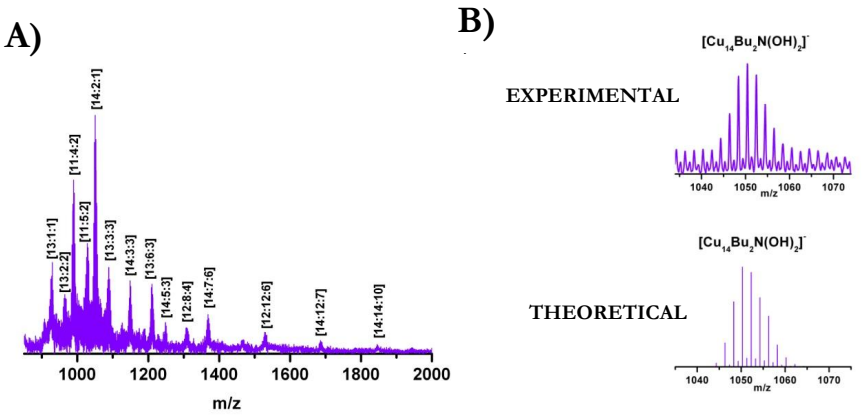

Figure 3. 12| *High m/z range LDI-TOF mass spectrum of copper clusters samples in water detected in negative ion mode. (A). Magnification showing one of the identified CuCLs together with its theoretical isotopic pattern: $[Cu_{14}Bu_2N(OH)_2]^-$ (B).*

Table 3. 3| *LDI-TOF results at the optimized low-mass range: m/z: 0 – 800 amu. The experimental and theoretical m/z main peaks are also showed.*

CLUSTER	**m/z** $_{experimental}$	**m/z** $_{theoretical}$
$[Cu_2]^-$	*124.2394*	*125.8592*
$[Cu_2(OH)_2]^-$	*160.1506*	*159.8647*
$[Cu_2BuN(OH)]^-$	*211.1231*	*213.9354*
$[Cu_2Bu_5N_2(OH)CO]^-$	*487.9152*	*484.2151*
$[Cu_2Bu_6N_2(OH)_2]^-$	*533.9081*	*530.2934*
$[Cu_2Bu_6N_2(OH)_2CO]^-$	*556.9602*	*558.2883*
$[Cu_3Bu_2N(OH)]^-$	*337.9690*	*333.9355*
$[Cu_3Bu_2N_2CO]^-$	*361.0189*	*359.9386*
$[Cu_3Bu_3N]^-$	*370.9870*	*376.9984*
$[Cu_3Bu_3N_2]^-$	*388.9199*	*390.0066*
$[Cu_3Bu_3N(OH)_2]^-$	*411.9307*	*410.0068*
$[Cu_3Bu_6N_2(OH)_2]^-$	*598.8597*	*595.2212*
$[Cu_4]^-$	*261.1897*	*253.7166*
$[Cu_4Bu_3N_3(OH)_2]^-$	*497.8980*	*500.9448*
$[Cu_4Bu_4N_3(OH)_3]^-$	*575.7745*	*575.0158*
$[Cu_5Bu_4N_2(OH)_3]^{2-}$	*312.1309*	*311.9711= 623.9422/2*

Table 3.4| *LDI-TOF results at the optimized high-mass range: m/z: 800-2000 amu. Experimental and theoretical m/z main peaks are also showed.*

CLUSTER	**m/z** $_{\text{experimental}}$	**m/z** $_{\text{theoretical}}$
$[Cu_{11}Bu_4N_2(OH)_2]^+$	*989.2878*	*988.5135*
$[Cu_{11}Bu_5N_2(OH)]^+$	*1028.0903*	*1028.5812*
$[Cu_{12}Bu_8N_4(OH)_2]^+$	*1308.4498*	*1309.7292*
$[Cu_{12}Bu_{12}N_6]^+$	*1528.2444*	*1532.0115*
$[Cu_{13}BuNO_2]^+$	*929.4922*	*929.1409*
$[Cu_{13}Bu_2N_2]^+$	*964.6708*	*968.2256*
$[Cu_{13}Bu_3N_3(OH)_3]^+$	*1088.5875*	*1090.3063*
$[Cu_{13}Bu_6N_3]^+$	*1210.8143*	*1210.5093*
$[Cu_{14}Bu_2N(OH)_2]^+$	*1050.3922*	*1051.1566*
$[Cu_{14}Bu_3N_3(OH)_3]^+$	*1148.7134*	*1153.2359*
$[Cu_{14}Bu_5N_3(OH)_2]^+$	*1248.4724*	*1250.3740*
$[Cu_{14}Bu_7N_6]^+$	*1368.4703*	*1372.5186*
$[Cu_{14}Bu_{12}N_7(OH)]^+$	*1685.7842*	*1688.8765*
$[Cu_{14}Bu_{14}N_{10}(OH)]^+$	*1845.6250*	*1845.0266*

(D.2) ESI-TOF results:

ESI-TOF experiments were also carried out due to the controversy over LDI fragmentation. As in LDI measurements, CuCLs peaks appeared only on the negative ionization mode, but no isotopic distribution has been observed. Therefore, the identification of the CuCLs would be very difficult. Despite of this, the assignation was carried out in comparison with the assigned LDI peaks. It should to be noted that using ESI-TOF technique m/z peaks appear at low mass range (100-600 amu) (Figure 3.13), however, the double or triple charge for some peaks allowed us to identify through to a Cu_{13} core. A summary of the main peaks is shown in Table 3.5 with their experimental m/z in comparison with the values obtained by LDI-TOF technique.

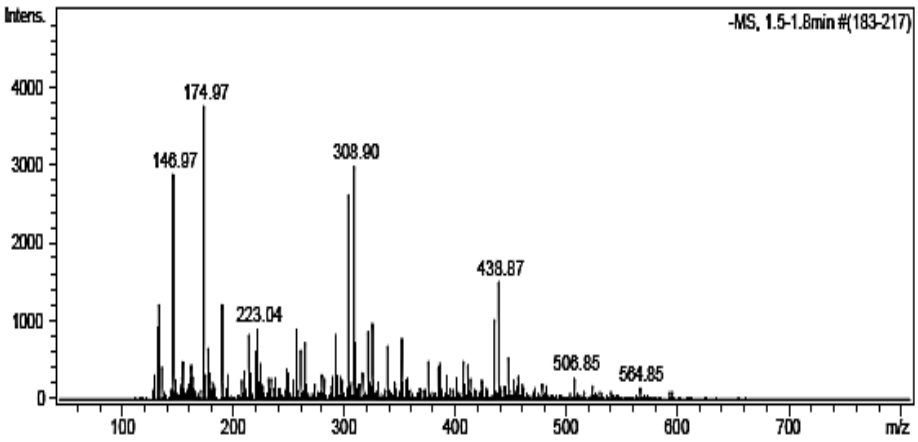

Figure 3. 13| *ESI-TOF spectrum of small CuCLs in aqueous solution in negative ion mode.*

Table 3. 5| *ESI-TOF results in negative ion mode compared with the identified clusters in LDI-TOF experiments.*

$CLUSTER_{ESI}$	m/z $_{ESI}$	m/z_{LDI}	$CLUSTER_{LDI}$
$[Cu_2(H_2O)]^-$	146.9684	125.8592	$[Cu_2]^-$
$[Cu_2N(OH)_2]^-$	**174.9673**	**160.1506**	**$[Cu_2(OH)_2]^-$**
$[Cu_{13}BuN(OH)_2]^{-4}$ $[Cu_{12}]^{-3}$	232.9385-931.754 254.9088-764.7264	929.4884 -	$[Cu_{13}BuNO_2]^-$ -
$[Cu_4]^-$	**265.1577**	**261.1897**	**$[Cu_4]^-$**
$[Cu_3BuN_2CO]^-$	308.9001	361.0189	$[Cu_3Bu_2N_2CO]^-$
$[Cu_{13}BuN(H_2O)]^{-3}$	**310.9113-932.7339**	**929.4865**	**$[Cu_{13}BuNO_2]^-$**
$[Cu_2Bu_4N_2CO_2]^-$	**434.8874**	**487.9121**	**$[Cu_2Bu_5N_2(OH)CO]^-$**
$[Cu_2Bu_5N_2(OH)_2CO]^-$	506.8545	556.9602	$[Cu_2Bu_6N_2(OH)_2CO]^-$
$[Cu_3Bu_6N(OH)_2]^-$	584.8534	598.8597	$[Cu_3Bu_6N_2(OH)_2]^-$

The comparison between both techniques led us to similar results obtaining mainly the presence of Cu_2, Cu_3 and Cu_{12} metal cores. Besides, these results agree nicely with the UV-Vis spectrum where the 257 and 275 nm bands were assigned to Cu_2 and Cu_3, respectively and with the PL results, which show by Jellium approach a Cu_{13} metal core.

MALDI-TOF experiments were also carried out by using DCTB (trans-2-[3-(4-tert-butylphenyl)-2-methyl-2-propenylidene] malononitrile) as a matrix. Results confirm the presence of small CuCLs (Annex C3).

(E) XPS analysis:

XPS analysis was carried out to investigate the oxidation state of Cu in the samples. Cu atoms at zero oxidation state can be distinguished from copper at higher oxidation states from the XPS spectrum by a shift in the Cu $2p_{3/2}$ core level peak to higher binding energies (BEs). Besides, when the oxidation state increases the appearance of characteristic shake-up satellite peaks around ~945 and ~965 eV for the Cu $2p_{3/2}$ and Cu $2p_{1/2}$ core levels are visible. However, great care has to be taken when we speak about clusters. Shift to higher binding energies is observed when the particle size becomes smaller; this behavior has been reported for different metals, such as Au[17], Pd[18] , Ni[19] and Cu[20]. The explanation for this effect is attributed to the "final state effect"[21] where the photocreated hole left behind the cluster lowers the kinetic energy of the outgoing photoelectron through the Coulomb attractive force. Ferreti et al.[22] have studied size selected copper clusters sputtered on a silicon surface by XPS observing the same effect. They pointed out three main characteristics on the XPS results with size decrease: (1) BE red shift, (2) Identical bulk spin-orbit coupling and (3) Enlargement of BE width band. Their results show the same bulk spin-orbit coupling (19.9eV) for all the studied clusters and the full width at half-maximum (FWHM) increase (respect to the bulk copper) due to a reduced screening of the core hole. [23] Moreover, it has to be pointed out that, in clusters, atoms can have different oxidation states depending on their position, Akola et al.[24] reported that, in thiolate-protected Au_{25} clusters, Au atoms can be in two oxidation states: Au (0) for the core atoms and close to Au (I) for outmost atoms complexed with the capping molecules. XPS survey spectra of the CuCLs/H_2O is showed in the Figure 3.14.A, as expected, the sample was composed mainly of C, O, N and Cu. Figure 3.14.B shows the Cu2p BE range for CuCLs/EtOH and in H_2O. The obtained Cu$2p_{3/2}$ binding energies (BE) values were 933.37, 933.51 for CuCLs in H_2O and in EtOH respectively. The lack of the characteristic shake-up satellite peaks around ≈ 945 eV for Cu (II) ions suggests that the clusters were not oxidized. Identical bulk spin-orbit (Cu$2p_{3/2}$ and Cu$2p_{1/2}$ BE difference = 19.9 eV) was found for the both samples like those studied by Ferreti.[22] It has to be pointed out that the obtained BE values are slightly higher than that corresponding to Cu_{bulk} (932.2-932.5 eV), which can be explained by the BE increase in metal clusters with decreasing cluster size. Besides, the Auger parameter (the sum of the binding energy of a particular core level peak and the kinetic energy of the corresponding Auger transition) was calculated by recording the Cu $L_3M_{4,5}M_{4,5}$ Auger spectrum. The KE_{bulk} =918.5 eV and our experimental result for CuCLs/H_2O was 917.38 eV, which is consistent with the results obtained by Ferreti[22] , where all the measured clusters show an Auger energy clearly shifted to smaller kinetic energies by more than 1 eV with respect to the

bulk. It has to be said that sometimes a small shakeup (associated to Cu (II)) is present on the sample. A RX irradiation during the time demonstrated the stability of the sample, but, after Ar^+ ion sputtering, removing of the Cu (II) was evident by the absence of the shakeup satellite peak.

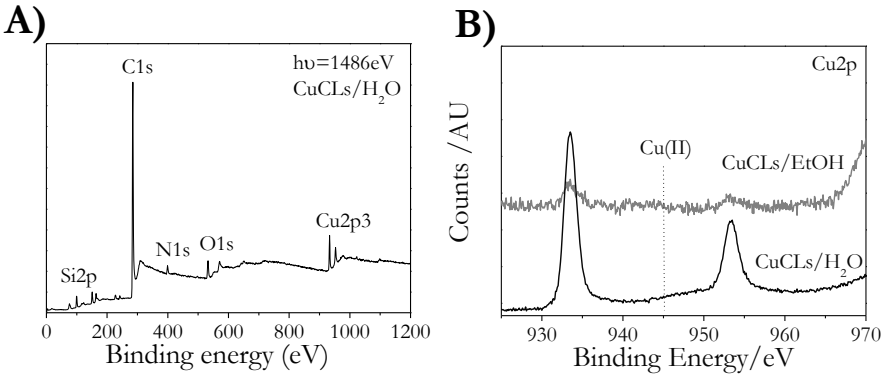

Figure 3.14| *XPS survey plot of CuCLs in water deposited onto Si acquired with a photon energy of 1486 eV (A). Cu $2p_{3/2}$ and Cu$2p_{1/2}$ peaks of CuCLs/H_2O (Cu_{13}) and CuCLs/EtOH (Cu_5) onto Si (B).*

(F) Cyclic Voltammetry study.

The electrochemical behavior of copper is of considerable interest in many areas of technology. The general features of a voltammogram on a 0.1M KOH solution reported on the anodic scan a small peak at -0.36V (Cu→Cu(OH)) followed by a larger peak at -0.05V which corresponds to the formation of a multilayer film of Cu^{+2} oxide and hydroxide . On the cathodic scan, a small cathodic peak was observed at -0.48V which can be attributed to the reduction of the Cu_2O to the metal Cu and the main reduction peak at -0.82V was associated with the reduction of $Cu(OH)_2$ to Cu_2O[25]. Thus, the absence of copper ions red-ox stability of the CuCLs were determined (study conditions were explained on Chapter 2). High stability of the clusters was obtained between 0.5 and -1.5 V due their large band gap.

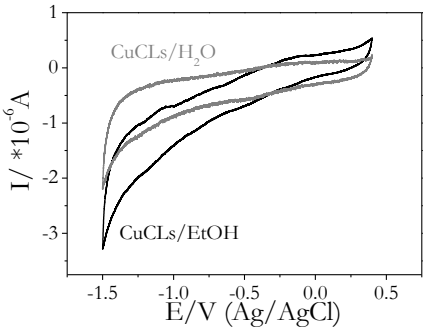

Figure 3. 15| *Cyclic voltammetry of CuCLs/EtOH (Cu_5) (black line) and CuCLs/H_2O (Cu_{13}) (gray line) in 0.1M KOH. Scan rate 10mV/s.*

3.3.5. Stability of CuCLs.

Fluorescence stability of metal clusters is an issue that should be explored for future applications. Shifts on the emission wavelengths can be associated to an oxidation process or aggregation of the clusters. Fluorescence of the as-synthesized CuCLs was therefore studied. The CuCLs were found to be very stable, showing the same emission spectra after even one year of being stored at room temperature and also at 4ºC (Figure 3.16). The emission peak remained unchanged at 300 nm and 408 nm for CuCLs in EtOH and in H_2O respectively.

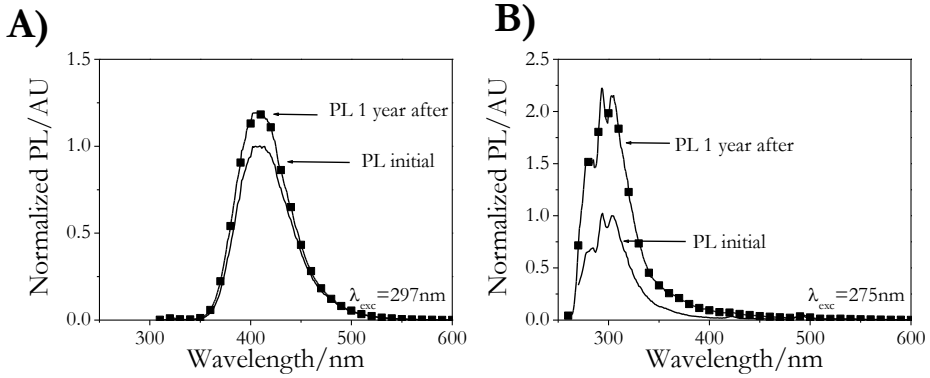

Figure 3.16| *PL spectra of CuCLs/EtOH (A) and CuCLs/H_2O (B) one year after the synthesis indicating the high stability of clusters.*

3.4. SUMMARY.

A direct one-step and environmentally friendly synthesis method was developed to produce fluorescent aqueous-soluble small copper clusters at 25ºC.

Size and therefore photoluminescent properties of copper clusters can be optimized by adjusting the purification method.

Different characterization techniques establish the small size of the copper clusters (Cu_NCLs, N<13 atoms).

Stability over the time was studied observing no photoluminescence changes for CuCLs solutions stored at 4ºC and also at room Tª.

REFERENCES.

[1] a) Adhikari B.; Banerjee A. *Chem. Mater. 22,* 4364 **(2010).** b) Shang L.; Dong S. *Chem. Commun. 9,* 1088 **(2008).** c) Zheng J.; Nicovich P. R.; Dickson R.M. *Annu Rev Phys Chem. 58,* 409 **(2007).** d) Rao T. U. B.; Pradeep T. *Angew. Chem. 122,* 4017 **(2010).**

[2] Rodríguez-Sánchez, L. PhD Dissertation: *"Electrochemical synthesis of Ag and Co nanoparticles. Kinetics formation and physicochemical properties"*. University of Santiago de Compostela **(2003).**

[3] Lisiecki I.; Pileni M. B. *J. Am. Chem. Soc. 115*, 3887 **(1993).**

[4] Zhao M.; Sun L.; Crooks R.M. *J. Am. Chem. Soc. 120*, 4877 **(1998).**

[5] OzinG.A.; Mitchell S.A.; McIntosh D.F.; Mattar S. *J. Phys. Chem. 87*, 4651 **(1983).**

[6] De Waele V.; Kecht J.; Tahri Z.; Mostafavi M.; Bein T.; Mintova S. *Sensors and Actuators B 126,* 338 **(2007).**

[7] Vázquez-Vázquez C.; Bañobre-López M.; Mitra A.; López-Quintela M.A.; Rivas J. *Langmuir 25,* 8208 **(2009).**

[8] a) Khatouri J.; Mostafavi M.; Amblard J.; Belloni *J. Chem. Phys. Lett. 191*, 351 **(1992).** b) Ershov B. G.; Janata E.; Michaelis M.; Henglein A. *J. Phys. Chem. 95,* 8996 **(1991).**

[9] de Heer W.A. *Rev. Mod. Phys. 65,* 611 **(1993).**

[10] Goswami N., Giri A., Bootharaju M.S., Xavier P.L., Pradeep T., Pal S.K. *Anal. Chem. 83,* 9676 **(2011).**

[11] Wei W. T., Lu Y. Z., Chen W. , Chen S. W., *J. Am. Chem. Soc. 133,* 2060 **(2011).**

[12] Ghijsen J.; Tjeng L.H.; van Elp J.; Eskes H.; Westerink J.; Sawatzky G.A.; Czyzyk M.T. *Phys Rev B 38*, 11322 **(1988).**

[13] a) Zhang X.; Zhang D.; Ni X.; Zheng H. *Solid-State Electronics 52,* 245 **(2008).**b) Singh D. P.; Neti N. R.; Sinha A.S.K.; Srivastava O.N. *J. Phys. Chem. C 111,* 1638 **(2007).** c) Ng C.H.B.; Fan W.Y. *J. Phys Chem B 110,* 20801 **(2006).**

[14] Muhammed M.A.H.; Pradeep T. *Chem. Phys. Lett. 449,* 186 **(2007).**

[15] Shibu E.S.; Muhammed M.A.H.; Tsukuda T.; Pradeep T. *J Phys Chem C 112,* 12168 **(2008).**

[16] a) Kabir M.; Mookerjee A.; Bhattacharya A.K. *Eur. Phys. J. D 31,* 477 **(2004).** b) Poater A.; Duran M.; Jaque P.; Toro-Labbe A.; Sola M. *J. Phys. Chem. B 110,* 6526 **(2006).**

[17] a) DiCenzo S.B.; Berry S.D.; Hartford E.H. Jr. *Phys. Rev. B 38,* 8465 **(1988).**

[18] Wertheim G.K.; DiCenzo S.B.; Buchanan D.N.E. *Phys Rev B 33*, 5384 **(1986).** b) Kaden W. E.; Wu T.; Kunkel W. A.; Anderson S.L. *Science 326,* 826 **(2009).**

[19] Pan J.S.; Tao J.G.; Huan C.H.A.; Zhang Z.; Chai J.W.; Wanga S.J. *Applied Surface Science 256,* 1088 **(2009).**

[20] a) Shin D.-W.; Dong C.; Mattesini M.; Augustsson A.; Mao S.; Chang C.L.; Persson C.; Ahuja R.; Nordgren J.; Wang S.X.; Guo J.-H. *Chem. Phys. Lett. 422,* 543 **(2006).** b) Shin D.-W.; Wang S.X.; Marshall A.F.; Kimura W.; Dong C.; Augustsson A.; Guo J. *Thin Solid Films 473,* 267 **(2005).**

[21] a) Zhang P.; Sham T. K. *Phys. Rev. Lett. 90*, 245502 **(2003).** (b) Moriarty P. Comment on "X-Ray Studies of the Structure and Electronic Behavior of Alkanethiolate-Capped Gold Nanoparticles: The Interplay of Size and Surface Effects. *Phys. Rev. Lett. 92*, 109601 **(2004).** (c) Zhang P.; Sham T. K.; Zhang and Sham Reply, *Phys. Rev. Lett. 92*, 109602 **(2004).**

[22] Nicoletta Ferreti PhD Dissertation: *"X-ray photoelectron spectroscopy of size selected copper clusters on silicon"*. Technische Universität Berlin, **(2009).**

[23] Jirka I. *Surf. Sci. 232*, 307 **(1990).**

[24] Akola J.; Walter M.; Whetten R.L.; Häkkinen H.; Grönbeck H. *J. Am. Chem. Soc. 130,* 3756 **(2008).**

[25] a) Ambrose J.; Barradas R.G.; Shoesmith D.W. *J. Electroanal. Chem. 47,* 47, **(1973).** b) de Chialvo M.R.G.; Salvarezza R.C.; Vasquez D.; Arvia A.J. *Electrochim. Acta 30,* 1501 (**1985).** c) Sander U.; Strehblow H.H.; Dohrmann J.K. *J. Phys. Chem. 85,* 447**(1981).**

CHAPTER 4.

Thermal Growth of Small Copper Clusters

4.1. INTRODUCTION.

Fluorescent metal clusters show great promise for biological imaging, sensing and photocatalytic applications. A wide palette of band gaps and therefore photoluminescent properties are desirable, which makes necessary the cluster size increase. Therefore, the synthesis control over the cluster size results in a big challenge in their future applications as well as the possibility of studying the evolution of their inherent properties with the size. As we explained on Chapter 1 advances on the Cu (0) clusters synthesis have been lately developed, but their size is smaller than 14 atoms. Consequently, the main purpose in this Chapter will be the obtaining and characterization of larger Cu (0) clusters. The strategy here proposed consists of a thermal control growth of the smaller clusters. Thermal treatments in solution of 2nm gold nanoparticles (AuNPs) stabilized with DDT (dodecanethiol) were studied by Zhong et al,[1] obtaining a size evolution until 5-6 nm diameter AuNPs. Also studies of solid AuNPs - DDT were developed by Teranishi et al.[2] and solid CuNPs by Dong et al.[3] The increasement of the clusters size by temperature annealing and therefore shifting their emission wavelength into the Vis region was developed by Chun-Sung et al.[4] They showed a clear PL shift in their Si clusters (emission wavelength 365nm) with 162ºC annealing obtaineing emissions at 420 nm, and finally higher temperatures led to Si nanoparticles with no PL properties. Thermal growth methods depend basically on the interaction between the *capping agent* (here tetrabutylammonium nitrate $TBANO_3$) and the metal core. This interaction will be crucial on the desorption, coalescence and aggregation process during the temperature treatment, which will determine the growth or ripening process. Four main growth steps can are assumed on this thermal evolution (Scheme 4.1): (1) Desorption of the tetralkyl ammonium salts from the metal core of small Cu(0) CLs. (2) Approximation of metal cores by attractive forces. (3) Coalescence of the metal cores. (4) Reorganization of the larger clusters. As it is illustrated in the Scheme 4.1, the basic concept of our thermal strategy was to explore the viability of a thermally activated coalescence of the small clusters toward the formation of larger clusters by the mechanism:

$$\mathbf{Cu_x^{a+} + Cu_y^{b-} \rightarrow Cu_{x+y}^{(a-b)+}}$$

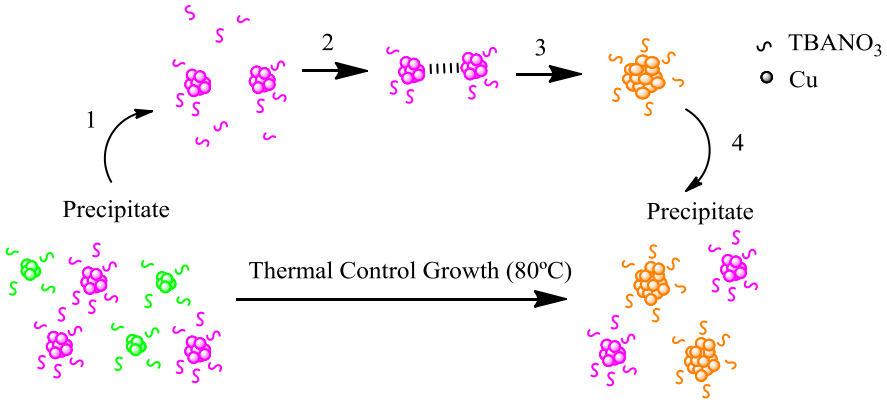

Scheme 4. 1| *Evolution of small* ***Cu(0)*** *clusters into larger CuCLs with thermal control growth.*

4.2. EXPERIMENTAL SECTION.

Small purified CuCLs (Cu_N, N≤13) in powder form were subjected to a thermal growth. 1mg of these CuCLs were dried at 80ºC (T^a < 100ºC, water boiling point, and also T^a<117ºC, $TBANO_3$ melting point) for 1 hour. A slight increase in temperature could also have a significant impact on the capping agent also. Therefore, thermal growth of the clusters must be performed with a temperature<temperature melting of the tetrabutylammonium salt. Then, 10 mL of acetonitrile (MeCN) was added and the mixture was vigorously stirring for three hours at ambient temperature to allow the clusters to redispersion. During the stirring process, the solvent changed from colorless to light yellow and finally to a light brown color. The product was then characterized by different techniques: MALDI MS, ESI MS, AFM, TEM, XPS, UV-Vis and fluorescence spectroscopy.

High-performance liquid chromatography (HPLC) was used as a purification process in order to separate the different clusters sizes. The HPLC chromatographs employed was Waters 600 controller pump capable of gradient elution and equipped with a Waters 2998 PDA detection system and multi-λ Waters 2475 fluorescence. Analytical (4.6x150 mm) and preparative columns (21.2x250 mm) were both C18 columns (octadecyl carbon chain).The mobile phase consisted of acetonitrile: water (65:35) mixtures. The analytical and preparative total flow rate, 1 mL/min and 20mL/min, respectively with injection total volumes of 10 and 190 μL. Fractions for fluorescence analysis were collected over the time intervals on the specific peaks of the chromatogram.

.

4.3. RESULTS AND DISCUSSION.

4.3.1. Optical characterization and band gap determination of large CuCLs.

The kinetic assembly of Cu (0) clusters by thermal control growth were governed by the changes on the electrostatic Van der Walls forces and steric interactions. This solvent effect restricted growth (size control) and temperature, has also been demonstrated in recent works on Ag_7 clusters[5] and on Au_{25} clusters. CuCLs exhibit a well-defined optical absorption spectrum with bands located 5.02eV (247nm) and 4.41eV (281nm) (Figure 4.1.A) commun for smaller clusters (Chapter 3) and a prominent peak at 2.89eV (428nm). UV-Vis absorption spectrum of small CuCLs in MeCN (E39, Chapter 3) is displayed as comparison. The red shift on the absorption band was not observed for the E39 sample (CuCLs in MeCN). Therefore, the new absorption band located at 428 nm was consistent with the expected size increase and not due to a solvathocromic effect. A similar absorption band (≈480nm) was mainly attributed by Ketch et al.[6] to the aggregation/coalescence processes of smaller copper clusters.

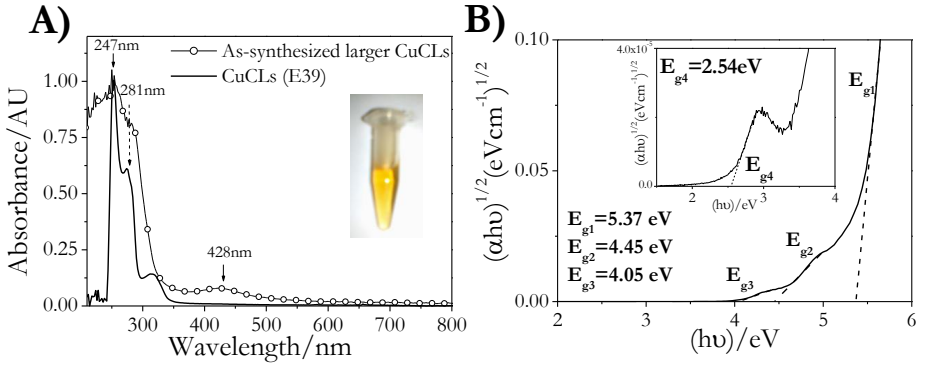

Figure 4. 1| *UV-Vis absorption spectrum of as-synthesized larger CuCLs (hollow circles) compared with CuCLs E39 (black line) in MeCN. Inset: Photograph of larger CuCls under daylight (A). Taut plot for a direct band gap fitting (2.54eV ≤ E_g≤5.37 eV) (B).*

The E_{gap} estimated from the Tauc approach (direct transition) gave us different values from 2.54 to 5.37eV (Figure 4.1.B). The excitation and emission spectra of the sample are shown in Figure 4.2.A-B. Strong emission was observed around 2.55eV (485nm) with excitation maxima at 3.26eV (380nm). The clusters also

exhibit strong emission at low wavelengths 3.23 eV (384nm) corresponding to the small CuCLs fraction still present on the sample. The obtained band gap values by fluorescence and Tauc approach agree. Figure 4.2.A shows the emission spectra of the CuCLs at different excitation wavelengths (297 nm ≤ λ_{exc}≤ 450 nm). Three different emission bands were found at 381, 401 and 480 nm. Emission at 475 nm was also observed by Kawasaki et al[7] in Cu nanocrystals with an average size of 2.3 nm.

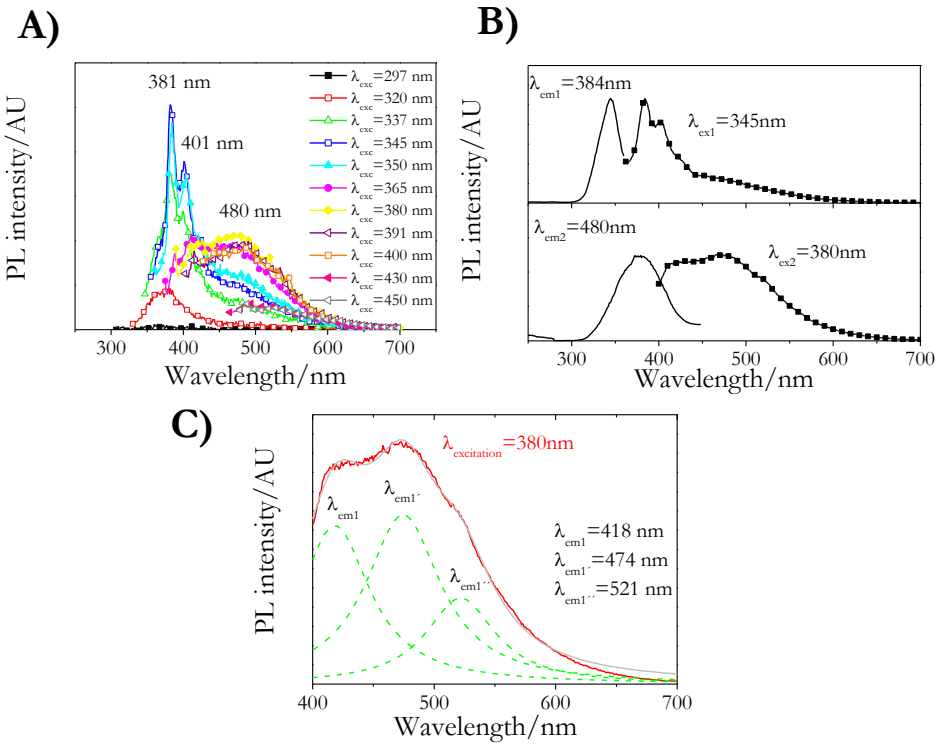

Figure 4. 2| *Photoluminescence spectrum of CuCLs exciting from 297 to 450 nm (A). Maximum excitation and emission spectrum of CuCLs: Top: λ_{exc}=345nm, λ_{emi}=384nm. Bottom: λ_{exc}=380nm, λ_{emi}=480nm (B). Lorentzian fitting of emission spectra of CuCLs. Green lines are the individual contributions, red and gray lines are the experimental data and the sum of the contributions respectively (C).*

Using the Jellium model three different sized CuCLs can be obtained, corresponding Cu_{10} to 381 nm, Cu_{11} to 401 nm and Cu_{20} to 480 nm. Figure 4.2.B displays the maximum excitation and emission spectra for the CuCLs. A large broadening emission was observed at 480 nm FMHW=151 nm, compared with

the emission at 401 nm (FMHW=42 nm). This broad emission can be fitted nicely by three Lorentzians functions (Figure 4.2.C). Fitted parameters are summarized on Table 4.1.

Table 4. 1| *Fitted parameters of the λ_{emi} =480 nm using three Lorentzians functions.*

	Central Wavelength/nm	Bandwidth/nm	Relative Heigth	Cu_N (Jellium model)
λ_{em1}	418.16	69.52	81.49	Cu_{13}
$\lambda_{em1'}$	474.63	76.59	89.74	Cu_{19}
$\lambda_{em1''}$	522.26	68.23	43.27	Cu_{25}

Therefore, the emission at 480 nm could be ascribed to the presence of differently sized fluorescent clusters (Cu_{13}+Cu_{19}+Cu_{25}, calculed by the Jellium model after the Lorentzian fitting) which can combine their emission bands to create the broadened fluorescence spectrum. Another explanation could be a vibrational coupling: when the system returns from the lowest vibrational level in the excited state to different vibrational levels in the ground state or transitions from higher excited states to the ground state could give the different bands. This would imply that emission from these states takes place before relaxation to lower excited states. Therefore, the objective will be differentiate the possibility of polydispersity on the CuCLs sample or monodisperse solution of only one cluster size with different excited to ground state transitions. Confirmation of the presence of various sized clusters would come from mass spectrometric studies and AFM measurements.

4.3.2. TEM and NC-AFM measurements.

Transmission electron microscopy (TEM) image (Figure 4.3.A) shows CuCLs forming aggregates (black dashed circle). Due to the poor resolution of the TEM images, NC-AFM technique was also used. The calculated average size was (0.98±0.41 nm). This value is slightly higher than those acquired for small CuCLs (Chapter 3), therefore, this indicated us the presence of larger copper clusters formed by more than one shell (Cu_{13} closed-shell icosahedra is 0.77 nm).

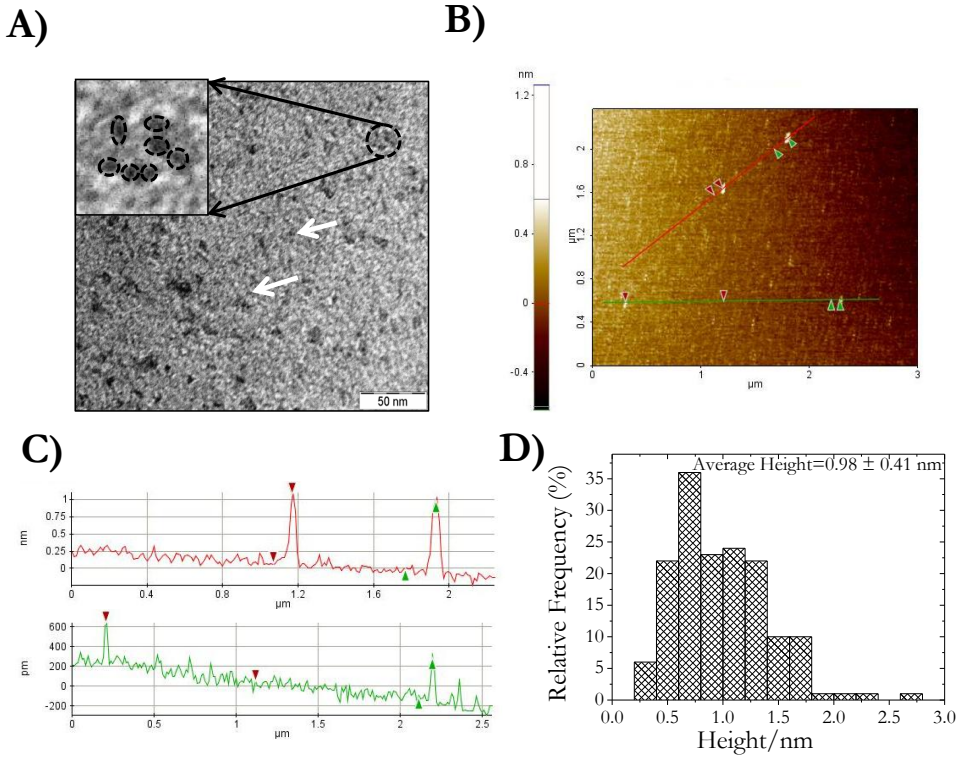

Figure 4. 3| *TEM image of CuCLs. Some of the clusters aggregates are marked with arrows. Inset: an aggregate magnification (A). AFM topography image of CuCLs deposited on mica substrate (rms ≈150 pm) (B). Section analysis of the solid lines is given on (C) and the corresponding histogram distribution height (D).*

4.3.3. Mass spectrometry study.

Different mass spectrometric techniques such as LDI-TOF (Figure 4.4), MALDI-TOF (Figure 4.5) and ESI-TOF (Figure 4.6) were acquired in order to study the cluster size. Besides, the laser fluence dependence study was study in order to determine their influence on the fragmentation (Figure 4.4.A from [1] to [4] increase). It was checked that isotopic Cu distribution is more easily obtained at high laser fluence intensities.

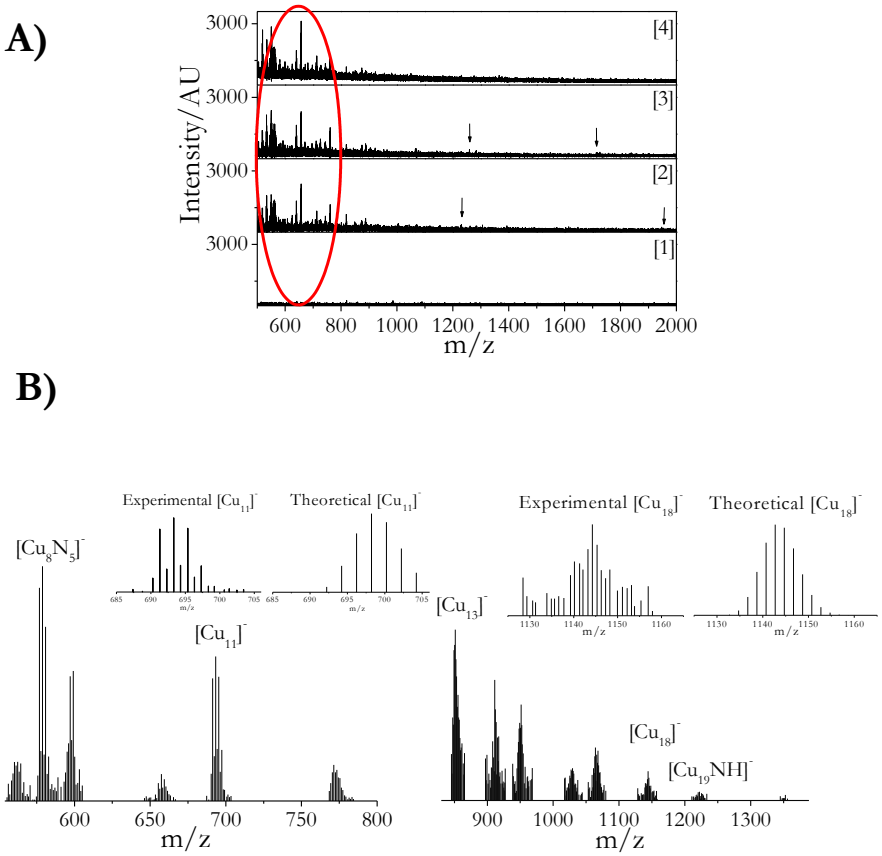

Figure 4. 4| *LDI mass spectra of CuCLs clusters at different laser intensities. The spectra indicate that the set of peaks from m/z 500 to 700 are fragments from larger clusters under high laser intensities (A). LDI-TOF in negative ion mode of CuCLs. Experimental and theoretical isotopic patters of one assigned clusters is showed as an example. Not assigned peaks correspond to fragments (B).*

However, increasing the laser fluence undesired fragmentation peaks appeared at low m/z range (red circle), meanwhile peaks at higher m/z values disappeared (marked with arrows). This behavior complicates the determination of the cluster formula. In despite of this, LDI-TOF in negative mode was acquired; the two highest mass peaks, m/z ≈ 579.06 and 693.07 amu can be assigned to cluster with a composition of $[Cu_8N_5]^-$ and $[Cu_{11}]^-$. On the high mass range, larger CuCLs were obtained, being the higher obtained at m/z ≈1222.05 amu corresponding to $[Cu_{19}NH]^-$. Due to the fragmentation process, it could be

possible that the Cu_{19} center was cleaved in Cu_8+Cu_{11} metal cores. In order to avoid this effect, MALDI-TOF (HCCA (4-hydroxy-α-cyanocinnamic acid) as matrix) and ESI-TOF mass spectrometry techniques was used. Four main peaks were assigned to CuCLs by using MALDI-TOF (Figure 4.5), corresponding to $[Cu_5O_2]^-$, $[Cu_{10}N_2O]^-$, $[Cu_{11}N_4]^-$ and $[Cu_{16}CN]^-$. It can be clearly seen the lower fragmentation on the high m/z range (Figure 4.5). But, some additional fragment peaks remain on the low m/z range.

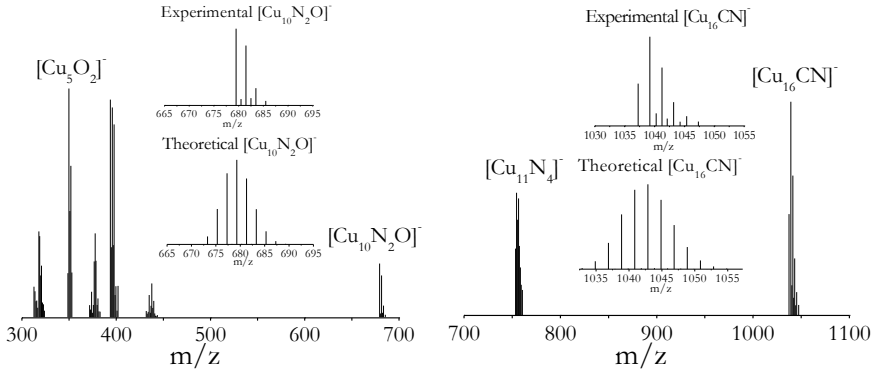

Figure 4. 5| *MALDI-TOF mass spectra in negative ion mode. Insets correspond to examples of theoretical and experimental assigned CuCLs.*

Figure 4.6 shows the ESI-TOF results with three intense peaks at m/z 365.41 amu, 670.03 amu and 1279.25 amu, corresponding to $[Cu_5O_3]^-$, $[Cu_{10}(OH)_2H]^-$ and $[Cu_{20}]^-$ clusters.

The agreement between the different techniques employed unequivocally confirmed the larger size of the clusters, as well as the presence of small clusters, allowing us to check the polidispersity of the sample and the origin of the different emissions. Detailed assignment with their theoretical and experimental m/z values and comparison between the three techniques are provided on Table 4.2.

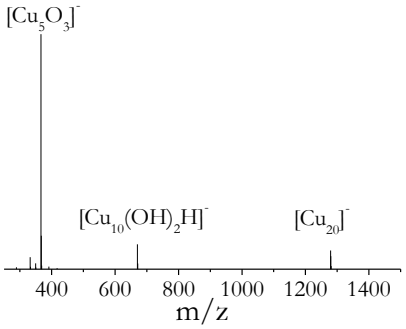

Figure 4. 6| *ESI-TOF mass spectrum (negative ion mode) of the CuCLs.*

Table 4. 2| *Assignments of the clusters in the negative mode corresponding to LDI-TOF, MALDI-TOF and ESI –TOF spectra.*

LDI-TOF			**MALDI-TOF**			**ESI-TOF**		
m/z_{exp}	m/z_{theo}	*Cluster*	m/z_{exp}	m/z_{theo}	*Cluster*	m/z_{exp}	m/z_{theo}	*Cluster*
			349.34	349.73	$[Cu_5O_2]^-$	365.41	365.74	$[Cu_5O_3]^-$
579.06	578.40	$[Cu_8N_5]^-$						
693.07	699.01	$[Cu_{11}]^-$	679.22	679.48	$[Cu_{10}N_2O]^-$	670.03	670.49	$[Cu_{10}(OH)_2H]^-$
			754.71	755.03	$[Cu_{11}N_4]^-$			
			1040.01	1041.07	$[Cu_{16}CN]^-$			
1143.75	1143.83	$[Cu_{18}]^-$						
1222.05	1222.39	$[Cu_{19}NH]^-$				1279.25	1270.92	$[Cu_{20}]^-$

4.3.4. XPS results.

XPS measurements were carried out in order to check the oxidation state of Cu in these CuCLs. Results (Figure 4.7) show a smaller shift of the $Cu2p_{3/2}$ peaks BE than the smaller CuCLs, which is consistent with the size increase of the sample.[8] Identical bulk spin–orbit coupling (19.9 eV) was found showing the presence of Cu (0).

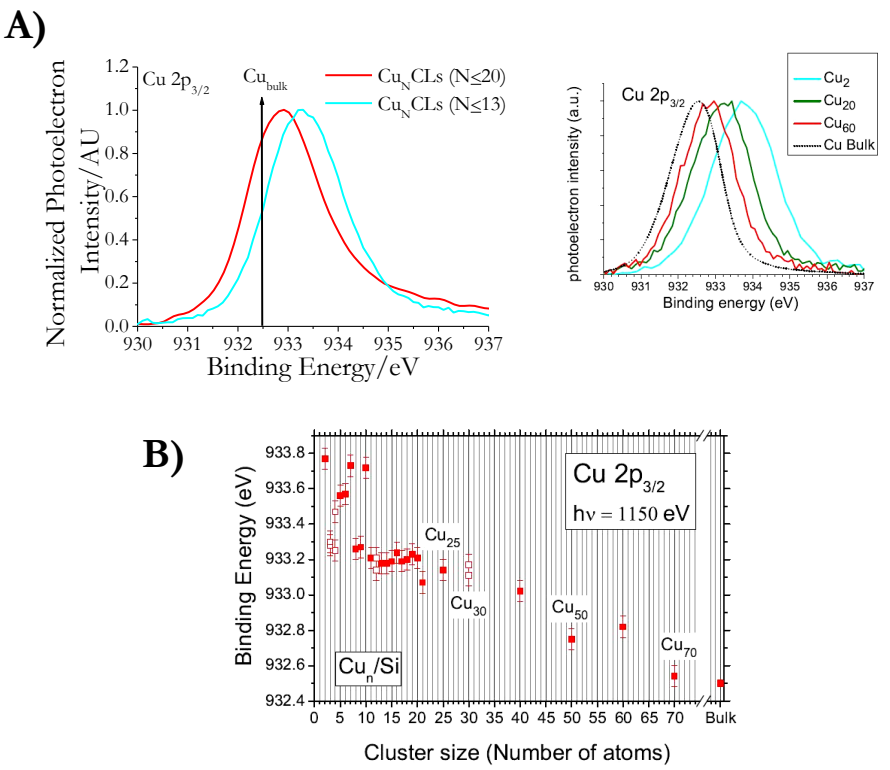

Figure 4. 7| *Cu 2p3/2 peak of small CuCLs (cyan line) and large CuCLs (red line).Arrow shows the BE value of bulk copper. Inset: Some BE,s of mass selected deposited CuCLs. A blue shift with respect to the bulk peak is observed for all clusters. (Image taken from reference 8) (A). Cu 2p3/2 BE' s as function of cluster size. A general trend with increasing cluster size is obvious. (Image taken from reference [8]) (B).*

As it can be seen on Figure 4.7.A the copper clusters here synthesized show a similar binding energy (BE) shift throught smaller values that those observed by

Ferreti (Inset Figure 4.7.A). Figure 4.7.B shows the general trend found by Ferreti for the BE with the cluster size. It has to be said that for smaller clusters of Cu_N ($N \leq 10$) the values change without a clear tendency. But from 10 to more than 70 atoms the trend is clear observing the approaching to the bulk value when the cluster size increase.

4.3.5. Stability of large clusters.

Stability of the as-synthesized larger clusters in aquous solutions and throughout the time have been studied. Aqueous solubilization of larger copper clusters is desirable for suitable in biological applications. Direct redispersion in water was unsuccesful and no emission was found, which indicates their instability in aqueous solutions. Hence, another aqueous solubilization method was tried, named "caustic extraction". Due to the miscible character of water and acetonitrile, phase transfer is not possible. However, the used process consisted of a direct staged contact between the MeCN phase and a concentrated caustic solution. Smiley[9] discovered that by adding NaOH or KOH concentrated solutions (50% weight of hydroxide aqueous solution) to an acetonitrile solution in the range 1:1 to 1:10 volume, two inmiscible phases are formed. By stirring this two phase system acetonitrile can be purified removing the H_2O and HCN impurities present on the MeCN. If we assume that larger CuCLs in MeCN can be surrounded by CN^- groups, when this purification is carried out, the clusters will go to the aqueous phase. Briefly, 2mL of CuCLs were added to a mixture in volume 2:1 (NaOH: MeCN). Initially, CuCLs remained in the interphase observed by a yellow colour. Vigorous stirring was maintained for 72 hours. The PL intensity at 480 nm on the aqueous phase CuCLs increased with time. After 1 hour stirring the most emissive specie was found to be Cu_7. After 20 hours Cu_{19} emission (477nm) appears (Figure 4.8.A). Time stability of CuCLs transferred to water was studied (Figure 4.8.B). No changes on the emission band were observed after one year. This fact point out the great stability of these clusters even in an aqueous media at room temperature.

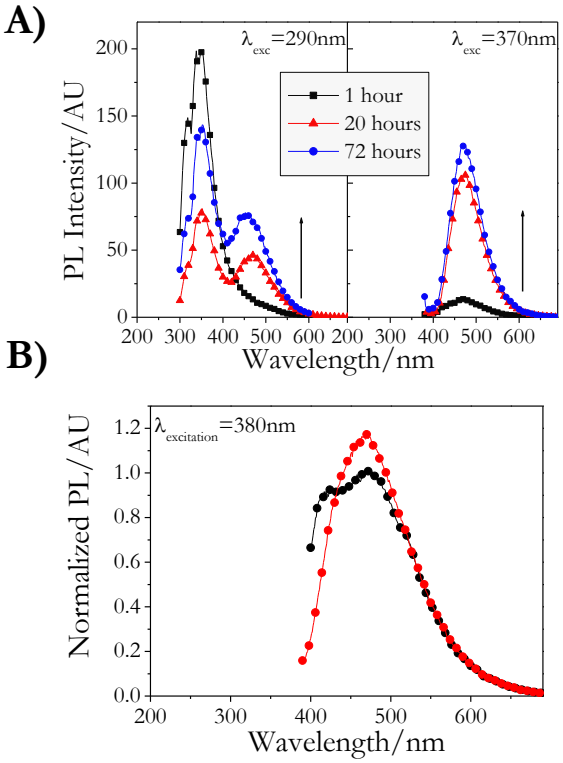

Figure 4. 8| *Emission spectra during the time of the aquous phase obtained by "caustic extraction" (A). Time stability emission spectra of* Cu_{19} clusters. *Black circles correspond to emission after synthesis and red circles to emission after 1 year (B).*

4.3.6. HPLC separation of large CuCLs.

The size-selective separation of polydisperse solutions of metal clusters has relevance in order to obtain monodisperse solutions required for applications such as catalysis or sensoring. It has been shown that monodisperse clusters can be obtained by different separation processes, such as fractionated precipitation,[10]size exclusion column chromatography (SEC)[11], HPLC[12], sequential size-selective precipitation[13] and gel electrophoresis.[14]

For this reason, Rodriguez Cobo E. has carried out an HPLC separation of the large Cu clusters synthesized in this Chapter (under the conditions summarized on Experimental Section)[15] . The method optimization was developed with an analytical column and then the sample was studied using a preparative column. Figure 4.9 shows the obtained chromatogram with a dominant set of peaks starting at 2.18 min.

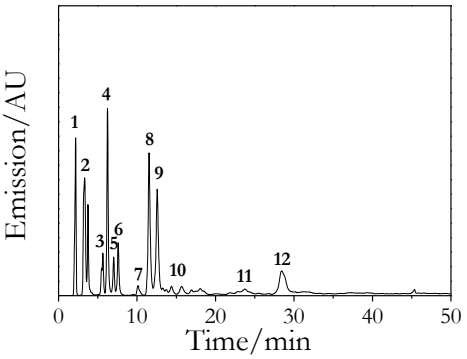

Figure 4. 9| *Chromatogram (emission detected at 296 nm y exciting at 270nm) of asprepared larger CuCLs. The mobile phase was 65:35 acetonitrile/water ratio at a flow rate of 20 mL/min, and the column was a preparative C18, isocratic separation. Different fractions were collected: 1=2.18 min, 2=3.31 min, 3=5.75 min, 4=6.25 min, 5= 7.02 min, 6=7.60 min, 7=10.10 min, 8=11.53 min, 9=12.57 min, 10=14.40 min, 11=15.81 min, 12=28.50 min.*

The "ideal" separation would be some order of cluster elution related to core cluster size. This question was studied by fluorescence spectroscopy of the different collected fractions (previously concentrated, Figure 4.10). It can be clearly seen that emissions at lower wavelengths (smaller clusters) (λ_{emi}=300 nm $\rightarrow Cu_5$ by Jellium) appear at the first collected fractions, from 1 to 7, mixture of smaller emissions (λ_{emi1}=300 nm+ λ_{emi2}=408 nm $\rightarrow Cu_5$ and Cu_{13} by Jellium) are observed from 8 to 10 fractions, and finally waste fraction spectra displays the emission at higher wavelengths, (λ_{emi}=460 nm$\rightarrow Cu_{18}$).

Fraction 1-7

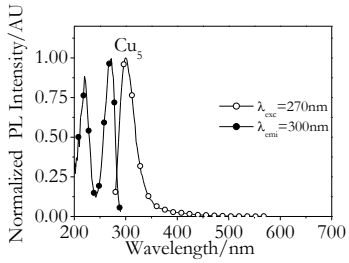

Fraction 8-12

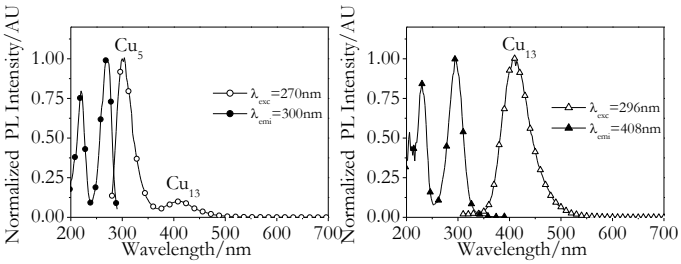

Waste

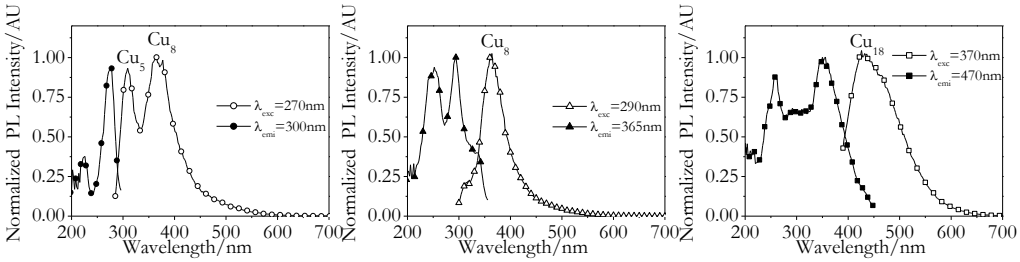

Figure 4. 10 | *Normalized PL spectra of the different obtained fractions and the waste after HPLC separation.*

The presence of larger clusters on the waste, can be explained by the detection PL method on the HPLC, the fixed excitation wavelength was not suitable for these clusters, and, therefore, they do not show any peak on the chromatogram. Additionally, this order of elution of the clusters is as if the

chromatographic separation behaved as a size exclusion process. In conclusion, PL results show that copper clusters differ in core size and can be separated. HPLC has to be regarded as an extremely promising tool to use with polydisperse samples of metal clusters, paying careful attention to the different factors that can have an influence in the elution order.

4.4. SUMMARY.

Thermal control growth of small copper clusters into larger clusters was successfully developed confirmed by the emission at higher wavelengths and the presence of different clusters sizes by mass spectrometric studies.

The "Caustic extraction" method was satisfactory in order to obtain the as-synthesized large CuCLs in aqueous medium.

Large CuCLs displayed high photoluminescence stability during one year stored at ambient temperature.

The polydisperse large CuCLs sample can be separated into different monodisperse fractions using the HPLC technique.

REFERENCES.

[1] Zhong C.J.; Zhang W.X.; Leibowitz F.L.; Eichelberger H.H. *Chem. Commun. 13*, 1211 **(1999).**

[2] Teranishi T.; Hasegawa S.; Shimizu T.; Miyake M. *Adv. Mater. 13*, 1699 **(2001).**

[3] Dong T.Y.; Wu H.-H.; Lin M.-Ch. *Langmuir 22,* 6754 **(2006).**

[4] Chun-Sung Y.; Kauzlarich S.M.; Wang Y.C.; Lee H.D.W.H. *J. Clu. Sci. 11,* 423 **(2000).**

[5] a) Wu Z.; Lanni E.; Chen W.; Bier M. E.; Ly D.; Jin R. *J. Am. Chem. Soc. 131*, 16672 **(2009).** b) Wu Z.; Jiang D.; Lanni E.; Bier M. E.; Jin R. *J. Phys. Chem. Lett. 1*, 1423 **(2010).**

[6] Ketch J.; Tahri Z.; De Waele V.; Mostafavi M.; Mintova S.; BeinT. *Chem. Mater. 18*, 3373 **(2006).**

[7] Kawasaki H.; Kosaka Y.; Myoujin Y.; Narushima T.; Yonezawa T.; Arakawa R. *Chem Comm 47,* 7740 **(2011).**

[8] Nicoletta Ferreti PhD Dissertation "*X-ray photoelectron spectroscopy of size selected copper clusters on silicon"*. Technische Universität Berlin, (**2009**).

[9] Smiley R.A.; Wilmington, Del. United States Patent, **(1981).**

[10] a) Price R. C.; Whetten R. L. *J. Am. Chem. Soc. 127,* 13750 **(2005).** b) Whetten R. L.; Khoury J. T.; Alvarez M. M.; Murthy S.; Vezmar I.; Wang Z. L.; Stephens P. W.; Cleveland C. L.; Luedtke W. D.; Landmann U. *Adv. Mater. 8,* 428 **(1996).**

[11] (a) Siebrands T.; Giersig M.; Mulvaney P.; Fischer C.-H. *Langmuir 9,* 2297 **(1993).** (b) Wilcoxon J. P.; Martin J. E.; Provencio P. *Langmuir 16,* 9912 **(2000).**

[12] (a) Jimenez V. L.; Leopold M. C.; Mazzitelli C.; Jorgenson J. W.; Murray R. W. *Anal. Chem. 75,* 199 **(2003).** (b) Song Y.; Jimenez V.; McKinney C.; Donckers R.; Murray R. W. *Anal. Chem. 75,* 5088 **(2003).** (c) Choi M. M. F.; Douglas A. D.; Murray R. W. *Anal. Chem. 78*, 2779 **(2006).** (d) Zhang Y.; Shuang S.; Dong C.; Lo C. K.; Paau M. C.; Choi M. M. F. *Anal. Chem. 81,* 1676 **(2009).**

[13] Yang X.; Su Y.; Paau M.Ch.; Choi M.M.F. *Anal. Chem. 84,* 1765 **(2012).**

[14] a) Schaaff T. G.; Knight G.; Shafigullin M. N.; Borkman R. F.; Whetten R. L. *J. Phys. Chem. B 102,* 10643 **(1998).** b) Gautier C.; Bürgi T. *J. Am. Chem. Soc. 133,* 11079 **(2006).**

[15] Rodríguez-Cobo E., PhD Dissertation:"*Synthesis, properties and functionalization of metal clusters"*. University of Santiago de Compostela. **(2012).**

CHAPTER 5.

Synthesis of Large Copper Clusters

5.1. INTRODUCTION.

In Chapter 4 we showed the thermal size growth of small CuCLs with their corresponding red PL shift. But the idea of a "**one step synthesis"** was the next goal. It is widely known by previous electrochemical studies that cluster size increase with the current density decreases.[1] We extended the electrochemical method to the synthesis of larger copper clusters. The effect of the current density and supporting electrolyte was studied. Large CuCLs with 25 atoms were obtained, which significantly improved their palette of applications. The large CuCLs were characterized by UV-Vis spectra, fluorescence spectroscopy, LDI-TOF, TEM and NC-AFM.

5.2. EXPERIMENTAL SECTION.

The electrochemical synthesis of large CuCLs has been carried out as it has been explained on the Chapter 2 (Experimental Details). The conditions are summarized in Table 5.1.

Table 5. 1| *Electrochemical synthesis conditions of larger CuCLs.*

Sample	ϱ/(mA/cm^2)	T^a/ºC	t/s	Solvent	Supporting electrolyte	Cathode	PL
E4	*5*	*25*	*800*	*MeCN*	*$TBANO_3$*	*Pt*	*YES*
E44	*5*	*25*	*800*	*MeCN*	*TBAAcO*	*Pt*	*YES*

5.3. RESULTS AND DISCUSSION.

5.3.1. Synthesis optimization.

Figure 5.1 shows the variation of the potential during the cluster. The potential becomes rapidily more negative attaining high overpotential values ≈ 1.06 V, very different to those achieved in Chapter 3 (≈0.2V). E39 potenciogram is shown as a comparison. After a certain time (≈40s) when it reaches a stationary state the potential remains approximately constant.

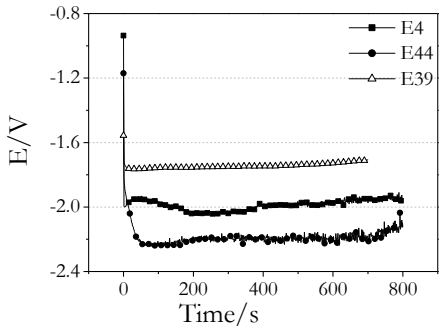

Figure 5. 1| *Change of the electrode potential during the cluster synthesis with different counterions. (Squares= NO_3^-) (Circles=AcO^-). E39 potenciogram is also showed as comparison (triangles).*

During the synthesis of Sample E4 a yellow precipitate was obtained while E44 has suffered a gradual color change, from colorless to olive green. The obtained precipitate in E4 was dried and redispersed in heptane. The UV-Vis spectra (Figure 5.2) of the E4 supernatant exhibited three absorbance bands at 244 nm (5.08eV), 275 nm (4.5 eV) and 300 nm (4.13 eV) (similar to small CuCLs, Chapter 3). The precipitate in heptane showed bands located at 226 nm (5.48 eV), 275 nm (4.5 eV) and a shoulder at 360 nm (3.44 eV). E44 absorbance peaks are located at 257nm (4.82eV), 292nm (4.24 eV), 345nm (3.59 eV) and a broad shoulder at 430nm (2.88eV). Both samples showed strong fluorescence. As we can see on Figure 5.2, emission of E4 supernatant appears at 350 and 420 nm, according to the Jellium model a mixture between Cu_7 and Cu_{13} will be present. The precipitate in pentane emits at 300 nm Cu_5 and E44 shows three emission bands at 360nm, 400nm and 520nm corresponding to $Cu_{8,}$ $Cu_{12\text{-}13}$ and Cu_{25}, by the Jellium model. Both syntheses show the presence of Cu_N clusters with 7-8≤N≤12-13. But only Cu_{25} core is obtained under the E44 conditions.

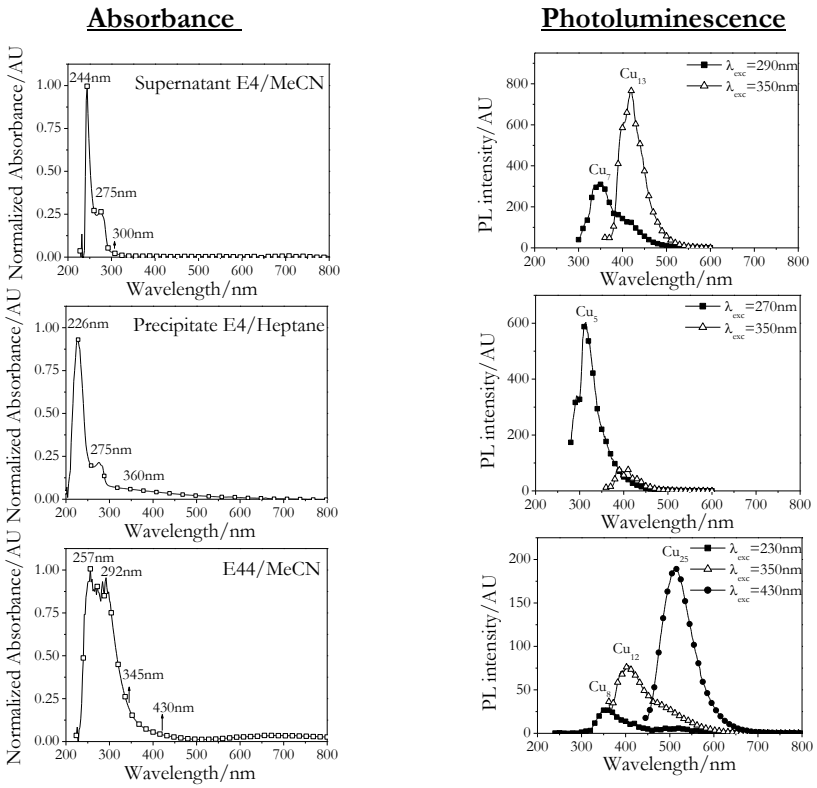

Figure 5. 2| *UV-Vis absorption and emission spectra of the different samples (E4 and E44) just after synthesis.*

A competition process can explain the synthesis of larger clusters. Our group[2] found that the reduction of the AcOTBA begins around -2.2 V, value that is achieved on the E44 sample. Therefore, the competition between the formation of small nuclei and the reduction of the counterion will happen at the same time giving less small Cu nuclei, and consequently a size increase of the initially formed clusters instead of the generation of smaller clusters. Thus, different characterization techniques would now be used in order to identify the Cu clusters present in the E44 sample.

5.3.2. Kinetic evolution during the synthesis.

The UV-Vis spectra evolution (Figure 5.3.A) displayed similar bands to small CuCLs located at ≈260 nm, ≈280 nm, ≈ 297 nm, ≈360 nm, but new bands appeared ≈314 nm and ≈ 650 nm, besides the change in their intensities. Different absorbance bands were fitted with Lorentzians functions and plotted versus the time (Figure 5.3.B). Herein, the most intense bands were 260 and 280 nm (assigned to a Cu_2 and Cu_3 cluster respectively) until the 300 s, but then the most intense was the absorption at 297 nm (related with a Cu_{13} cluster).

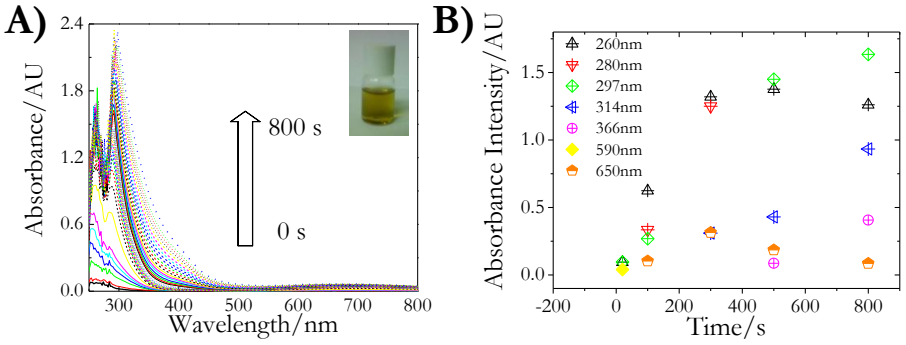

Figure 5. 3| *Absorbance versus time during the electrochemical synthesis of CuCLs. Time between successive spectra is ⊿t =20 s . Inset shows a photograph of the E44 sample.(A). Absorbance versus time for the peaks centered at 260, 280, 297, 314, 366, 590 and 650 nm (fitted by Loretzians) during the synthesis.*

The comparison between kinetic evolution on small and larger copper clusters synthesis reveals differences. As we have observed on Chapter 3, the most intense absorption bands were located at 257 and 275 nm, but now on larger CuCLs the most intense are located at 257 and 297 nm. Besides, the band at 360 nm increase the intensity and a new band appear from the intial stages of the synthesis at 650 nm. Therefore, it can be concluded the presence of Cu_{13} on this sample also (absorption at 297 nm emission at 408 nm), but the band edge located near the 430 nm can be the responsible of the emission at 520 nm corresponding to Cu_N with N>13.

5.3.3. Band gap determination.

Energy band gaps (E_g) of large CuCLs were calculated by using the Jellium model: 3.42, 3.03 and 2.38 eV (emission energy) corresponding to Cu_5, Cu_8 and Cu_{25} metal cores. This result agreed with the E_{gap} calculated by the direct transition Tauc approach (Figure 5.4.A) which also displayed four different E_g values between 2.32 eV and 4.26 eV. The values are summarized in Table 5.2. It should be noted that the Cu_8 and Cu_{13} metal cores correspond to stable "magic numbers" (Cu_8) and "geometric favorable structure" (Cu_{13}).

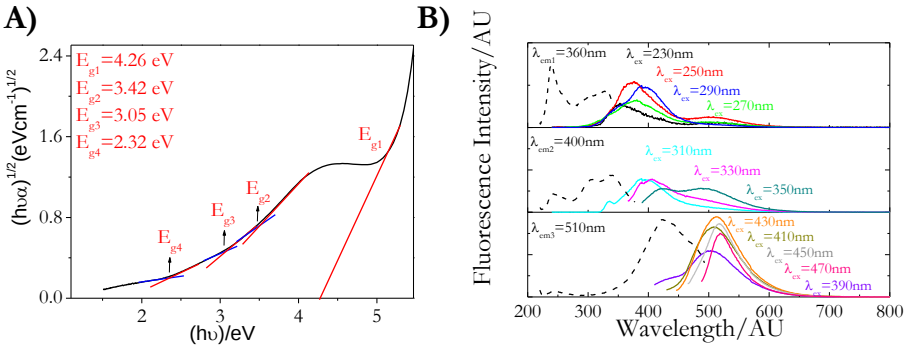

Figure 5. 4| *Tauc plot for a direct band gap fitting (2.32 eV≤E_g≤4.26 eV) (A). Emission and excitation spectrum of fluorescent large CuCLs with different excitation wavelengths from 230 to 470 nm (B).*

Table 5. 2| *Comparison between the Band gap values calculated from the Tauc approach and derived from the emission wavelengths.*

E_g/eV	3.42	3.05	2.32
$E_{emission}$/eV (nm)	3.42	3.03	2.38
Cluster core by Jellium	Cu_8	Cu_{13}	Cu_{25}

5.3.4. TEM and NC-AFM measurements.

TEM and NC-AFM were performed in order to study the cluster size. Results obtained by TEM confirm the polydispersity of the sample showing an average diameter of 1.37±0.34nm (Figure 5.5.A). NC-AFM heights display a closer value: 1.12±0.5nm (Figure 5.5.C). Therefore, the larger size of the as-synthesized clusters was confirmed.

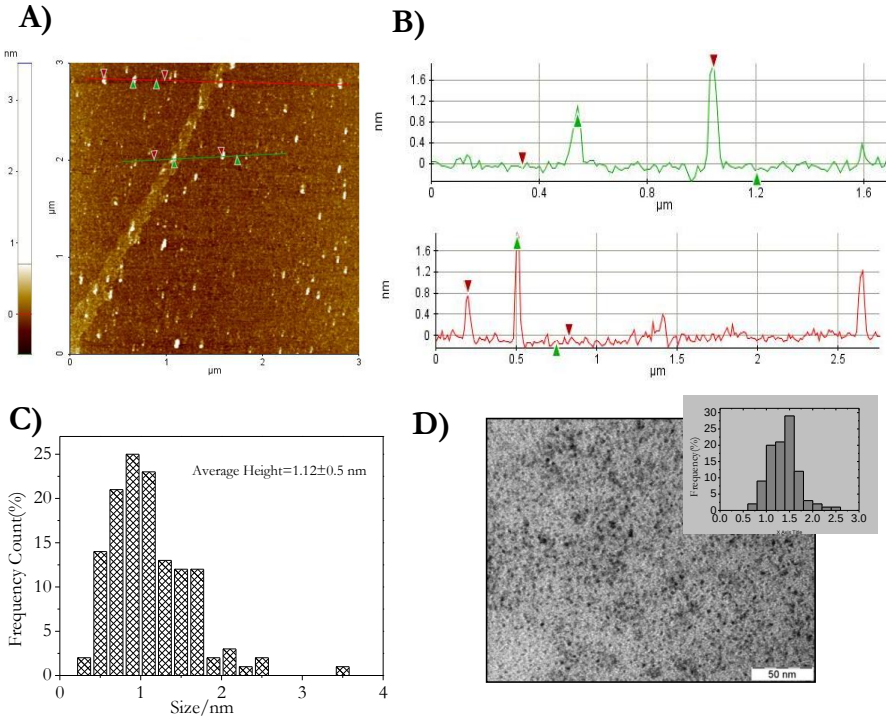

Figure 5. 5| *NC-AFM topography image of CuCLs deposited on mica substrate (rms ≈150 pm).(A) Section analysis of the solid lines is given on (B) and the corresponding histogram distribution height (C). TEM image of CuCLs. Inset: histogram distribution (D).*

5.3.5. Aqueous solubility and mass spectrometry studies.

The aqueous solubilization of larger clusters was carried out by a direct process: 3mL of CuCLs were dried on the rotary evaporator at 60ºC (lower temperature than acetonitrile boiling point: 80ºC and TBAAc melting point: 96.5ºC) giving a brown gel, which was subsequently redispersed in water (Aqueous Fraction). This gel was not very soluble in water and the insoluble precipitate was again redispersed in acetonitrile (MeCN Fraction). Both fractions were studied by UV-Vis absorption (Figure 5.6.A), fluorescence spectroscopy (Figure 5.6.B) and LDI-TOF mass spectrometry (Figure 5.7). UV-Vis of MeCN fraction shows a decrease on the 245 nm absorbance whereas the spectrum of the aqueous fraction displays an absorbance band at 245nm. Fluorescence emission at 408 nm (Cu_{13} clusters) indicated that smaller CuCLs are soluble in water while lager clusters are not.

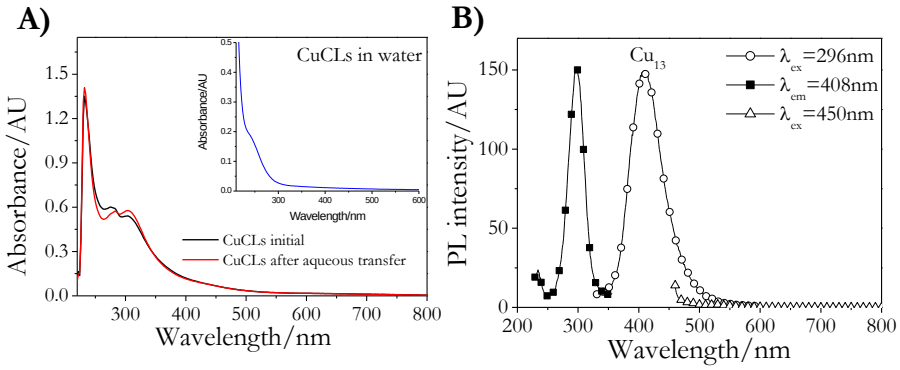

Figure 5. 6| *UV-Vis spectra of large CuCLs initial (black line), aqueous transfer (inset, blue line) and insoluble precipitate redispersed in MeCN (red line) (A) Emission spectra of CuCLs in water (B).*

Taking into account PL and absorption results, CuCLs redispersed in water should mainly composed by Cu_{13} metal cores (emission at 408nm). LDI-TOF measurements were carried out on both fractions. Therefore, different sets of peaks are expected from aqueous fraction to acetonitrile aliquots. As it can be seen on Figure 5.7 the most intense group of peaks on both spectra corresponds to low m/z values: 609.20 and 649.52 amu corresponding to $[Cu_9NC_2]^-$ and $[Cu_{10}N]^-$ for MeCN and aqueous fraction respectively. However, there are a set of peaks present only on the MeCN fraction: 1289.11 and 1627.24 amu which can be assigned to: $[Cu_{19}CN_5]^-$ and $[Cu_{25}NCN]^-$ respectively. On the basis of the LDI-

mass spectra results, the final product in the aqueous fraction only comprises small CuCLs.

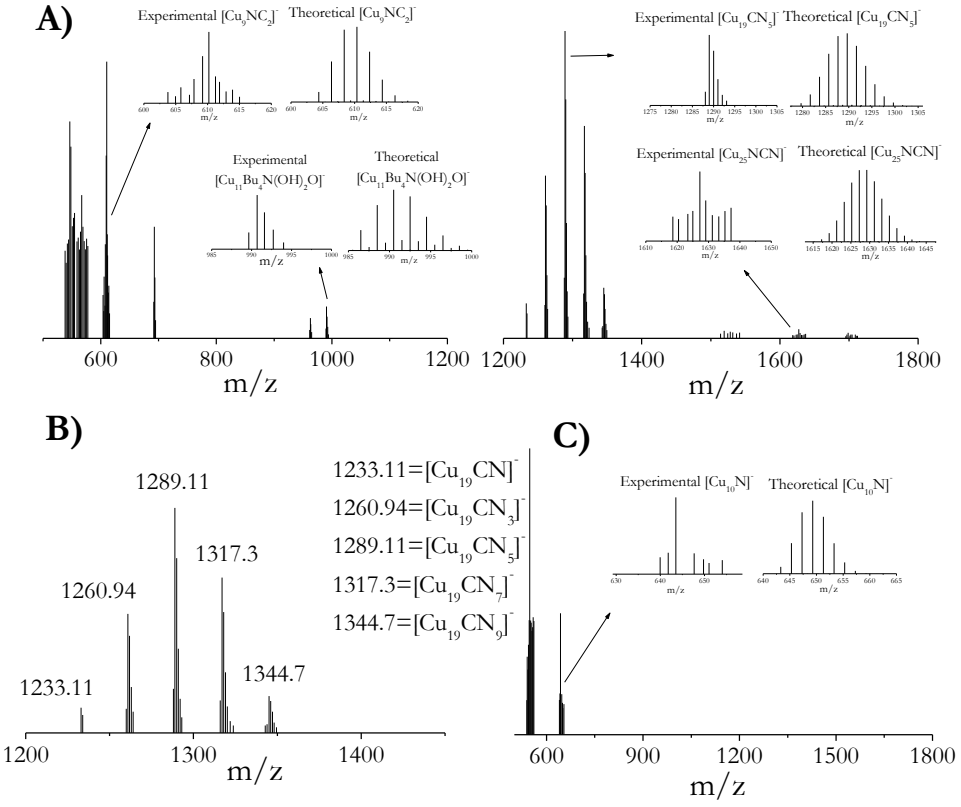

Figure 5. 7| *LDI-TOF mass spectra of CuCLs in MeCN (A). Magnification of the set of peaks from 1200 to 1400 range (B). LDI-TOF of CuCLs in water (D). All the spectra were collected in negative ion mode. Magnification of some peaks are shown as example with their theoretical isotopic patterns.*

A comparison between the different m/z values found on the MeCN and the aqueous fractions is displayed in Table 5.3. It can be concluded that the initial sample is formed by a mixture of CuCLs with the presence until a Cu_{25} core. However, aquous fraction only shows the presence of small CuCLs with a Cu_{10} core.

Table 5. 3| *LDI-TOF results in negative ion mode for the MeCN and aqueous fraction at the optimized high mass range from 400 to 1800 amu with their experimental and theoretical m/z peaks and their corresponding assignation.*

MeCN Fraction			**Aqueous Fraction**		
m/z_{exp}	**m/z_{theo}**	**Cluster**	**m/z_{exp}**	**m/z_{theo}**	**Cluster**
609.20	*609.94*	*$[Cu_9NC_2]^-$*	*649.52*	*649.47*	*$[Cu_{10}N]^-$*
990.69	*991.48*	*$[Cu_{11}Bu_4N(OH)_2O]^-$*			
1233.11	*1233.39*	*$[Cu_{19}CN]^-$*			
1260.94	*1261.40*	*$[Cu_{19}CN_3]^-$*			
1289.11	*1289.41*	*$[Cu_{19}CN_5]^-$*			
1317.30	*1317.43*	*$[Cu_{19}CN_7]^-$*			
1344.70	*1345.44*	*$[Cu_{19}CN_9]^-$*			
1627.24	*1628.67*	*$[Cu_{25}NCN]^-$*			

5.4. SUMMARY.

One step electrochemical synthesis of large CuCLs with Cu_N ($8 \leq N \leq 25$) were successful developed and their size were characterized by NC-AFM and mass spectrometry techniques.

Only small copper clusters with a Cu_{10} core were aqueous soluble.

These visible-light absorption copper clusters are a promising materials on future applications as visible photocatalysts.

REFERENCES.

[1] a) Reetz M. T.; Helbig W. *J. Am. Chem. Soc. 116*, 7401 **(1994).** b) Rodríguez-Sánchez M.L.; Rodríguez M.J.; Blanco M.C.; Rivas J.; López-Quintela M.A. *J. Phys. Chem. B 109,* 1183 **(2005).** c) Reetz M. T.; Winter M.; Breinbauer R.; Thurn-Albrecht T.; Vogel W. *Chem. Eur. J. 7*, 1084 **(2001).**

[2] Rodríguez-Sánchez, L. PhD Dissertation: *"Electrochemical synthesis of Ag and Co nanoparticles. Kinetics formation and physicochemical properties"*. University of Santiago de Compostela **(2003).**

CHAPTER 6.

Photoluminescence Stability of CuCLs

6.1. INTRODUCTION.

The great photoluminescence properties of metal clusters (such as, size tunable emission wavelength, high luminescent quantum yields, high photobleaching threshold and excellent photostability) in comparison with traditional organic dyes and quantum dots, are very useful in a wide range of applications. Therefore, the study of the PL stability of CuCLs is a very important factor. Here different stability studies, such as (1) thermal, (2) dispersion, (3) photochemical (i.e. photobleaching) and (4) pH changes stability are studied. Besides, the possible application as metal ions detectors in aqueous medium by the fluorescence quenching of our CuCLs is also carried out.

6.2. EXPERIMENTAL SECTION.

Photoluminescence stability of the different sized copper clusters (CuCLs) was studied in this Chapter. The solvatochromic effect was carried out by drying the original solvent and replacing it with the same volume of the selected solvent. Photobleaching was measured over the time of the different CuCLs samples by continuous irradiation exciting at their maximum excitation wavelength: small CuCLs (Cu_5) (Chapter 3) (λ_{exc}=270 nm), medium CuCLs ($Cu_{19\text{-}20}$) (Chapter 4) (λ_{exc}=360 nm), and bigger (Cu_{25}) (Chapter 5) (λ_{exc}=430 nm). Oxygen PL susceptibility was performed by bubbling O_2 during five minutes inside the quartz cuvette (2mL volume of CuCLs solution). The pH was adjusted with NaOH (basic pH) or HNO_3 (acid pH). Thermal studies were made by heating the CuCLs in solution at the desired temperature. Capping replacement was carried out by: (1) phase exchange between 5mL of Cu_{13} clusters aqueous solution and 10 mL of 1mM 1-hexanethiol in toluene stirring for seven hours at ambient temperature (Scheme 6.1) and (2) solubilization of the solid Cu_{13} clusters (1.5 mg) in 4 mL aqueous solution of 3-mercaptopropionic acid (2M) and L-Glutathione (0.1M) stirring for 20 hours at 40 ºC. For metal sensing an aliquot of CuCLs (1000 ng/mL, 240µL) was added to 2720 µL of water containing various concentrations of metal ions. The solution was mixed thoroughly and left to react at room temperature for 20 seconds.

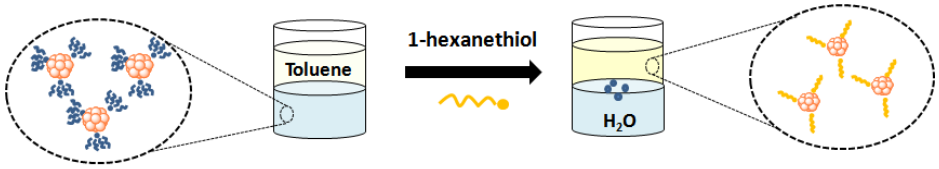

Scheme 6. 1| *Schematic representation of the phase transfer of Cu_{13}CLs from aqueous to toluene layer by hexanethiol.*

6.3. RESULTS AND DISCUSSION.

6.3.1. Photoluminescence stability.

(A) Photostability.

Many applications require that the CuCLs fluorescence remain stable over long periods of time under UV irradiation. In other words, they have not to display photobleaching. Photobleaching can be referred to as reversible/irreversible discrete intensity fluctuations from an "on" (fluorescent) to an "off" (non-emissive) state due to transitions of the individual molecules to non-fluorescent states such as the triplet[1]. There are different parameters determining the photobleaching process, which in some cases tend to be sensitive to the environment. No photobleaching was observed on smaller (Cu_5), medium ($Cu_{19\text{-}20}$) and large (Cu_{25}) clusters after 1000 minutes irradiation (Figure 6.1) at their maximum excitation wavelength.

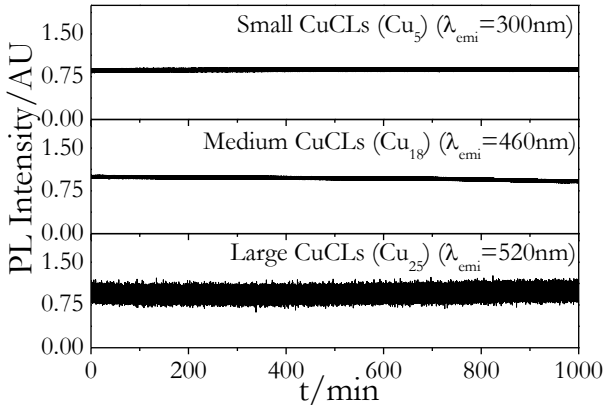

Figure 6. 1| *Photobleaching study of small CuCLs in EtOH (λ_{exc}=270nm, λ_{emi}=300nm), medium CuCLs in water ((λ_{exc}=360nm, λ_{emi}=460nm) and large CuCLs in MeCN (λ_{exc}=430nm, λ_{emi}=520nm)during irradiation time of 1000 minutes. Collection time for each point 1s.*

(B) Quantum yield and lifetime.

The fluorescence quantum yield (QY) is the ratio of photons absorbed to photons emitted through fluorescence. In other words, the quantum yield gives the probability of the excited state being deactivated by fluorescence rather than by any another non-radiative mechanism.Quantum yield of the small Cu_{13} CLs in water is ≈ 13 % (relative to quinine sulfate standard). Mooradian[2] and El-Sayed[3] studied the phenomenon of the fluorescence in copper films and copper nanoparticles respectively, getting emission bands at around 2.06eV (600-610nm) with extremely low quantum yields (10^{-10} and 10^{-5}, respectively). Recent studies on CuCLs have shown QY between 0.15 and 4.4 %.[4] Therefore, our copper clusters display the larger QY up until now.

The lifetime measurements were also determined for the small CuCLs (Cu_{13}) in water and Cu_8+Cu_{20} in MeCN. The decay profile of the CuCLs was monitored at an excitation wavelength of 300 and 282 nm, and 408 - 345 nm emission respectively. The numerical fitting of the luminescence collected at 408 nm (Cu_{13}) and 345 nm (Cu_8) required a sum of four exponentials to be adequately fitted. By comparing both samples, Cu_{13} exhibit a large component of a few tens of picoseconds and several slow components of nanoseconds, which is not shown in Cu_8.

Table 6. 1| *Luminescence Lifetimes (LT) and Their Relative Amplitudes (RA) for Cu_{13} and Cu_8 clusters.*

Cu_{13}		***Cu_8+Cu_{20}***	
LT (ns)	RA(%)	LT (ns)	RA(%)
0.013	21.80	0.04	7.30
0.28	5.77	0.35	6.37
1.48	8.51	1.42	10.6
5.47	3.44	6.23	1.24

In the case of Cu_8+Cu_{20} mixture, we observe an increase of the lifetime components, one explanation for this trend could be related with their sizes, displaying higher lifetime components for larger sizes. However, this assumption and their corresponding mechanism will require further investigation.

(C) PL Chemical stability.

The effect of different parameters such as pH, solvent environment, O_2 or Tª on the PL quenching of metal clusters is widely known. Therefore, an exhaustive study of these variables was studied on the small CuCLs solutions.

(C.1) pH stability.

pH photoluminescence dependance of CuCLs in water was studied. PL intensity of Cu_5 clusters, λ_{emi}=300nm remained nearly constant in a wide pH range: 4.7-10.7 (as it can be seen in Figure 6.2.A), but pronounced changes appeared for Cu_{13} clusters λ_{emi}=408nm. It can be clearly seen how Cu_{13} PL is gradually enhanced with pH from 6 to 12, but decays gradually from 6 to 3 (Figure 6.2.B), (meanwhile emission peak position: 408 nm remains unalterable). This pH effect can indicate that the Cu_{13} cores should have basic sites relevant to the emission due to the quenching observed in acidic media. Cu_5 clusters, on the other hand, displayed high pH stability, which came from their high band gap: E_g ≈5.3 eV.

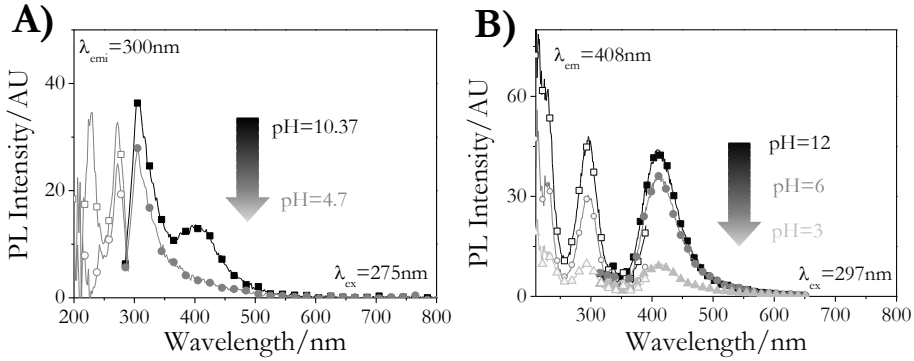

Figure 6. 2| *pH dependent excitation and emission spectra of CuCLs (Cu_5) (A) and (Cu_{13}) (B) when pH is switched between 12 and 3.*

(C.2) Solvatochromic effect.

Small CuCLs (Cu_{13}) with maximum emission wavelength at 408 nm were redispersed in different solvents, such as: pentane, chloroform, and ethanol (Figure 6.3) in order to study the possible solvatochromic effect. A well-resolved vibronic structure was observed when the polarity decreased. Shifts on the

excitation wavelengths are observed, but not on the emission. Therefore, the stability of the Cu_{13} clusters on different enviroments can be checked.

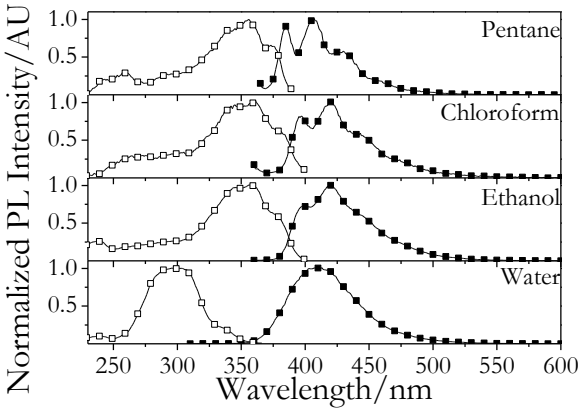

Figure 6. 3| *Excitation (black squares)-Emission (hollow squares) spectra (maximum intensity) of copper clusters in different solvents. (Pentane) (λ_{exc} = 355nm, λ_{emi} =406nm). (Chloroform) (λ_{exc}=350nm, λ_{emi}=418nm). (Ethanol) (λ_{exc} =350nm, λ_{emi} =420nm). (Water) (λ_{exc} =297nm, λ_{emi} =406nm).*

(C.3) O_2 quenching.

Oxygen is known in fluorescence to be like a potent quencher of fluorophores. In the quenching reaction, ground state of oxygen may react with triplet state specie under the formation of highly reactive singlet oxygen:

$$S_0\ (h\nu) \rightarrow S_1\ (ISC) \rightarrow T$$

$$T + {}^3O_2 \rightarrow S_0 + {}^1O_2$$

The singlet oxygen can react with surrounding molecules, including excited as well as ground state molecules. This reaction normally destroys the *"fluorophore"*. Here aqueous Cu_{13}CLs solution was investigated under oxygenated conditions. The oxygen-saturated Cu_{13} clusters solution exhibited the same intensity emission at 408 nm with no evidence of oxygen quenching (Figure 6.4). These results may indicate that CuCLs fluorescence is oxygen independent.

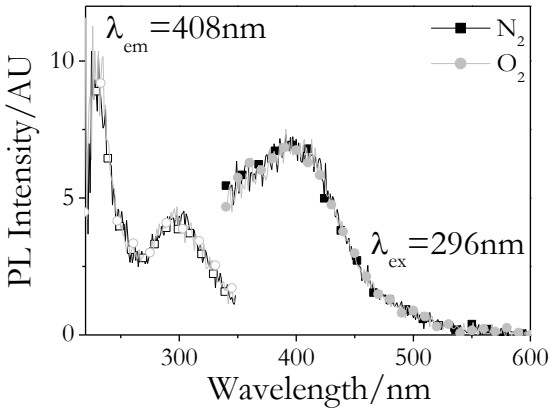

Figure 6. 4| *Fluorescence stability of O_2 (gray line) and N_2 (black line) saturated small Cu_{13} clusters in aqueous solutions.*

(C.4) Temperature effects:

Temperature is a determinant factor on the emission intensity. Normally, metal clusters decrease their PL intensity with temperature increase[5] although, Pradeep et al found that the intensity increased with an increasing temperature.[6] Here, Cu_{13}CLs were studied under different temperatures (Figure 6.5) observing a monotonous decrease on the PL intensity. However, it is worth noting that the fluorescence emission properties are reversible, when the sample returns to an ambient temperature they display the same PL intensity. The explanation of this PL decrease is a ***non-radiative relaxation.*** Two factors may cause this decrease: (1) thermal activation of non-radiative trapping or (2) thermal escape from the clusters, which becomes prominent by increasing the temperature with any change in emission peak position. There is a non-linear dependence of the fluorescence intensity on temperature (Figure 6.5, Inset) and it required an increase of 40K (from 278K to 318K) for a 50% decrease of the fluorescence emission intensity.

Photoluminescence Stability of CuCLs

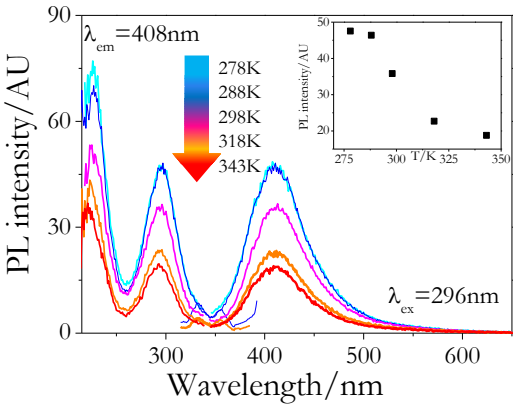

Figure 6. 5| *Fluorescence spectra as a function of the temperature from 278K to 300K of* Cu_{13} *clusters in aqueous solution (Inset: PL intensity vs Temperature in K).*

6.3.2. Capping molecules-ligand exchange.

As described on Chapter 2, tetrabutylammonium salts were used as capping agent. To further investigate the effect of the capping agent on the PL stability, the ligand exchange with different thiols was studied for the small copper clusters: Cu_{13}, as a convenient approach for producing functionalizated subnanometer copper clusters. Three different thiols were used: 1-hexanethiol, 3-mercaptopropionic acid (3-MP) and L-glutathione (L-Glu). During the process, thiol is expected to replace $TBANO_3$ because of the affinity of the sulfur to copper. On the two-phase method, the clusters are expected to be obtained in the organic phase. On the solid solubilization, the clusters would be completely solved, but the results have been not completely satisfactory. These thiols have a tendency to precipitate at ambient temperature, and consequently the clusters may precipitate with them. In spite of this, optical absorption and fluorescence spectra of the resulting supernatant solution obtained after the reaction was compared for both thiols in Figure 6.6. It can be observed that the supernatant absorption (gray line) for both thiols display an intensity increase (comparing with the initial thiol solution black line) around 285 and 270 nm for 3-MP and L-Glu respectively (marked by arrows). However, it should be noted a blue emission shift from 408 to 300 nm (Figure 6.6).

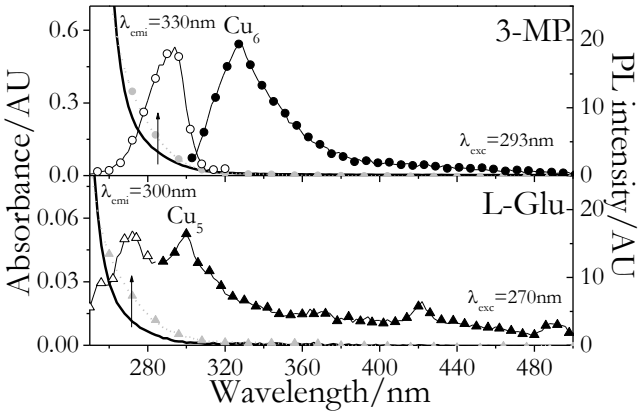

Figure 6. 6| *UV-Vis and PL spectra of Cu_{13} solid clusters after thiol exposure (24 hours, 50ºC).*

This should be related with the Cu_{13}CLs etching leading to the formation of smaller CuCLs, which by the Jellium model correspond to Cu_6 and Cu_5 centers. This study will involve a deeper investigation, but our preliminary results show a possible easy functionalization of these CuCLs needed in order to a specific bind into different molecules, substrates or surfaces. The two-phase exchange between 1-hexanethiol/toluene and Cu_{13}CLs/H_2O has proceed through seven hours vigorous stirring, observing an organic phase color change from colorless to light yellow. Figure 6.7.A shows the absorption spectra of the Cu_{13} clusters in the organic phase with absorption maximum band at 300 nm after the first hour of stirring and two absorption bands after 7 hours stirring located at 289 nm and 360 nm. The retention of the absorption profile of the aqueous copper clusters on 300nm after the phase transfer confirms the retention of the Cu_{13} core. An increase of the PL during the stirring time was also observed in the organic phase (Figure 6.7.B). The emission band of the phase-transferred clusters displayed a well-resolved vibronic structure with two main peaks at 397nm and 417nm (according to the polarity solvent decrease explained on the Figure 6.3). The phase transfer happen due to the great affinity of the thiol group for the Cu (0), therefore the electrostatic attracted tetrabutylammonium salt was replaced by the thiol.

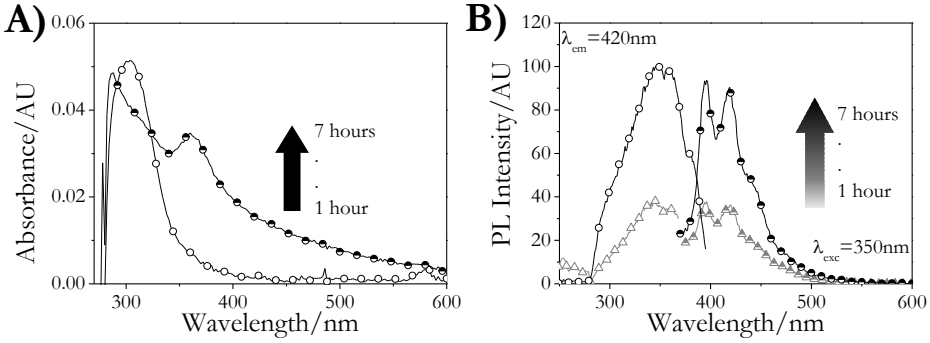

Figure 6. 7| *UV-Vis spectra of the time dependent phase-transfer of the CuCLs (A) and excitation and emission spectra of the CuCLs at different stirring time (B).*

The obtained results clearly established that the emission is an inherent property of the copper core, and the same electronic transition can be accessed for both ligands ($TBANO_3$ and C_6SH). Although the excitation spectrum could be modified, emission always happen between the same energy levels, implying that they are metal derived. This phase transfer via electrostatic interactions is

fast and versatile and can be carried out under ambient conditions. The previous results indicate again the high stability of our copper clusters which could be functionalizated by other thiols in order to introduce additional functionalities to the sub-nanometric fluorescent copper clusters.

6.3.3. Fluorescent CuCLs as ion nanosensors.

Metal-selective fluorescent nanosensors are attracting extensive attention nowadays. Several metal ions have been studied by fluorescence quenching of the metal clusters, such as: Hg(II)[7], Cr(III)[8], Cu(II)[9], Fe(III)[10], Pb(II)[11,4a,4d]. Fluorescent water soluble CuCLs was studied as potential nanosensors of different ions in solution. The CuCLs in water (Cu_{13}) (Chapter 3) was very luminescent, however, in the presence of Pb^{+2}, the fluorescence of the Cu_{13} clusters was found to be quenched by Pb^{+2}, which can be used as a selective and reversible "turn on-off" indicator for Pb^{+2} (Scheme 6.2).

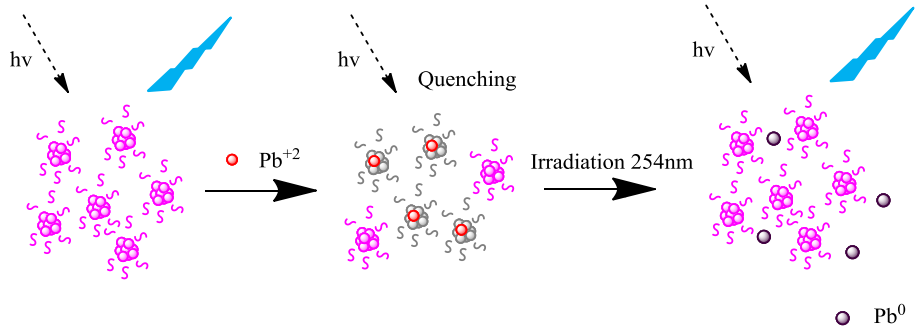

Scheme 6. 2| *Schematic illustration of the fluorescent Cu_{13} CLs for Pb^{+2} "off-on" detection.*

To further evaluate the analytical detection of Pb^{+2} different concentrations (0.048, 4.83, 12.1, 19.3, 28.96, 38.61, 57.92, 77.2 and 96.52 μM) were added to CuCLs sample. As it can be seen in Figure 6.8.A upon addition of increasing concentrations of Pb^{+2}, a gradual decrease in the fluorescence was observed at 408nm. From Figure 6.8.B it can be seen that the fluorescence ratio (F_0/F) is sensitive to the [Pb^{+2}]. The Stern Volmer plot (typical for static or dynamic quenching) shows a modified form, which is associated with the presence of accessible and inaccessible fluorophores[12], this result agrees with the data provided in Chapter 3, where the Cu_{13} CLs are identified as Cu_{13} but also exist smaller Cu cores in the sample. Hence, the Cu_{13} can be the "accessible"

fluorophore and the smaller clusters the inaccessible fluorophores. For a limited range of quencher concentrations, the modified Stern-Volmer plot appears to be linear (from 0.048 to 20 μM) ($y=0.9136+0.0134[Pb^{+2}]$, $R^2=0.9908$).

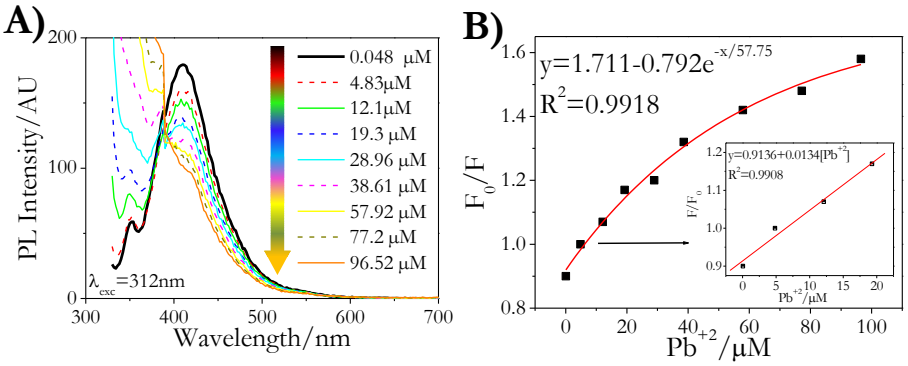

Figure 6. 8 | *Emission spectrum representing the quenching effect of different concentrations of Pb^{+2} on fluorescent Cu_{13}CLs (A). Plot of fluorescence quenching (F_0/F) of the CuCLs at 408 nm incubated with different concentrations of Pb^{+2}(B).*

Next, we investigated the selectivity of our CuCLs toward Pb^{+2} ions. The data presented in Figure 6.9 were collected at 20 μM concentrations. The results confirm the high selectivity of the CuCLs toward Pb^{+2} ions. Other metal ions had minor or negligible quenching effects on the fluorescence intensity of the CuCLs. Larger CuCLs (Cu_{20}) (Chapter 4) were also studied on the sensing of Pb^{+2}, almost no PL quenching effect can be observed. This behavior is still under study, because the real mechanism of CuCLs PL quenching is not well understood. Some authors associated the quenching to possible interactions between the ion and the capping agent, but our case will need a deep study. Finally, reversibility and recyclability of the CuCLs as fluorescent sensors were evaluated. Fluorescence quenching also is also time dependent, and CuCLs with 500nM can be quenched within 72 hours. Subsequent irradiation by a UV lamp (λ_{exc}=254 nm) for 21 hours were able to recover the quenched fluorescence to its initial intensity (Figure 6.10). The recovery mechanism is believed to consist of the Pb^{+2} reduction by the e^- transfer from the excited cluster. However, other studies will be necessary in order to explain the quenching recovering cycles allowed by this system.

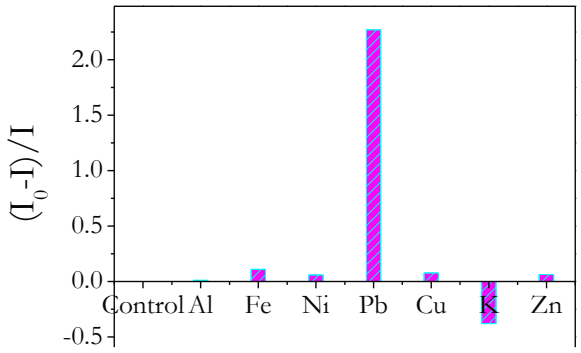

Figure 6. 9| *Selectivity of the CuCLs towards 20 µM metal ions concentrations (λ_{exc}= 312 nm).*

.

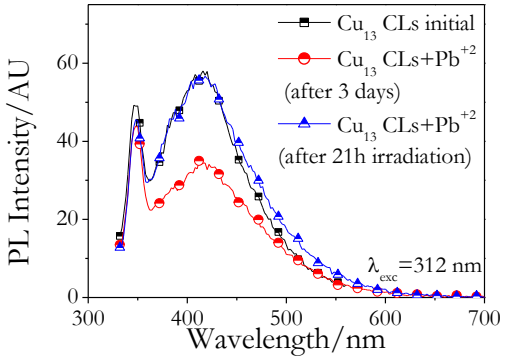

Figure 6. 10| *PL spectra of CuCLs emission during the time and recovering of the PL intensity after exposure to UV radiation.*

6.4. SUMMARY.

The bright emission, high photostability and chemical stability of CuCLs make them attractive alternatives to conventional fluorophores.

CuCLs ligands exchange took place by using different thiols.

Fluorescent small CuCLs have demonstrated satisfactory results on the detection of Pb^{+2} ions. Besides the inherent CuCLs photoluminescence can be recovered under UV light irradiation. This fact makes possible the use of the CuCLs as an "off-on recyclable nanosensors.

REFERENCES.

[1] a) Basché T.; Kummer S.; Bräuchle C. *Nature 373,* 132 **(1995).** b) Ha T.; Enderle T.; Chemla D. S.; Selvin P. R.; Weiss S. *Chem. Phys. Lett. 271,* 1 **(1997).** c) Yip W. T.; Hu D. H.; Yu J.; Vanden Bout D. A.; Barbara P. F. *J Phys Chem. A 102*, 7564 **(1998).**

[2] Mooradian A. *Phys. Rev. Lett. 22,* 185 **(1969).**

[3] Darugar Q.; Qian W.; El-Sayed A. M.; Pileni M.P. *J.Phys.Chem B 110,* 143 **(2006).**

[4] a) Goswami N.; Giri A.; Bootharaju M. S.; Xavier P.L.; Pradeep T.; Pal S.K. *Anal. Chem. 83,* 9676 **(2011).** b)Xie J. P.; Zheng Y. G.; Ying J. Y. *J. Am. Chem. Soc. 131*, 888 **(2009).** c) Wei W. T.; Lu Y. Z.; Chen W.; Chen S. W. *J. Am. Chem. Soc. 133*, 2060 **(2011).** d) Kawasaki H.; Hamaguchi K.; Osaka I.; Arakawa R. *Adv. Funct. Mater. 21,* 3508 **(2011).** e) Zhang H.; Huang X.; Li L.; Zhang G.; Hussain I.; Li Z.; Tan B. *Chem. Commun. 48,* 567 **(2012).**

[5] a) Yu P.; Wen X.; Toh Y.-R.; Tang J. *J. Phys. Chem. C 116,* 6567 **(2012).** b) van Wijngaarden J.T.; Toikkanen O.; Liljeroth P.; Quinn B.M.; Meijerink A. *J. Phys. Chem. C 114,* 16025 **(2010).**

[6] a) Shibu E. S.; Muhammed M. A. H.; Tsukuda T.; Pradeep T. *J. Phys. Chem. C 112,* 12168 **(2008).** b) Shibu E. S.; Pradeep T. *Int. J. Nanosci. 8,* 223 **(2009).**

[7] a) Adhikari B.; Banerjee A. *Chem. Mater. 22*, 4364 **(2010).** b) Xie J.; Zheng Y.; Ying J.Y. *Chem. Commun. 46*, 961 **(2010).** c) Wei H.; Wang Z.; Yang L.; Tian S.; Hou CH.; Lu Y. *Analyst 135,* 1406 **(2010).** d) Huang Ch-Ch.; Yang Z.; Lee K-H.; Chang H.-T. *Angew. Chem. 119,* 6948 **(2007).**

[8] Liu S.; Lu F.; Zhu J.-J. *Chem. Commun. 47,* 2661 **(2011).**

[9] a) Zhang M.; Ye B.-C. *Analyst 136*, 5139 **(2011).** b) Durgadas C. V.; Sharma C. P.; Sreenivasan K. *Analyst 136,* 933 **(2011).** c) Liu H.; Zhang X.; Wu X.; Jiang L.; Burda C. Zhu J.-J. *Chem. Commun. 47,* 4237 **(2011).**

[10] Ho J.A.; Chang H.-C.; Su W.-T. *Anal. Chem. 84*, 3246 **(2012).**

[11] Yuan Z.; Peng M.; He Y.; Yeung E.S. *Chem. Commun. 47,*11981 **(2011).**

[12] Joseph R. Lakowicz, *Principles of Fluorescence Spectroscopy*, Springer, **(2006).**

CHAPTER 7.

Catalytic Activity of CuCLs

7.1. INTRODUCTION.

The main goal in catalysis is to find highly selective catalysts for particular reactions. In this sense, catalysis by noble metal nanoparticles and clusters is now becoming very important because of the high selectivity displayed by these materials.[1] The great catalytic activity of metal clusters is considered to be due to their intrinsic electronic properties, which are characterized by the appearance of a bandgap at the Fermi level. It has been shown that the bandgap mainly depends on the number of atoms of the cluster.[2] Over the past few years, size-dependent catalytic activity of clusters has been studied for different kind of reactions. For example, recent works for selective oxidation and hydrogenation processes have been explored by Zhu[3] and Liu[4], using well defined $Au_n(SR)_m$ clusters as model catalyst; and a strong size dependence has also been reported[5] for this catalyst against the selective oxidation of stryrene. Ag clusters supported on alumina also show a size-dependent catalytic activity on the chemoselective reduction of nitrostyrene,[6] and selected supported silver clusters enhance the reduction of several nitro com-pounds.[7] Although it is well-known that Cu(I) or Cu(II) complexes are good catalyst for different types of reactions,[8] the catalytic properties of Cu(0) clusters (CuCLs) have not received much attention up to now, mainly because of the lack of synthesis procedures. Catalytic activities of supported CuCLs have been reported for the cyclotrimerization reaction[9a] showing high selectivity; for the Suzuki cross-coupling reaction of various aryl halides with phenylboronic acid;[9b] for the cycloaddition of azides with terminal alkynes[9c] and very recently[10] for the electroreduction of oxygen.

The catalytic properties of Cu(0) clusters (CuCLs) are very important not only because the cluster bandgap may play an important role in the catalytic properties, but also because the Fermi level of Cu, which determines the position of the HOMO/LUMO energies (valence, VB, and conduction bands, CV, respectively in normal semi-conductors), is very different from Au or Ag. Therefore, different catalytic behaviors can be expected. Here, we report the size-dependent catalytic properties of unsup-ported Cu (0) CLs for the reduction reaction of methylene blue (MB) by hydrazine (N_2H_4). The reaction forms the colorless leucomethylene blue (LMB), which can be trans-formed again to blue MB just by allowing the oxygen to enter into the reaction media. This reaction has been used before to evaluate the catalytic activities of various nanocatalysts, including Ag,[11] Au,[12] Pd,[13] Pt,[14] and Cu-based nanoparticles.[15] In our case, this clock reaction has been chosen because of its reversible color change, which can be conveniently used for the study of the recycling properties of the cluster catalysts.

On the other hand, photocatalysis has attracted considerable interest nowadays. Photocatalytic reactions consist on the excitation of electrons from the valence band to the conduction band of one semiconductor upon light irradiation. The corresponding excited electrons and holes can be employed in reduction and oxidation reactions, respectively. Therefore, photocatalysis process is believed to be capable of eliminating organic or inorganic pollutants in water via oxidation or reduction mechanism (Scheme 7.1).[16] Titanium dioxide (TiO_2) has been considered as a suitable material for various photocatalytic applications because of its strong oxidizing power, low cost and high stability.[16c,17] However, a large bandgap (3.2 eV) of anatase TiO_2 restricts its application only to the narrow range of ultraviolet (only about 3-5% of total sunlight). From the viewpoint of field applications, such as water and air treatments,[18] hydrogen production from water splitting,[19] development of substrates with self-cleaning properties[20] however, the large band gap of TiO_2 and the difficulty in catalyst recovery are recognized to be the major disadvantages of powdered TiO_2.[21] In this context, typical photocatalysts have been modified in order to enchance their solar photocatalytic activity, by doping or by combination with other materials.[22]

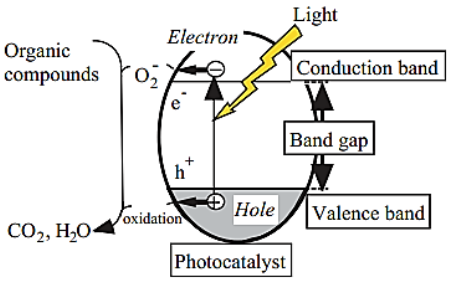

Scheme 7. 1| *Photocatalyst mechanism.*

Therefore, the study of the photocatalytic properties of the as-synthesized clusters was also studied. The reaction consisted on the photodissolution of a silver nanofibers sample in presence of clusters under the corresponding irradiation light.

7.2. EXPERIMENTAL SECTION.

Catalytic experiments were carried out with CuCLs of three different sizes (Chapter 3 and 4). Small CuCLs synthesized on Chapter 3 (CuCLs in EtOH named as Cu_5 and in H_2O named Cu_{13}) and larger CuCLs obtained on Chapter 4 (CuCLs in MeCN named as Cu_{20}) will be used in this experiment. As we explained previously CuCLs are very stable showing the same emission spectra after more than one year stored at ambient temperature. The high stability of clusters is due to their large HOMO-LUMO bandgap, which –contrary to Cu nanoparticles or bulk Cu- makes them very stable against oxidation of reduction. The reduction of MB in water, using N_2H_4 as the reducing agent, in the presence of CuCLs was studied by UV-Vis spectroscopy following the absorbance at the λ_{max} of MB (665nm). Kinetic studies were first carried out using the Cu_{13} clusters. The aqueous solution of MB was mixed first with DI water, then CuCLs and finally hydrazine hydrate (fresh, made daily) were added. The pH was adjusted with $NaOH/H_2O$ solution. Concentration of CuCLs is referred as the copper total concentration. Kinetic experimental conditions are summarized on Table 7.1.

Photocatalytic experiments were carried out by Pérez Mariño A.M.[23] with different CuCls sizes: small CuCLs, named as Cu_{13} (Chapter 3) and large CuCLs, named as Cu_{25} (Chapter 5). UV photodissolution of silver nanofibers (AgNF, suministred by Nanogap) has been carried out with 6μL of AgNF + 5 μL Cu_{13}CLs ([Cu_{13}CLs] $\approx 4.33.10^{-7}$M) reached a final volume of 1511 μL with water. Visible photodissolution of AgNF was done with 3 μL of AgNF + 200 μL Cu_{25}CLs ([Cu_{25}CLs] $\approx 6.56.10^{-8}$M) reached a final volume of 3003 μL with water. UV-lamp employed was a UV pen ray (S/N: 90-0012-01 0210) with λ_{exc}=254 nm , and $2000 \leq I_{maximum} \leq 4100$ μW/cm^2. Vis lamp was a tungsten lam of 60W. UV-Vis spectra was recorded during the irradiation observing the evolution of the AgNF associated absortion band located at 406 nm. As a comparison, blank solutions were also performed under identical experimental conditions. Aliquots of the samples were also measured by TEM and SEM techniques.

Catalytic Activity of CuCLs

Table 7. 1| *Reduction of MB by N_2H_4 catalysed by CuCLs under different experimental conditions.*

Reaction	*Cluster*	*[CuCLs]x10^5 /M*	*[N_2H_4]/ M*	*[MB]x10^{-5} /M*	*K_{obs}x10^4 /s^{-1}*	*R*	*SD*	*pH*
1	**-**	**-**	**0.06**	**3.3**	**0.78**	0.8673	0.04	9
2	**Cu_{13}**	**0.27**	**0.06**	**3.3**	**4.46**	0.9824	0.10	9
3	**Cu_{13}**	**0.54**	**0.06**	**3.3**	**8.78**	0.9963	0.06	9
4	**Cu_{13}**	**1.08**	**0.06**	**3.3**	**9.65**	0.9873	0.13	9
5	**Cu_{13}**	**1.76**	**0.06**	**3.3**	**19.6**	0.9940	0.12	9
6	**Cu_{13}**	**3.24**	**0.06**	**3.3**	**26.3**	0.9995	0.02	9
7	**Cu_{13}**	**1.76**	**0.03**	**3.3**	**14.4**	0.9817	0.16	9
8	**Cu_{13}**	**1.76**	**0.06**	**3.3**	**19.6**	0.9940	0.12	9
9	**Cu_{13}**	**1.76**	**0.12**	**3.3**	**10.7**	0.9823	0.13	9
10	**Cu_{13}**	**1.76**	**0.18**	**3.3**	**17**	0.9949	0.07	9
11	**Cu_{13}**	**1.76**	**0.2**	**3.3**	**26.7**	0.9993	0.02	9
12	**Cu_{13}**	**1.76**	**0.06**	**3.3**	**3.75**	0.9992	0.03	6.5
13	**Cu_{13}**	**1.76**	**0.06**	**3.3**	**7.6**	0.9999	0.01	7.5
14	**Cu_{13}**	**1.76**	**0.06**	**3.3**	**10.1**	0.9839	0.11	8.5
15	**Cu_{13}**	**1.76**	**0.06**	**3.3**	**19.9**	0.9953	0.06	9.5
16	**Cu_{13}**	**0.06**	**0.06**	**3.3**	**23.1**	0.9845	0.08	11.5
17	**Cu_5**	**1.76**	**0.06**	**3.3**	**27.4**	0.9824	0.16	-
18	**Cu_{20}**	**1.76**	**0.06**	**3.3**	**-**	-	-	-

7.3. RESULTS AND DISCUSSION.

7.3.1. CuCLs AS CATALYST.

(A) Cu_{13} as effective catalyst.

Figure 7.1 shows the progress of the reaction in presence and absence of Cu_{13} clusters for the experiments R1 and R8 of Table 7.1. In absence of Cu_{13} (Figure 7.1.1) the absorbance intensity remains almost unaltered in agreement with the literature[12,15c] but in presence of clusters (Figure 7.1.2) a fast reduction of MB is observed, which indicates that the Cu_{13} clusters catalyze this reaction.The absorbance versus time (Figure 7.1.3) for the catalytic reaction follows an exponential decrease:

$$\mathbf{lnA=-k_{obs}t,} \qquad \mathbf{Eq.1}$$

where A=Absorbance, t= time, and k_{obs}= observed reaction rate constant. Figure 7.2 shows a good linear relationship of lnA versus t for all the performed experiments.

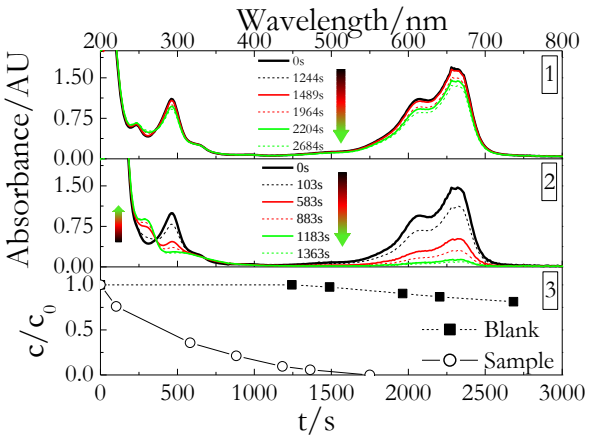

Figure 7. 1| *(1) UV-Vis spectra of the reduction of MB with N_2H_4 as a function of time in absence (1) (Table 7.1-Reaction 1) and in presence (2) of Cu_{13}CLs (Table 7.1-Reaction 8). Comparison of the MB reduction for 1 and 2 (3).*

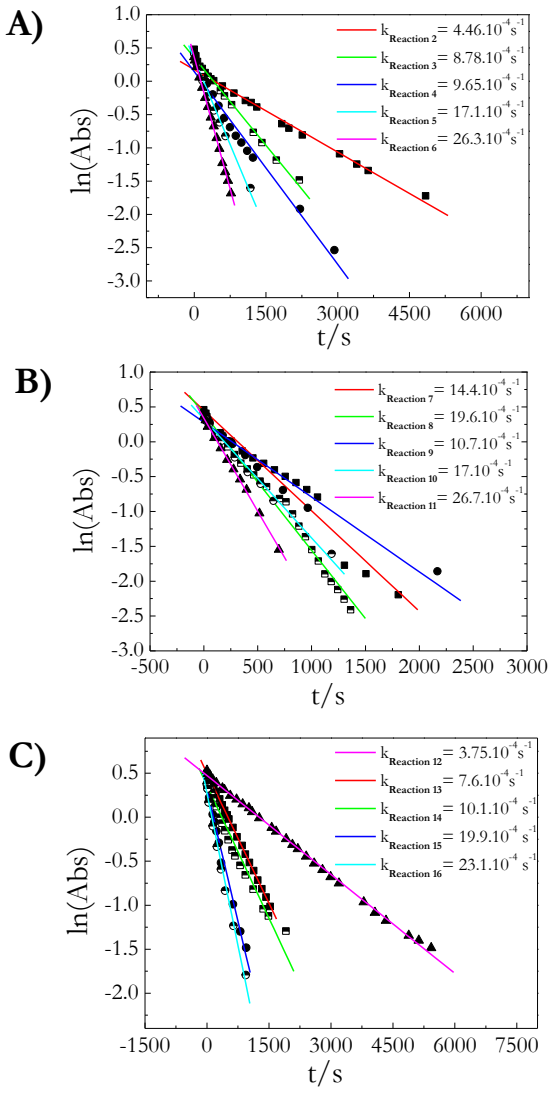

Figure 7. 2 | *Plot of ln (absorbance) vs time for different Cu_{13} concentrations (Table 7.1, Reactions 2-6) with their corresponding fitted values of k_{obs}.(A) Plot of ln (absorbance) vs time for different hydrazine concentrations (Table 7.1, Reactions 7-11) with their corresponding fitted values of k_{obs}.(B) Plot of ln(absorbance) vs time for different pHs (Table 7.1, Reactions 12-16) with their corresponding fitted values of k_{obs}.(C)*

In order to determine the order of the reaction for the N_2H_4 and the catalysts, the reaction was carried out at different Cu_{13}CLs concentrations (Table 7.1, reactions 2-6) and N_2H_4 concentrations (Table 7.1, reactions 7-11). It is observed that k_{obs} increases linearly with [Cu_{13}CLs] (Figure 7.2-A and 7.3):

$$\mathbf{k_{obs} = k_{obs}'[Cu_{13}],}$$

being kobs´ = 70.6±6.2 M^{-1} s^{-1} . Besides, also k_{obs} increases linearly with the concentration of the reducing agent (N_2H_4) (Figure 7.2-B and 7.3):

$$\mathbf{k_{obs} = k_{obs}''[N_2H_4],}$$

being k_{obs}'' = 0.010 ± 0.003 M^{-1} s^{-1}. From this behavior one can see that

$$\mathbf{k_{obs} = k^0\ [N_2H_4]\ [CuCLs]}$$

k^0 obtained from the variations of [Cu_{13}] and [N_2H_4] is (1.2 ±0.1) 10^3 M^{-2} s^{-1} and (0.6±0.2) 10^3 M^{-2} s^{-1}, respectively. Therefore, $<k^0>$ = (0.9± 0.3) 10^3 M^{-2} s^{-1}.

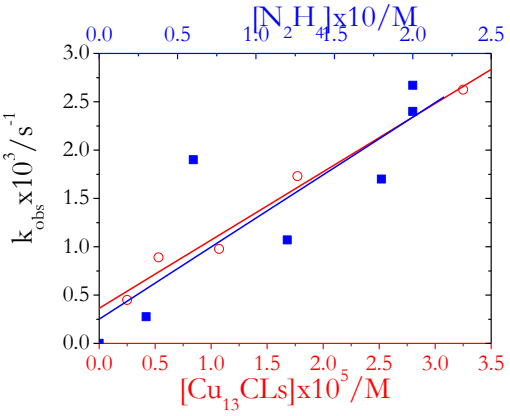

Figure 7. 3| *Plot of k_{obs} vs [Cu_{13}CLs] and [N_2H_4].(Reactions from 2 to 11,Table 7.1).*

From these results, the following mechanism for the catalytic reaction can be proposed:

$$(1)\ MB + Cu_{13\ cluster} \leftrightarrow MB - Cu_{13\ ads},\ K$$
$$(2)\ MB\text{-}\ Cu_{13\ ads} + N_2H_4 \rightarrow LMB,\ k$$

After the adsorption equilibrium between MB and Cu_{13} forming an intermediate MB-$Cu_{13\ ads}$, a posterior collision between this intermediate and the reduction agent, N_2H_4, allows two electrons to be transferred to the MB, mediated by the CuCLs, with a rate constant $k = k^0/K$.

(B) Effects of the cluster size on the catalysis.

Once we had shown that sub-nanometer Cu_{13} clusters are a promising and reusable catalyst for the MB reduction, we checked the cluster size role in the catalytic behavior. Small (Chapter 3, Cu_5) and large CuCLs (Chapter 4, Cu_{20}) were then used for the catalytic studies under the conditions of the Reactions 17 and 18 (Table 7.1) respectively. As can be seen in Figure 7.4 the smallest CuCLs (Cu_5) are even more efficient than the Cu_{13} clusters. However, the largest clusters (Cu_{20}) do not catalyze the reaction. These results show that the cluster's size is crucial for the catalytic activity.

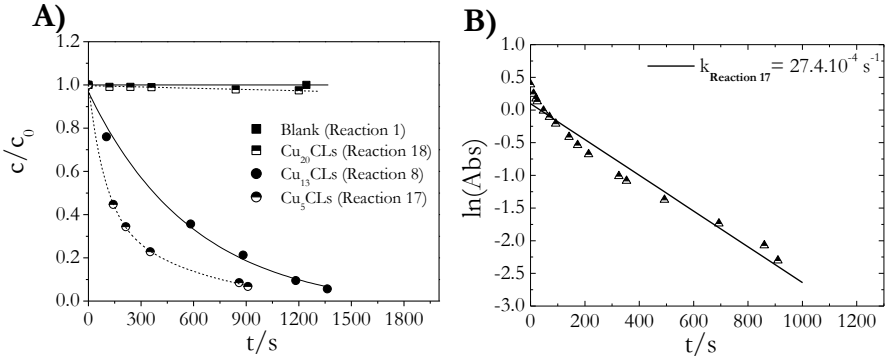

Figure 7. 4| *Comparison of the rate of reduction of MB without and with different sub-nm Cu cluster catalysts. (A) Plot of ln (absorbance) vs time for the Cu_5CLs (Table 7.1, Reaction 17) with its corresponding fitted value of k_{obs} (B).*

(C) Mechanistic aspects.

The observed size-dependent catalysis with CuCLs can be explained taking into account that the previous mechanism of a cluster-mediated electron transfer from the donor (N_2H_4) to the acceptor (MB) has to proceed through the conduction band of the CuCLs, as it is schematically depicted in Scheme 7.2. Redox potentials for N_2H_4 ($E^0_{N2H4/N2}$ = -1.16V) and MB ($E^0_{MB/LMB}$ in the range of 0V, for pH =7[24] to 0.4V for basic pHs (value calculated by cyclic voltammetry giving a result (vs SHE)) are also shown. The position of the HOMO/LUMO frontier orbitals for the three cluster catalysts depend not only on E_g, but also on the position of their Fermi levels. Previous DFT studies[25] have shown that the chemical potential in Cu clusters changes with the size of the clusters, according to the following equation $\mu(eV) = -\Phi + CN^{-1/3}$, where is Φ the work function and C is a constant, which represents the different dependence of the ionization potential and the electron affinity on the cluster size. Therefore, the Fermi level of Cu clusters can be described by a similar expression: E_F (eV) = - E_F (Cu_{bulk}) + $CN^{-1/3}$. Theoretical calculated values of C for Cu clusters in vacuum are in the range 0.1eV-1eV.[25]

Scheme 7. 2| *Schematic energy diagram showing the catalytic activity of different CuCLs (Cu_5, Cu_{13} and Cu_{20}) used for the MB reduction by N_2H_4. After finishing the catalytic reduction, MB can be recovered by shaking the sample in oxygen atmosphere, and a new catalytic reaction cycle can be carried out.*

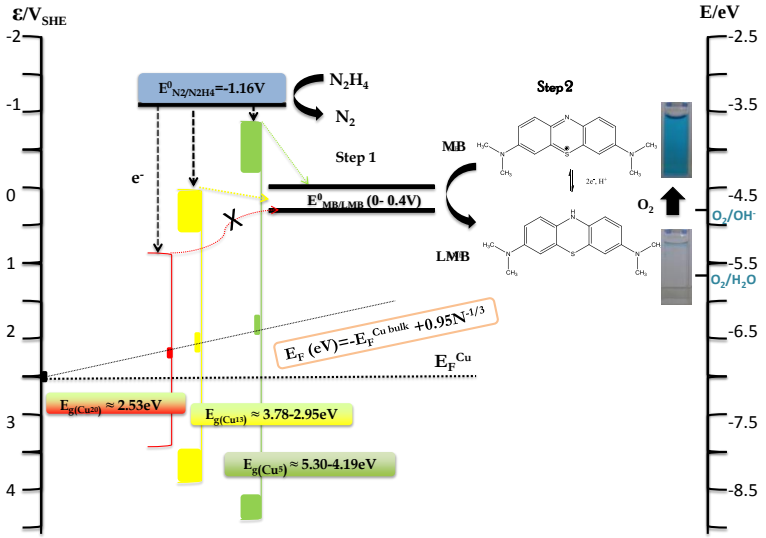

It can be noted that the interpretation based on Scheme 7.2 can also explain the high electrocatalytic activity of CuCLs for the oxygen reduction reaction (ORR) recently reported by Wei et al.[10] One can see that only clusters with sizes ≈≥7 could catalyze the ORR because their LUMO is located below the redox potential for the ORR at basic pHs (0.4V). Besides, although our clusters are in solution and protected with tetrabutylammonium nitrate, so that the change of the chemical potential with the cluster size could be different from the DFT calculations, one can clearly see that a value of C ~1eV agrees nicely with our experimental results. With this value of the constant C, the LUMOs of Cu_5 and Cu_{13} are located above the MB redox potential and below the hydrazine redox potential, allowing the clusters to be catalytically active, being this activity larger for the Cu_5 clusters because of their larger driving force. However, the largest Cu_{20} clusters would be inactive because their LUMO frontier orbitals are located below the MB redox potential.

Changes on the catalytic activity of Cu_{13} CLs were observed with the pH (Figure 7.5), observing that the reaction becomes slower when the pH is reduced. This behavior can be also interpreted on the basis of the proposed mechanism. As it was mentioned above, the redox potential of MB increases with the pH. Therefore, the driving force will increase when the pH also does, giving rise to an increase of the catalytic activity.

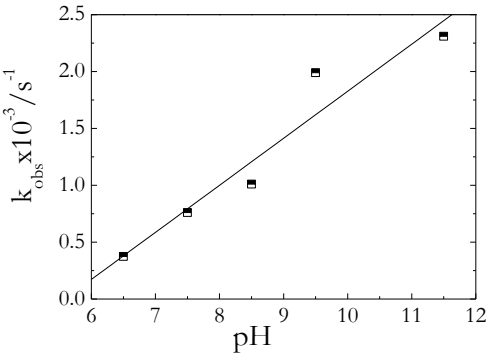

Figure 7. 5| *Plot of k_{obs} vs pH. (Reactions from 12 to 16 on Table 7.1).*

(D) Recycling studies.

We also studied the recycling properties of the catalysts. As can be observed in Figure 7.6.A, Cu_{13} clusters retain their catalytic activity for, at least, 42 cycles. It is interesting to note that the catalytic activity even increases at the second and subsequent cycles with respect to the first round (Figure 7.6.B), which indicates that the assumed adsorption equilibrium between CuCLs and MB was not totally established when the first round was initiated.

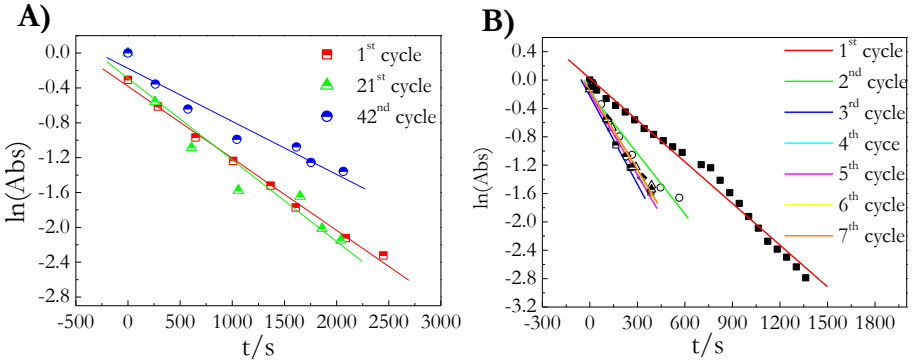

Figure 7. 6| *Plot of ln(Abs) vs time for the catalytic MB reduction at different reaction cycles (A) Plot of ln (absorbance) vs time for the first 7 reaction cycles(B) by using (Cu_{13} clusters).*

Furthermore, in order to check that the concentration of clusters remains the same after each reaction cycle, we used the fluorescent properties exhibited by the clusters. The Cu_{13} clusters have an emission band at λ_{em} = 425nm (λ_{exc} = 335nm), which is close to the emission of the reduced form of methylene blue (LMB, $\lambda_{em} \approx 470$nm)[26] in aqueous solution. Therefore, one needs to decompose the combined emission band in mixtures of LMB and Cu_{13} clusters. This can be seen in Figure 7.7, showing the band decomposition by Lorentzians in the inset. By this procedure, it was checked that the PL properties of clusters also remain constant after each reaction cycle.

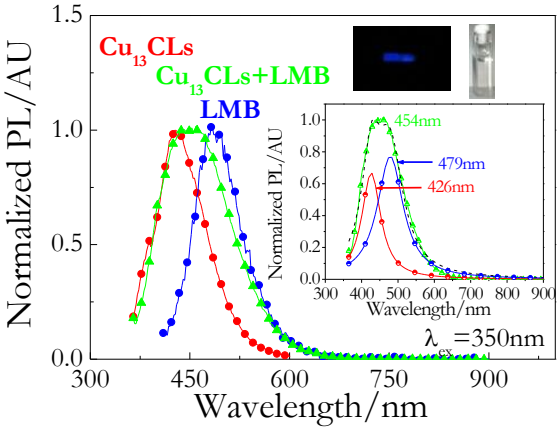

Figure 7. 7| *Emission spectra of Cu_{13} (red line), LMB (blue) and Cu_{13+LMB} (green). Inset 1 shows the Cu_{13+LMB} emission band (black) fitted by Lorentzians (blue and green lines). Inset 2 displays the blue color emitted by Cu_{13+LMB} exciting at 350nm.*

7.3.2. CuCLs AS PHOTOCATALYST: PHOTODISSOLUTION OF AgNFs.

(A) Cu_{13} and Cu_{25} as effective photocatalyst.

The phenomenon of photodissolution was previously developed in our group by Attia-Attia Y.[27] studying the gold nanorods (AuNRs) photodissolution under UV light in presence of different metal clusters. A decrease on the absorption spectra accompanied by a plasmon band shift was observed, being mainly associated with a nanorod length decrease. This phenomenon can be explained due to the remained Ag clusters still present on the solution (which were used as catalyst on the nanorods formation). As described before, metal clusters display fluorescence, but if the media presents an specie susceptible of oxidation or reduction, then the exciton generated by the irradiation can form electrons and holes which can act as reduction/oxidation agents instead of been recombined to give the fluorescence emission. In order to evaluate the photocatalytic activity of the CuCLs, a similar experiment to AuNRs photodissolution was developed. Silver nanofibers (AgNFs) were used instead AuNRs, as it was explained on the Experimental Section. UV-Vis absorption band intensity at 406 nm (relative to the AgNFs concentration) decreases was studied during the irradiation time. Negligible intensity changes were observed in the blank solutions; only a 15.17% under UV light and no changes under Vis light (after 24 hours irradiation). In contrast, a dramatically decrease was observed in presence of CuCLs obtaining a 86.2 % and 38 % decrease in presence of Cu_{13} and $Cu_{25,}$ respectively (Figure 7.8). Silver nanofibers morphological changes were also observed using TEM and SEM techniques (Figure 7.9). As can be seen in Figure 7.9.A-B AgNFs/ Cu_{13} under UV irradiation displayed corrosion/irregularities. It should be noted the change on the fiber diameter from 100 nm to 130 nm. This fact should be attributed to the initial dissolution of Ag^0 to Ag^+ and posterior reduction of Ag^+ ions under UV light.

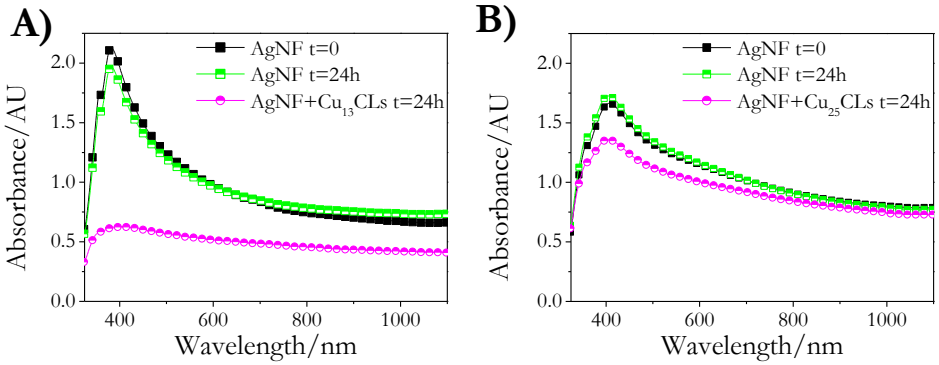

Figure 7. 8| *UV-Vis spectrum of AgNFs irradiated with UV light (λ=254 nm) during 24 hours in presence of $Cu_{13}CLs$ (A) and UV-Vis spectrum of AgNFs irradiated with Vis light during 24 hours in presence of $Cu_{25}CLs$ (B).*

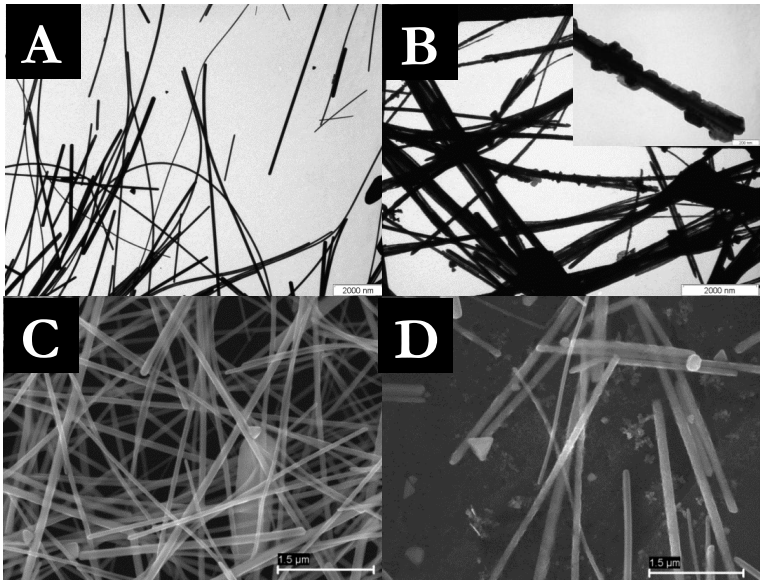

Figure 7. 9| *TEM images of the AgNFs before (A) and AgNFs + $Cu_{13}CLs$ after 24 hours UV irradiation (B). SEM images of the AgNFs before (C) and AgNFs+$Cu_{25}CLs$ after 24 hours Vis irradiation (D).*

(B) Mechanistic aspects.

If the absorption of the CuCLs to the silver nanofibers (AgNFs) surface is assumed, the photocatalytic mechanism can be described as follows:

The photoluminescence properties of the CuCLs (Chapter 3, 5 and 6), cause the promotion of the electrons peresnt on the valence band (HOMO) to the conduction band (LUMO) when they are irradiated with the suitable energy light with the corresponding fluorescence emission when the electron returns to their valence band. However, if we taking into account the presence of new species on the media the system is slightly different and new mechanism can be proposed. Copper clusters are supposed to be adsorbed onto the surface of the AgNFs (on the system AgNF/CuCLs). This consequently gives a high efficiency charge transfer between them. When CuCLs were irradiated under the suitable light the promotion of an electron from the VB to the CB (Step 1 on the Scheme 7.3) led to the formation of an electron hole (h^+) on the VB. Subsequently, the holes of the e^-/h^+ formed pair were occupied by an e^- causing the dissolution of the AgNFs ($Ag^0 \rightarrow Ag^+$) (Step 2 on the Scheme 7.3). Finally, the e^- located on the CB were captured from any e^- acceptor present on the media, here principally associated to the molecular oxygen (O_2) (Step 3 on the Scheme 7.3).

Scheme 7. 3 | *Schematic energy diagram showing the photocatalytic activity of different CuCLs (Cu_{13} and Cu_{25}) used for the AgNFs photodissolution.*

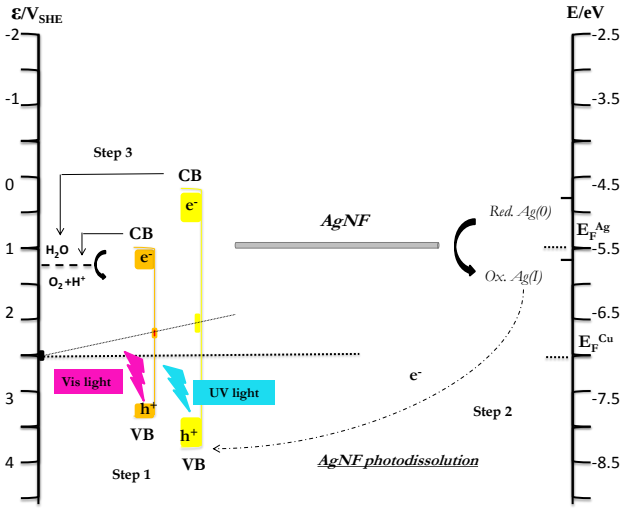

7.4.SUMMARY.

Cluster size dependent catalytic properties of small CuCLs in the clock redox MB-LMB reaction have been demonstrated.

It has also been observed that CuCLs show not only very significant catalytic effects, but also a high reusability efficiency, which could be used for other types of redox reactions, with important technological applications.

Photocatalytic properties were also demonstrated on the photodissolution of silver nanofibers reaction.

REFERENCES.

[1] Lei Y.; Mehmood F.; Lee S.; Greeley J.; Lee B.; Seifert S.; Winans R. E.; Elam J. W.; Meyer R. J.; Redfern P. C.; Teschner D.; Schlögl R. ; Pellin M. J.; Curtiss L. A.; Vajda S. *Science 328*, 224 **(2010).**

[2] Calvo-Fuentes J.; Rivas J.; López-Quintela M.A. in Encyclopedia of Nanotechnology, Bhushan, B. (Ed.) DOI 10.1007/978-90-481-9751-4 (Springer Science+Business Media B.V., Dordrecht, in press).

[3] Zhu Y.; Qian H.; Drake B.A.; Jin R. *Angew. Chem. Int. Ed. 49*, 1295 **(2010).**

[4] Liu Y.; Tsunoyama H.; Akita T.; Xie S.; Tsukuda T. *ACS Catalysis 1*, 2 **(2011).**

[5] Zhu Y.; Qian H.; Zhu M.; Jin R. *Adv. Mater. 22*, 1915 **(2010).**

[6] Shimizu K.; Miyamoto Y.; Satsuma A. *J. Catal. 270*, 86 **(2010).**

[7] Leelavathi A.; Rao T.U.B.; Pradeep T. *Nanoscale Research Letters 6*, 1 **(2011).**

[8] (a) Gong J., Yue H., Zhao Y., Zhao S., Zhao L., Lv J., Wang S., Ma X. J. Am. Chem. Soc. **2012**, DOI: 10.1021/ja3034153. (b) Bandini M.; Benaglia M.; Sinisi R.; Tommasi S.; Umani-Ronchi A. *Org. Lett.* 9, 2151 **(2007).** (c) Munro-Leighton C.; Delp S.A.; Blue E.D.; Gunnoe T.B. *Organometallics 26,* 1483 **(2007).**

[9] (a) Judai K.; Abbet S.; Wörz A.S.; Ferrari A. M.; Giordano L.; Pacchioni G.; Heiz U. *J. Mol. Catal. A: Chem. 199*, 103 **(2003).** (b)Thathagar M. B.; Beckers J.; Rothenberg G. *J. Am. Chem. Soc.* 124, 11858 **(2002).** (c) Durán Pachón L., van Maarseveen J.H., Rothenberg G. *Adv. Synth. Catal. 347,* 811 **(2005).**

[10] Wei W.; Lu Y.; Chen W.; Chen S. *J. Am. Chem. Soc. 133*, 2060 **(2011).**

[11] Patel A.C.; Li S.; Wang C.; Zhang W.; Wei Y. *Chem. Mater. 19*, 1231 **(2007).**

[12] (a) Wu J.; Zhang X.; Yao T.; Li J.; Zhang H.; Yang B. *Langmuir 26,* 8751 **(2010).** (b) Wei Q.; Zhong Z.; Nie Z.; Li J.; Wang F.; Li Q. *Microporous Mesoporous Mater. 117,* 98 **(2009).**

[13] Zhao Y.; Aoki K. *Chem. Phys. Lett. 430*, 117 **(2006).**

[14] Kundu S.; Huitink D.; Liang H. *J. Phys. Chem. C 114,* 7700 **(2010).**

[15] (a) Saha A.; Ranu B. *J. Org. Chem. 73*, *6867* **(2008).** (b) Wang Y.; Biradar A.V.; Wang G.; Sharma K.K.; Duncan C.T.; Rangan S.; Asefa T. *Chem. Eur. J. 16*, 10735 **(2010).** (c) Pande S.; Jana S.; Basu S.; Sinha A. K.; Datta A.; Pal T. *J. Phys. Chem. C 112*, 3619 **(2008).**

[16] a) Hoffmann M.R.; Martin S.T.; Choi W.; Bahnemann D.W. *Chem. Rev. 95,* 69 **(1995).** b) Linsebigler A.L.; Lu G.; Yates Jr. J.T. *Chem. Rev. 95,* 735 **(1995).** c) Fujishima A.; Rao T.N.; Tryk D.A. *J. Photochem. Photobiol. C 1*, 1 **(2000).**

[17] Du J.; Lai X.; Yang N.; Zhai J.; Kisailus D.; Su F.; Wang D.; Jiang L. *ACS Nano 5,* 590 **(2011).**

[18] Zhang Y; Tang ZR; Fu X; Xu Y J *ACS Nano 4*, 7303 **(2010).**

[19] a) Silva C.G.; Juárez R.; Marino T.; Molinari R.; García H. *J Am Chem Soc 133,* 595 **(2011).** b) Li Q.; Guo B.; Yu J.; Ran J.; Zhang B.; Yan H.; Gong J.R. *J Am Chem Soc 133,* 10878 **(2011).**

[20] Roy S.C.; Varghese O.K.; Paulose M.; Grimes C.A. *ACS Nano 4*, 1259 **(2010).**

[21] Beydoun D.; Amal R.; Low G.K.C.; Mc Evoy S. *J. Phys. Chem. B 104*, 4387, **(2000).**

[22] a) Lee J.S.; You K.H.; Park Ch. B. *Adv. Mater. 24,* 1084 **(2012).**

[23] Pérez Mariño A. M., Final Degree Project: *"Silver Nanofibers photodissolution catalyzed by Sub-nanometer Atomic Clusters"*. University of Santiago de Compostela **(2012).**

[24] Mills A.; Wang, J. *J. Photochem. Photobiol. A: Chem. 127*, 123 **(1999).**

[25] Crispin X.; Bureau C.; Geskin V.; Lazzaroni R.; Brédas J.-L. *Eur. J. Inorg. Chem.* 1999, 349 **(1999).**

[26] Lee S.-K.; Mills A. *J. Fluoresc. 13*, 375 **(2003).**

[27] Attia Attia, Y., PhD Dissertation: *"Directed wet-chemical synthesis of metallic nanoparticles of different sizes and shapes: control mechanisms"*. University of Santiago de Compostela **(2012).**

CONCLUSIONS AND FUTURE WORK.

CONCLUSION REMARKS

As we have shown on the different chapters of this thesis electrochemical synthesis has been developed as a direct one-step and environmentally friendly method to produce fluorescent copper clusters at 25ºC, which was one of the main points of this study. Besides this, applications of the as-synthesized copper clusters have been also studied, and different conclusions can be extracted from this work.

First, it was the first time that fluorescent copper clusters were synthesized by using the electrochemical technique. The synthesis of copper clusters has been optimized (Chapter 3,4 and 5), observing the best conditions on small CuCLs synthesis were: aqueous medium, $10mA/cm^2$ as current density, tetrabutylammonium nitrate as supporting electrolyte, 800 seconds duration and platinum as a cathode. Although a cheaper synthesis has been studied by using aluminium instead platinum as cathode, their optimization needs to be studied in future work. Furthermore, it was the first time also that larger copper clusters were obtained (with Cu_N, N= copper atom number, $20 \leq N \leq 25$) by using a thermal growth from solid clusters and also under different electrochemical synthesis conditions, being here, the best synthesis conditions: aprotic medium such as acetonitrile as solvent, tetrabutylammonium acetate as supporting electrolyte, 800 s duration, $5mA/cm^2$ current density and Pt as cathode.

Characterization of copper clusters has been difficult, but using the combination of different techniques such as UV-Vis, fluorescence, AFM, XPS, MALDI-TOF, CV…we were able to stablish their size, being the clusters Cu_N: Cu_5, Cu_8 and Cu_{13} the most stable configurations for smaller CuCLs and Cu_{20} and Cu_{25} for larger clusters.

Another important aspect ro point out is the copper clusters samples purification. Good results were obtained by using centrifugation+redispersion purification, "Caustic extraction" method and also HPLC technique.

In general, the stability over the time was succesful for all clusters sizes, observing no PL changes for CuCLs solutions stored at 4ºC and also at ambient Tª (Chapter 6). Besides, they displayed high photostabilty. Small copper clusters did not show solvatochromic emission effect and are independent of $[O_2]$, but they are sensitive to pH and temperature changes, being basic pH and low temperatures the optimal conditions to the high emission intensity. CuCLs thiol

functionalization has been successful. This high photo and chemical stability make CuCLs attractive alternatives to conventional fluorophores.

Finally, different applications for the CuCLs have been studied. Firstly, a detection fluorescence assay with small copper clusters (Cu_{13}) has been developed for Pb^{+2} ions (Chapter 6). The remarkable sensitivity (483nM) and selectivity (200-fold over other tested ions) of this sensing application makes copper clusters suitable like nanosensors. Moreover, photoluminescence can be recovered and suitable for another detection cycle. Secondly, catalytic studies with copper clusters (Chapter 7) reveals a size dependent activity on the the clock redox MB-LMB reaction. This catalytic behavior can be explained by assuming an electron transfer stage mediated by the Cu cluster catalysts. On the other hand photocatalytic studies also reveals size dependent activity on the photodissolution of silver nanofibers, showing good results for small and large copper clusters by using the suitable irradiation light.

CONCLUSIONES GENERALES

Tal y como se ha mostrado a lo largo de los diferentes capítulos de esta tesis, se han obtenido satisfactoriamente diferentes tamaños de clústeres de cobre (CuCLs) fluorescentes mediante el método de síntesis electroquímica. Del mismo modo, se ha realizado un estudio de las posibles aplicaciones de estos clústeres extrayendo diferentes conclusiones.

En primer lugar, ha sido la primera vez que se han logrado sintetizar clústeres de cobre fluorescentes mediante el método electroquímico. Se ha desarrollado la optimización del método de síntesis de clústeres de cobre de diferentes tamaños (Capítulos 3,4 y 5). Las condiciones de síntesis óptimas para obtener clústeres de cobre de pequeño tamaño resultaron ser: medio acuoso, con una densidad de corriente de $10mA/cm^2$, usando nitrato de tetrabutilamonio como electrolito soporte durante 800 segundos y un cátodo de platino. Hay que decir, que, a pesar de los intentos de economizar el método de síntesis (mediante el uso de un cátodo alternativo de aluminio) se hacen necesarios un mayor número de estudios para su futura optimización. Por otra parte, también ha sido la primera vez que se han obtenido clústeres de cobre de mayor tamaño (Cu las condiciones óptimas para obtener clústeres de mayor tamaño (con Cu_N, N= número de átomos de cobre, $20 \leq N \leq 25$) tanto mediante un crecimiento térmico controlado a partir de clústeres de pequeño tamaño en estado sólido, así como bajo diferentes condiciones de síntesis: un medio aprótico (acetonitrilo), con acetato de tetrabutilamonio como electrolito soporte, usando una densidad de corriente de $5mA/cm^2$, 800 s de duración y un cátodo de platino.

La caracterización de los clústeres de cobre ha sido ardua, pero mediante la combinación de los diferentes resultados obtenidos usando diferentes métodos (UV-Vis, fluorescence, AFM, XPS, MALDI-TOF, CV…) su tamaño ha sido determinado. Como resultado se han obteniendo clústeres de pequeño tamaño con N= número de átomos de Cu, Cu_N: Cu_5, Cu_8 y Cu_{13} y clústeres de mayor tamaño: Cu_{18-20} y Cu_{25}.

Otro de los puntos más importantes de este trabajo ha sido la purificación de las muestras de clústeres de cobre. Dada la necesidad de elevada pureza de las muestras en futuras aplicaciones se estudiaron diferentes métodos de purificación, tales como: centrifugación y redispersión, extracción cáustica y también mediante el uso de la técnica de separación HPLC, obteniendo en todos ellos buenos resultados.

En general, la estabilidad de los clústeres de cobre sintetizados también ha sido un punto muy importante. Todos los tamaños de clústeres de cobre presentan estabilidad en el tiempo. No se observaron cambios en la fluorescencia en las disoluciones de CuCLs guardadas tanto a 4ºC como a temperatura ambiente, mostrando, además, gran fotoestabilidad. Los clústeres de pequeño tamaño no muestran efecto solvatocrómico y su fluorescencia es independiente de la concentración de oxígeno en el medio, pero son susceptibles a cambios en el pH y en la temperatura. Las condiciones óptimas han sido obtenidas usando pH básicos y bajas temperaturas. Además se ha conseguido la funcionalización con diferentes tioles. Esta gran fotoestabilidad y estabilidad química los señala como futuras alternativas a los fluoróforos convencionales.

Finalmente se ha llevado a cabo el estudio de posibles aplicaciones para los clústeres de cobre sintetizados. En primer lugar un ensayo de deteción de iones de plomo basado en el quenching de la fluorescencia con clústeres de pequeño tamaño (Cu_{13}) (Capítulo 6). Su gran sensibilidad (483nM) y selectividad hace los clústeres de cobre una gran promesa en su uso como nanosensores. Además, el hecho de que la fluorescencia pueda ser recuperada y reutilizada en otro ciclo de detección los señala como posibles candidatos a sensores "off-on". En segundo lugar, la actividad catalítica de los clústeres de cobre (Capítulo 7) ha resultado ser dependiente del tamaño en la reacción clock del MB-LMB. Este comportamiento catalítico se explica mediante una transferencia de electrones mediada por los clústeres de cobre. Por otro lado estudios fotocatalíticos también muestran actividad dependiente del tamaño en la reacción de fotodisolución de nanofibras de plata, exhibiendo buenos resultados para clústeres de diferente tamaño empleando la irradiación adecuada.

FUTURE WORK

Research on metal clusters has attracted a big interest nowadays. Great progress has made in this field toward the synthesis and applications of silver and gold clusters. However, copper clusters are less studied at the moment, therefore, as demonstrated in this thesis, a lot of work involving copper clusters needs to be done. A part of future work was summarized as following:

1) Synthesis and purification of different copper clusters sizes in aqueous medium needs to be improved. Due to their great photoluminescence properties they can be used on biomedical applications. Therefore, an exhaustive study on this field can contribute to an inexpensive method of biological markers design. Besides, synthesis of copper clusters needs to be scalable and affordable, allowing the obtaining of a high clusters's concentration in each synthesis. Besides, another important point will be the functionalization of copper clusters with different ligands and also the etching process in order to obtain smaller clusters sizes from the larger ones.

2) Catalytic size dependent properties of copper clusters were observed. However, copper clusters can be effective in another reactions used as homogeneous catalyst or even supported catalyst onto different surfaces. This point must be studied.

3) Studies about copper clusters sensing/elimination of Pb^{+2} and other metal ions and the CuCLs recycling will be other important point in future works.

4) Photocatalytic properties by copper clusters give promising results, a deep research on this field would be necessary in order to apply them as possible self-cleaning funcionalizated surfaces.

5) Electrocatalytic studies on the ORR reaction have also great interest in order to find cheaper catalyst for this kind of reaction.

ANNEX C3.

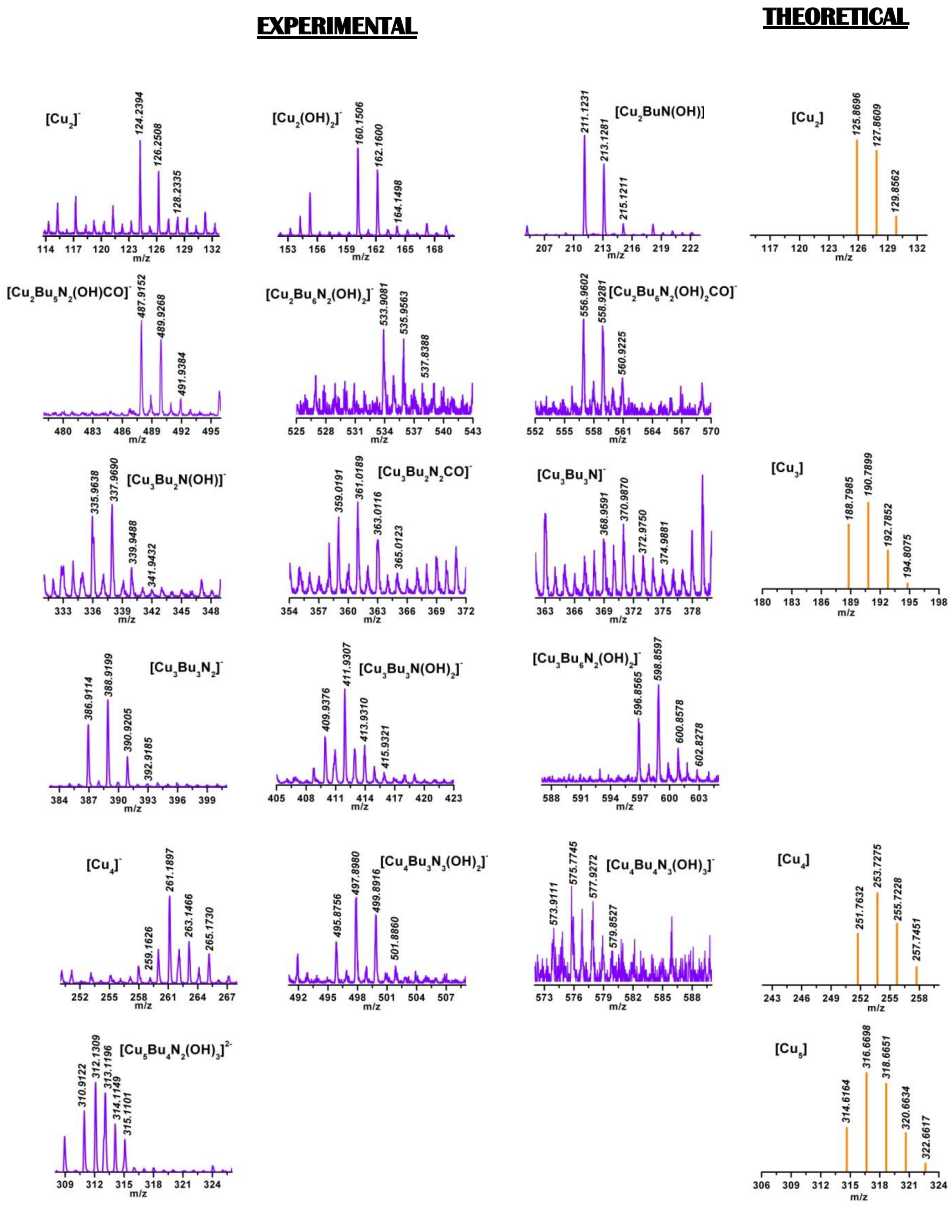

Figure Annex C3. 1| *Magnifications of the isotopic patterns found for different Cu clusters in the m/z range 0 to 800 amu by LDI-TOF mass spectroscopy in negative ion mode. Cu_N clusters with $2 \leq N \leq 5$ (N=number of copper atoms) with different fragments of the tetrabutylammonium salt and/or hydroxyl groups are clearly detected.*

Annex C3

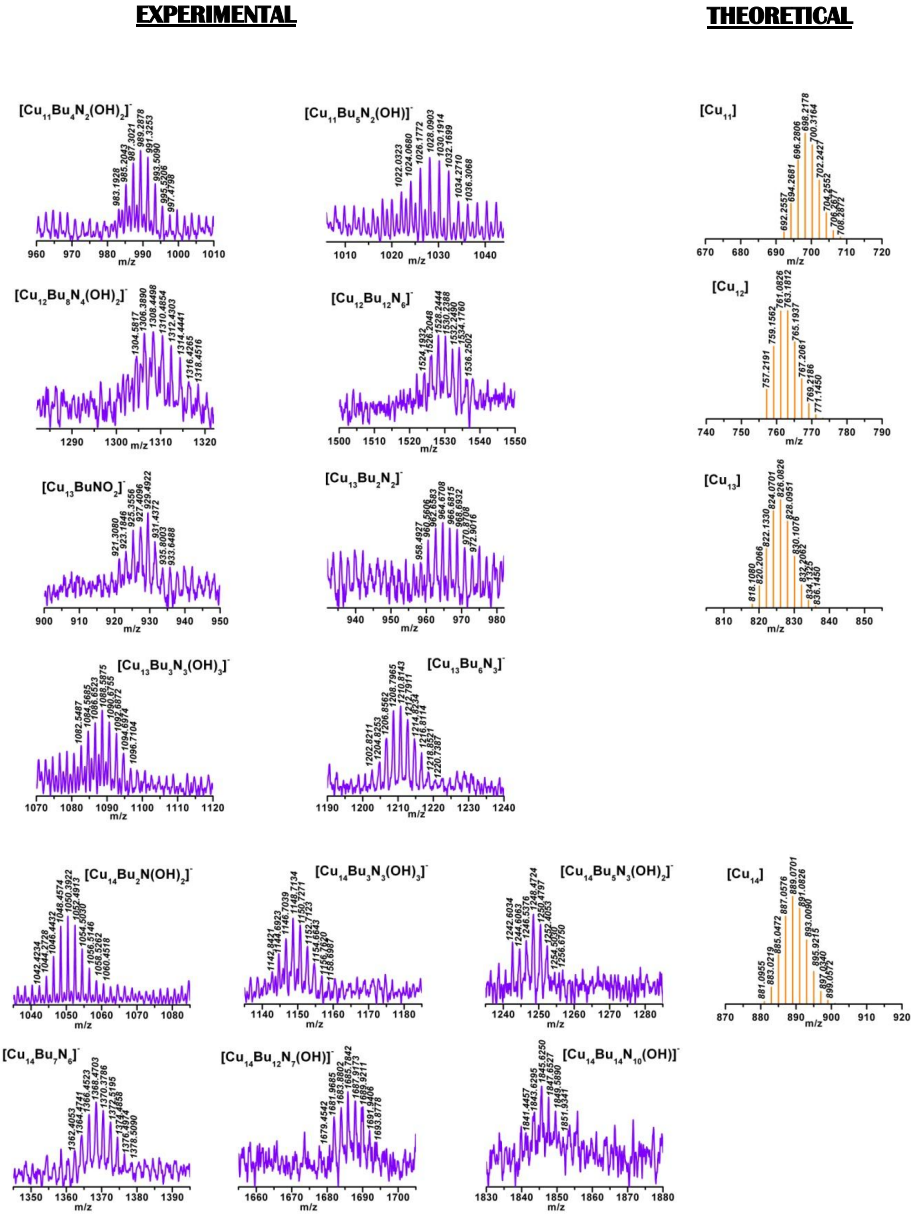

Figure Annex C3. 2| *Magnifications of the isotopic patterns found for different Cu clusters in the m/z range 800 to 2000 amu by LDI-TOF mass spectroscopy in negative ion mode. CuN clusters with 11≤N≤14 (N=number of copper atoms) with different fragments of the tetrabutylammonium salt and/or hydroxyl groups are clearly detected.*

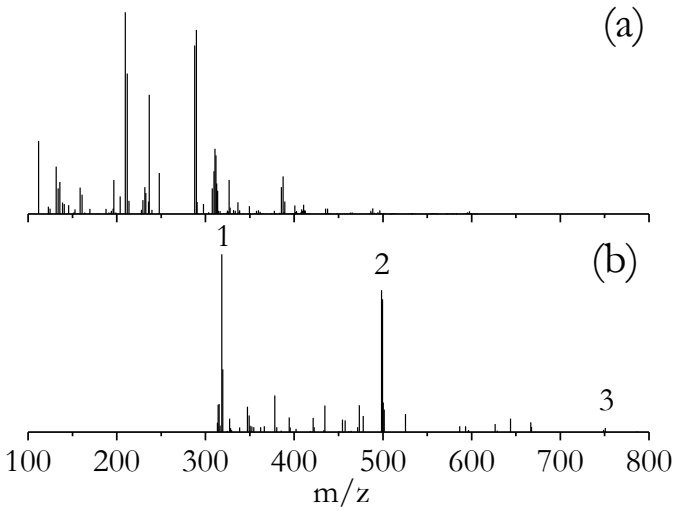

Figure Annex C3. 3| *Comparison between the LDI-TOF spectrum of CuCLs (Cu_{13}) in water (a) and MALDI-TOF CuCLs dissolved in acetonitrile and DCTB in dicloromethane with a volume ratio: CuCLs: DCTB = 1:100 (b) in negative ion mode showing m/z peaks 1=318.37 $[Cu_5]^-$, 2=498.05 $[Cu_4Bu_3N_3(OH)_2]^-$ and 3=750.43 $[Cu_{10}(H_2O)_2O]^-$. MALDI results confirm the presence of small CuCLs.*

Photoreduction synthesis of copper clusters by simple irradiation of copper precursors salts under UV light (254 nm pen ray) were carried out under the conditions summarized on Table Annex C3.1.

Table C3. 1| *Experimental conditions of photoreduction CuCLs synthesis.*

	Solvent	$[Cu^{+2}]$/mM	Precursor	Irradiation/h	Precipitate
E1	H_2O	0.8	$Cu(NO_3)_2$	6	YES (E1´)
E2			CuOAc	7	YES (E2´)
E3	MeCN: H_2O		$Cu(NO_3)_2$	9	NO
E4			CuOAc	7	NO

The mechanism can be explained as the same proposed by Loginov et al.[1] for the photochemical synthesis of colloidal metals adsorbed on quartz:

$$[M^{x+}L_n]_s \underset{}{\overset{h\nu}{\rightleftharpoons}} \{M^{(x-1)+}L_{n-1}, L^{\cdot}\}_s \longrightarrow [M^{(x-1)+}L_{n-1}]_s + L + S^{\cdot}$$

$$[M^{(x-1)+}L_{n-1}]_s \overset{h\nu, S^{\cdot}}{\rightleftharpoons} (M^0)_s \overset{}{\rightleftharpoons} (M_N{}^0)_s$$

Where M=metal, L=ligand and S= solvent. The used solvents (water and acetonitrile) can generate radicals which are strong reductants. Blue and orange precipitates were generated on aqueous solutions synthesis for nitrate and acetate counterions respectively. Precipitates redispersed in acetonitrile show strong emission (E1´and E2´) at small wavelengths. Best synthesis conditions are E1´and E4 experiments. The PL results agreed with small CuCLs synthesized by electrochemical synthesis and excludes the possibility of some interference due to the degradation of the tetrabutylammonium salts during the electrochemical synthesis.

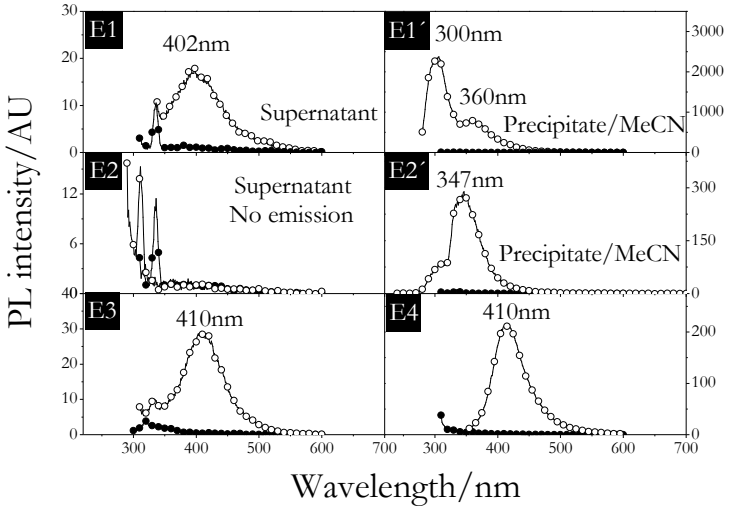

Figure Annex C3. 4| *PL spectra of different photoreduction experiments (Table C3.1).Black circles correspond to the emission of the copper salts initially and open circles correspond to the samples after the irradiation.*

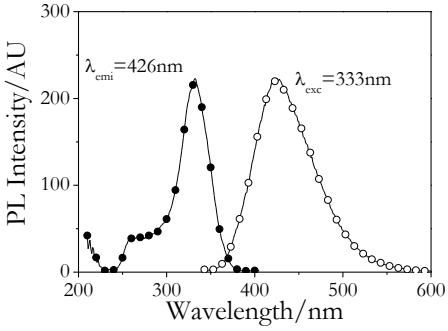

Figure Annex C3. 5| *PL spectrum of CuCLs in aqueous solution synthesized using an Aluminium cathode under the same conditions of E31.*

[1] Loginov A.V., Gorbunova V.V., Boitsova T.B. *Journal of Nanoparticle Research 4*, 193 **(2002).**

RESUMEN

Capítulo 1

Introducción

La nanotecnología ha despertado mucho interés desde comiezos del S. XXI, aunque, fue en 1850 cuando Michael Faraday comenzó sus estudios sobre partículas metálicas coloidales. El objetivo de la nanotecnología consiste en la síntesis, caracterización, diseño, aplicaciones y manipulación de la materia a escala de muy pequeño tamaño. Se define como "**nanopartículas"** a aquellas partículas formadas por agregados de átomos metálicos donde al menos una de sus dimensiones tiene un tamaño de dos a varias decenas de nanómetros y **"clústeres metálicos"** aquellos cuyo tamaño es comparable a la longitud de onda de Fermi de un electrón, <2 nm, y finalmente, **"clústeres sub-nanométricos"** clústeres con un tamaño menor de 1 nm. Al reducir el tamaño a escala nanoscópica se ha comprobado que existe una dependencia del tamaño con las propiedades ópticas, electrónicas y magnéticas debido al confinamiento y cuantización de los electrones de conducción en un pequeño volumen. Todo esto proporciona unas asombrosas propiedades físico-químicas a los clústeres metálicos, los cuales se han convertido en importantes líneas de investigación recientemente. Esta tesis se centrará en la síntesis, caracterización, estudio de las propiedades físicas y ópticas y en las potenciales aplicaciones de diferentes tamaños de clústeres de cobre (CuCLs). Los clústeres metálicos muestran propiedades intermedias entre átomos metálicos y el metal masivo, exhibiendo propiedades ópticas y electrónicas que dependen del tamaño. Inicialmente, la densidad de estados energéticos para el metal masivo es continuo, pero a medida que disminuye el tamaño, esto se va reemplazando progresivamente por niveles discretos de energía y el espaciado entre estos se va incrementando. Cuando estos espaciados exceden de la energía térmica, se abre una "banda vacía" en el metal, esta diferencia entre niveles de energía se denomina "Gap Energético". Este "Gap Energético" es una de las características más relevantes de los clústeres, un band-gap HOMO-LUMO que depende del tamaño (similar al de los semiconductores). Cuanto mayor sea este band-gap mayor estabilidad les confiere a los clústeres. Este band-gap será aproximadamente >1eV para clústeres pequeños y <1ev para aquellos clústeres de mayor tamaño.

Respecto a las propiedades ópticas de los clústeres, a diferencia de las nanopartículas, estos no presentan banda de resonancia plasmónica (banda de absorción característica para cada metal resultante de la interacción entre el campo eléctrico oscilante de una onda electromagnética con los electrones libres de conducción presentes en la superficie de la nanopartícula), sino que se

caracterizan por bandas de absorción discretas a menores longitudes de onda que las nanopartículas debido a su comportamiento quasi-molecular. Además, novedosas propiedades fluorescentes surgen de este comportamiento en clústeres metálicos, debido a transiciones electrónicas entre el orbital inferior ocupado (HOMO) y el orbital superior desocupado (LUMO). Dado que estas transiciones dependen del valor del band-gap, las bandas de emisión lo harán del mismo modo, observándose un desplazamiento en la longitud de onda de emisión hacia valores mayores cuanto mayor es el tamaño del clúster, es decir, cuanto menor es su band gap. La fluorescencia que presentan estos pequeños clústeres los hace muy atractivos para su aplicación en biomedicina, así como nanosensores de biomoléculas, iones ó proteínas. Además de las propiedades fluorescentes, un amplio abanico de aplicaciones se abre para estos nuevos materiales; por ejemplo se ha observado un comportamiento inusual de gran actividad catalítica en pequeños clústeres, lo cual se relaciona con un insuficiente nivel de coordinación entre los átomos que forman el clúster. Aunque los estudios realizados se basan sobre todo en clústeres soportados en otro material, los clústeres metálicos parecen ser una gran promesa como catalizadores en diferentes tipos de reacciones, siendo la ORR (electrorreducción de oxígeno) una de las más interesantes, debido a la posibilidad de encontrar nuevos materiales que posibiliten, abaraten y mejoren esta reacción, fundamental en la creación y mejora de las pilas de combustible.

Capítulo 3

Síntesis de CuCLs pequeños

Los clústeres metálicos fluorescentes tienen gran interés hoy en día debido a sus propiedades y a su posible aplicación como marcadores fluorescentes en estudios biomédicos. Por ello se buscan clústeres solubles en medio acuoso y con elevada fotoestabilidad. En este capítulo se muestra la síntesis de clústeres de cobre fluorescentes en medio acuoso de pequeño tamaño mediante el método electroquímico. La optimización de la síntesis se ha llevado a cabo en base al estudio de la influencia de diferentes parámetros, concluyendo que las condiciones de síntesis óptimas son: 10mA/cm^2 de densidad de corriente, cátodo de platino, nitrato de tetrabutilamonio como electrolito soporte en medio acuoso usando un tiempo de síntesis de 800s. El método de purificación usado consistió en el centrifugado del precipitado obtenido con agua ó etanol, cuyo resultado ha sido clústeres de tamaño de 13 y 5 átomos de cobre, respectivamente. La fluorescencia de ambas muestras corresponde a una longitud de onda de emisión de 408 nm (Figura 3.1.A) para los clústeres de cobre (Cu_{13}) y de 300 nm (Figura 3.1.B) para los clústeres de cobre (Cu_5).

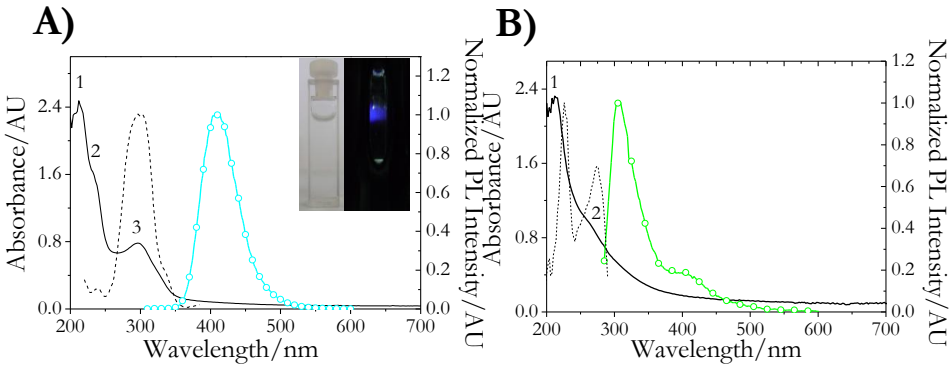

Figura 3. 1| *Espectros de absorción y emisión de clústeres de cobre Cu_{13} longitud de onda de excitación 296 nm y emisión a 408 nm (A) y Cu_5 longitud de onda de excitación 275 nm y emisión a 300 nm (B).*

Las muestras son transparentes bajo luz ambiente, pero son azules cuando se irradia con luz ultravioleta (300 nm), cómo se observa en la imagen de la Figura 3.1.A. El band-gap de ambas muestras de clústeres se ha calculado mediante la aproximación de Tauc así como con el modelo de Jellium, observando resultados similares. Obteniento un band gap de 3.25 eV mediante Tauc y 3.04 eV por

Jellium para el Cu_{13} y 4.15 eV por Tauc y por Jellium para Cu_5. El tamaño de estos clústeres se ha determinado mediante el uso del microscopio de fuerzas atómicas en modo no contacto obteniendo un tamaño medio de 0.6±0.27 nm (Figura 3.2.A) y de 0.42±0.21 nm (Figura 3.2.B) para los clústeres de Cu_{13} y Cu_5 respectivamente. Comprobando de este modo el tamaño sub-nanométrico de nuestros clústeres de cobre.

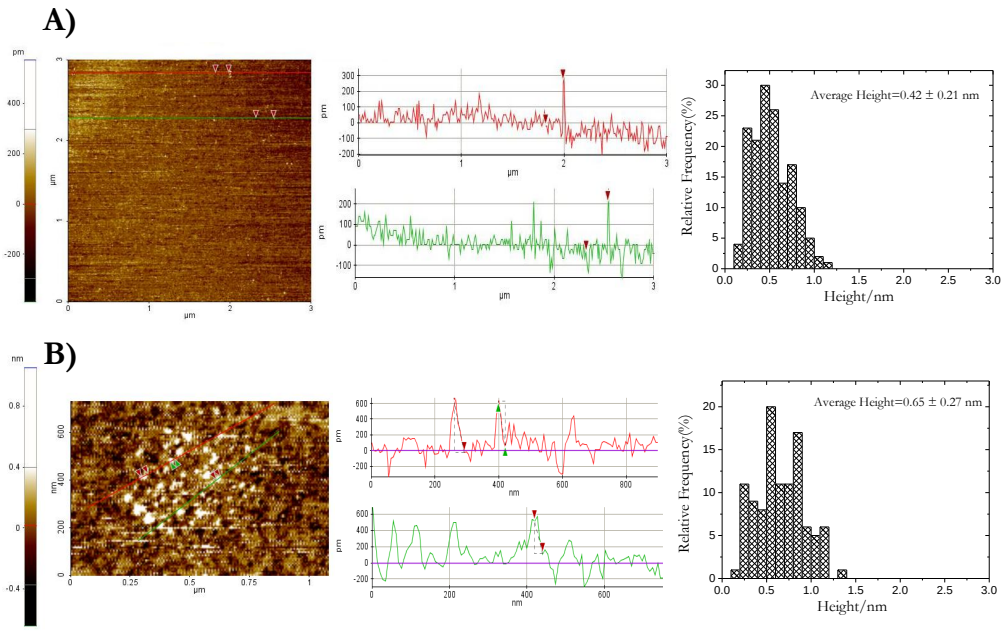

Figura 3. 2| *Imágenes topográficas del microscopio de fuerzas atómicas (NC-AFM) de los clústeres de Cu_5 (A) y Cu_{13} (B) depositados en un sustrato de mica. Análisis de las secciones de las líneas mostradas en la topografía se observan en el medio y el correspondiente histograma de distribución de alturas se muestra a la derecha de la imagen.*

Diferentes técnicas de espectrometría de masas tales como LDI-TOF (Desorción/Ionización por Láser - tiempo de vuelo), MALDI-TOF (Desorción/Ionización por Láser Asistida por Matriz-tiempo de vuelo), ESI-TOF (electrospray-tiempo de vuelo) han sido empleadas para la determinación del tamaño de estos clústeres de cobre. Los resultados obtenidos revelan tamaños de clúster (Cu_N, N= nº de átomos) con N≤13 átomos de cobre, observando una mayor fragmentación de los núcleos metálicos usando la técnica de LDI-TOF.

Las disoluciones de clústeres obtenidas (Cu_{13} y Cu_5) presentan una gran estabilidad en el tiempo (almacenados tanto a temperatura ambiente como a 4ºC en nevera), obteniendo aproximadamente la misma intensidad de fluorescencia incluso un año después de ser sintetizados.

Capítulo 4

Crecimiento térmico de CuCLs de pequeño tamaño.

Como se ha explicado anteriormente, las propiedades fluorescentes de los clústeres dependen de su band gap, y por lo tanto, de su tamaño. Debido a esto, un control del tamaño de clúster se hace necesario para la obtención de muestras de clústeres con diferentes propiedades. La estrategia aquí propuesta se basa en el crecimiento de los clústeres de cobre de 13 átomos (en estado sólido) mediante un tratamiento térmico controlado. Los métodos de crecimiento térmico dependen básicamente de la interacción entre el agente protector y el núcleo metálico, siendo esta interación crucial en los procesos de desorción, coalescencia y agregación, los cuales determinan el proceso de crecimiento. El mecanismo propuesto para la formación de clústeres mayores partiendo de aquellos clústeres de menor tamaño se puede explicar mediante la expresión:

$$Cu_x^{a+} + Cu_y^{b-} \rightarrow Cu_{x+y}^{(a-b)+}$$

El procedimiento experimental se basa en el tratamiento a 80ºC de 1mg de clústeres de cobre pequeños (Cu_{13}) durante una hora, redispersándolos a continuación en 10mL de acetonitrilo bajo intensa agitación durante tres horas. Se observa un cambio de color en el disolvente pasando de transparente a marrón claro. El producto obtenido se ha caracterizado inicialmente mediante espectroscopía UV-Vis y fluorescencia (Figura 4.1).

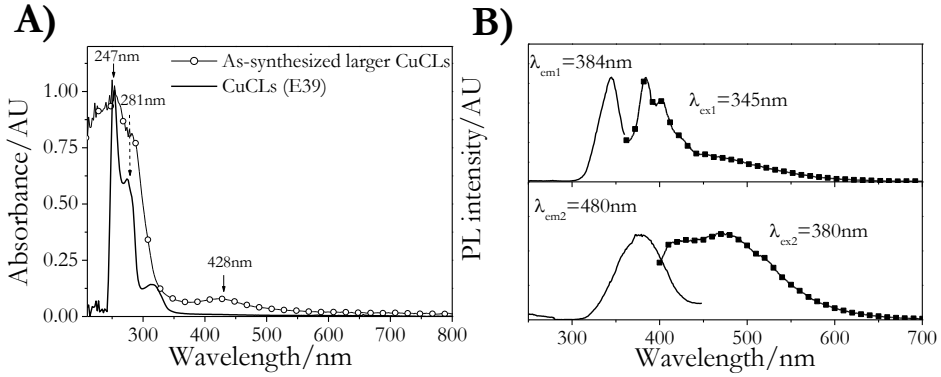

Figura 4. 1| *Espectro de absorción UV-Vis (A) y de fluorescencia (B) de clústeres de cobre crecidos térmicamente.*

La muestra de clústeres de mayor tamaño presenta una banda de absorción definida a 428 nm, no observada previamente para aquellos clústeres de menor tamaño (Cu_N, N≤13). Además, la existencia de una banda de emisión a 485 nm, corrobora el crecimiento de dichos clústeres. Mediante el modelo de Jellium se suponen dos tamaños de clústeres existentes en esta muestra: Cu_{10} y Cu_{20}. Sin embargo, se hace necesario destacar el ancheamiento de la banda de emisión a 480 nm (FMHW=151 nm), superior al observado en la emisión a 400 nm (FMHW=42 nm). Esta emisión se podría considerar proveniente de la suma de las emisiones de tres clústeres diferentes. Para comprobar esta hipótesis se puede realizar el ajuste de esta banda mediante funciones Lorentzianas. El resultado obtenido ha sido un buen ajuste empleando tres Lorentzianas, lo cual indicaría tres posibles bandas de emisión localizadas estas a 418, 474 y 522 nm. De tal modo, mediante el modelo de Jellium se pueden asociar a clústeres de Cu_{13}, Cu_{19} y Cu_{25}, respectivamente. La verdadera confirmación de la existencia de diferentes tamaños de clústeres vendrá dado por un análisis más exhaustivo empleando otras técnicas de caracterizaciçon, tales como espectrometría de masas y medidas con el microscopio de fuerzas atómicas. La topografía obtenida mediante el microscopio de fuerzas atómicas (Figura 4.2) nos ha dado un tamaño medio de clúster de 0.98±0.41 nm. Este valor es considerablemente más elevado que aquel obtenido para clústeres de cobre pequeños.

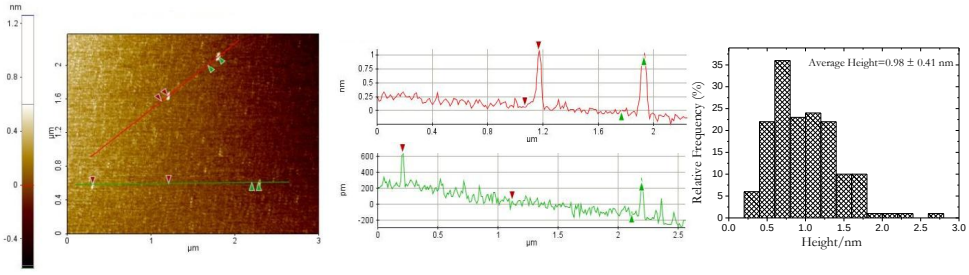

Figura 4. 2| *Imagen topográfica del microscopio de fuerzas atómicas (NC-AFM) de los clústeres crecidos térmicamente depositados en un sustrato de mica. Análisis de las secciones de las líneas mostradas en la topografía se observan en el medio y el correspondiente histograma de distribución de alturas se muestra a la derecha de la imagen.*

Por otro lado el uso de diferentes técnicas de espectroscopía de masas (LDI-TOF, MALDI-TOF y ESI-TOF) posibilita la determinación del tamaño de los clústeres aquí sintetizados. El resultado obtenido muestra diferentes tamaños de

clústeres entre 5 y 20 átomos de cobre en el núcleo metálico. A pesar de que los resultados difieren ligeramente entre las técnicas empleadas, mediante MALDI y ESI (técnicas que producen una menor fragmentación) se observan similitudes, ya que ambas técnicas proporcionan tamaños de entre 5 y 10 átomos, cabe destacar a su vez, que mediante MALDI el clúster mayor detectado consta de 16 átomos de cobre mientras que por ESI se detectaron clústeres de cobre de hasta 20 átomos. Estos resultados concuerdan con la aproximación de Jellium mediante la emisión que nos daba la existencia de Cu_{10} y Cu_{20}. Por lo tanto se puede observar que el crecimiento de los clústeres mediante tratamiento térmico controlado ha sido satisfactorio.

Dada la naturaleza polidispersa de la muestra obtenida se ha llevado a cabo una separación de la misma mediante el uso de la técnica de HPLC (realizada por Eldara Rodríguez Cobo) logrando la separación de dichos clústeres en base a la fijación de una longitud de onda de excitación de la muestra, obteniendo las distintas alícuotas en base a su señal en el cromatograma. La zona del cromatograma que no muestre actividad fluorescente será recogida como resto. Los clústeres de menor tamaño (Cu_5) saldrán en las primeras alícuotas, seguidos por los clústeres de Cu_{13} y finalmente la emisión correspondiente a los clústeres de mayor tamaño (Cu_{20}) se detectó en el resto. Este resultado parece indicar una separación de tamaños selectivo mediante la fijación de una longitud de onda de excitación a la cual los clústers sean receptivos.

Capítulo 5

Síntesis de CuCLs de mayor tamaño.

El objetivo en este capítulo reside en la síntesis en un solo paso de clústeres de mayor tamaño. Con este fin se ha procedido al estudio de diferentes cambios en las condiciones de síntesis. El resultado ha sido la obtención de clústeres de cobre de mayor tamaño que los obtenidos hasta el momento, con diferentes bandas de emisión localizadas en 360 nm (3.42 eV), 409 nm (3.03 eV) y 520 nm (2.38 eV) (Figura 5.1). Estos valores de energía obtenidos a partir de la emisión coinciden perfectamente con los diferentes band gaps obtenidos por la aproximación de Tauc. El tamaño de los CuCLs de esta muestra fue estudiada por medidas con el microscopio de fuerzas atómicas en modo no-contacto obteniendo tamaños de 1.12±0.5 nm.

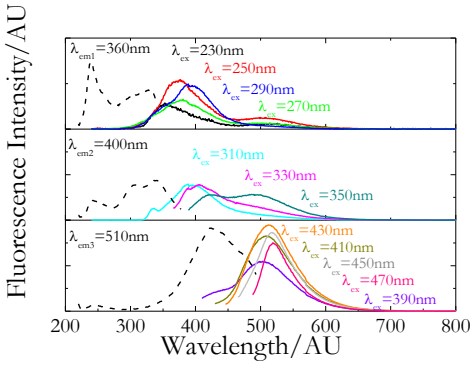

Figura 5. 1| *Espectro de fluorescencia de los clústeres de mayor tamaño obtenidos directamente mediante síntesis electroquímica donde se observan los tres rangos de emisión con sus respectivas excitaciones.*

Se ha logrado obtener mediante el estudio de espectrometría de masas (LDI-TOF) un tamaño de hasta 25 átomos de cobre, lo cual era lo esperado mediante el modelo de Jellium. Además se han identificado otros clústeres de núcleo Cu_{19} y $Cu_{9\text{-}11}$, lo cual explica la existencia de mútiples bandas de emisión en el espectro de fluorescencia.

Capítulo 6

Estabilidad de la fluorescencia de los CuCLs.

Las novedosas propiedades fluorescentes de los clústeres metálicos (tales como longitudes de onda de emisión dependientes del tamaño, altos rendimientos cuánticos y gran fotoestabilidad) en comparación con los tintes orgánicos tradicionales ó los quantum dots, los hace muy prometedores en un amplio rango de aplicaciones. Debido a esto, el estudio de la estabilidad fluorescente de los clústeres de cobre se hace necesario. Para ello se han llevado a cabo estudios de estabilidad térmica, de dispersión, estabilidad fotoquímica, estabilidad frente al pH, etc.

Se comprobó que todos los clústeres de cobre sintetizados (Cu_5, Cu_{13}, Cu_{20} y Cu_{25}) poseen estabilidad frente a la irradiación continuada a su longitud de onda máxima de excitación hasta 16 horas. La estabilidad frente a cambios de pH también ha sido estudiada, observando mejores resultados en un amplio rango de pHs = 4.7 a 10.37 para los clústeres de menor tamaño (Cu_5) que para los clústeres de Cu_{13} (estables en pHs de 6-12). Este resultado confirma la mayor estabilidad de aquellos clústeres de menor tamaño (tal y como cabría esperar debido a su gran band gap). Se observó también que los clústeres de Cu_{13} son sensibles a la temperatura, obteniendo una mayor intensidad de fluorescencia a menores temperaturas. La funcionalización de estos clústeres de cobre ha sido un gran punto a considerar, dado que su posteror aplicación biológica depende en gran medida de aquellos grupos funcionales de los ligandos que los protegen para poder dirigirlos a un determinado uso. Para ello se llevaron a cabo diferentes pruebas de funcionalización de los clústeres de cobre Cu_{13} tanto en fase sólida como por transferencia de fase mediante el uso de tioles. El resultado fue satisfactorio para el método de transferencia de fase (de acuosa a orgánica) usando 1-hexanotiol, observando la misma longitud de onda de emisión en la fase orgánica tras 7 horas de agitación. La funcionalización en fase sólida no ha resultado tan clara, dado que tras la redispersión en medio acuoso usando L-glutationa y 3-mercaptopropiónico, en lugar de observar la típica emisión de estos clústeres a 408 nm, se observan dos bandas diferentes una a 300 nm y otra a 330 nm, respectivamente, lo cual parece indicar una fragmentación de los clústeres en otros de menor tamaño. Esta técnica conocida como "etching" es muy estudiada hoy en día para conseguir clústeres de menor tamaño partiendo de otros mayores. Por lo que es una línea de investigación a considerar en futuros trabajos.

Capítulo 7

Actividad catalítica de los CuCLs.

La gran actividad catalítica de los clústeres metálicos es debida a sus propiedades electrónicas intrínsecas, las cuales se caracterizan por la aparición de un band gap en el nivel de Fermi. Como se ha dicho anteriormente, el band gap depende principalmente del número de átomos del clúster. Por lo tanto, clústeres de diferentes tamaños mostrarán diferente actividad catalítica frente a una misma reacción. Como objeto de estudio se han elegido dos tipos de reacciones para probar la actividad catalítica de nuestros clústers: una reacción clock (reducción del azul de metileno (MB) a leuco azul de metileno) y una fotodisolución (disolución de nanofibras de plata mediada por los clústeres de cobre). Se han estudiado tres tamaños diferentes de clústeres de cobre Cu_5, Cu_{13} y Cu_{20} para catalizar la reacción redox del azul de metileno, observando que el comportamiento catalítico depende del tamaño del clúster, explicándose por un proceso de transferencia de electrones mediado por el clúster de cobre desde el donante de electrones (hidracina) al aceptor (azul de metileno) por medio de la banda de conducción de los clústeres (Esquema 7.1). De este modo se explica que la reacción no ocurre en presencia de los clústeres de cobre Cu_{20} (cuyos orbitales LUMO se encuentran debajo del potencial redox del azul de metileno), pero es satisfactoria para los otros dos tamaños de clústeres.

Esquema 7. 1| *Esquema del diagram de energía donde se observa la actividad catalítica de diferentes tamaños de clústeres (Cu_5, Cu_{13} y Cu_{20}) usados en la reacción de reducción del MB.*

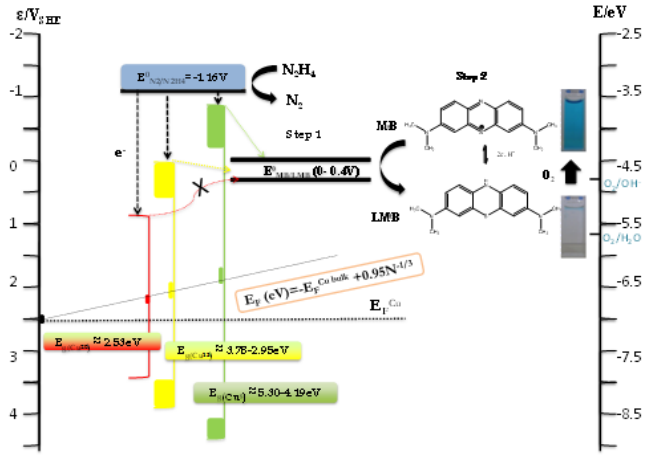

Se ha estudiado además la capacidad de reciclado de los clústeres de cobre obteniendo resultados efectivos para los clústeres de Cu_{13} de hasta 42 ciclos.

Por otra parte, la actividad fotocatalítica de los clústeres de cobre ha sido realizada por Ángel M. Pérez Mariño mediante la reacción de fotodisolución de nanofibras de plata (cedidas por la empresa Nanogap). Se han empleado dos tipos de tamaños de CuCLs: clústeres de pequeño tamaño Cu_{13} y de mayor tamaño Cu_{25}. Los clústeres de cobre de pequeño tamaño Cu_{13} fueron irradiados con luz UV y los de mayor tamaño Cu_{25} con luz visible observando en ambos la fotodisolución de las nanofibras de plata. El mecanismo propuesto (Esquema 7.1) se basa en la excitación de un electrón de la VB de los clústeres mediante la irradiación con la luz adecuada a la CB (Etapa 1), dejando un hueco h^+ en la VB. Este hueco será rellenado con un electrón proveniente de la fotodisolución de $Ag^0 \rightarrow Ag^+$ de las nanofibras de plata (Etapa 2). Finalmente, el electrón situado en la CB de los clústeres será captado por una especie captora de electrones, como por ejemplo en nuestro caso el O_2 (Etapa 3).

Esquema 7. 2| *Mecansimo de fotodisolución de fibras de plata en presencia de clústeres de cobre de diferentes tamaños bajo irradiación adecuada a cada band gap.*

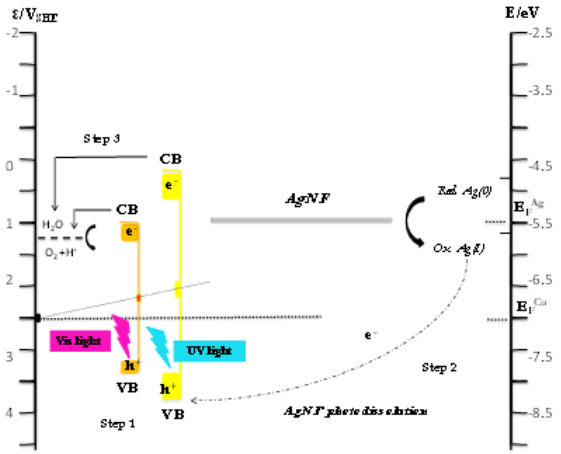

AGRADECIMIENTOS

En este apartado me gustaría resumir el agradecimiento a todas aquellas personas que me han brindado su apoyo durante esta etapa de mi vida, y, sin las cuales esta tesis no se habría hecho realidad.

En primer lugar, me gustaría expresar mis agradecimientos a mis directores de tesis, el profesor Manuel Arturo López Quintela y el profesor José Rivas Rey, por haberme brindado la oportunidad de trabajar en su grupo de investigación y haber hecho posible este trabajo. Les agradezco su confianza y colaboración así como haber inculcado en mí el espíritu investigador. Por todo eso: muchas gracias.

Me gustaría también agradecer a la profesora María del Carmen Blanco, por su inestimable apoyo e instrucción durante este tiempo.

Del mismo modo querría agradecerle a Purificación Domínguez por su ayuda en esta etapa.

A la entidad que ha financiado mis estudios: el International Iberian Nanotechnology Laboratory (INL), la cual me ha permitido llevar a cabo este doctorado.

Del mismo modo no puedo olvidarme de todos esos amigos y compañeros conocidos en mi estancia en el laboratorio, los cuales de forma diferente han aportado su granito de arena a este trabajo. A Ana (por ser genial), a Bea (por todos nuestros momentos), a Cintia (por todas las risas), a Pauli (por su optimismo), me ha encantado compartir este camino con vosotras. A Rosalía, David, Eldara, Paula, Yolanda, Atanu, Yuri, Ana, Marta, Esther, Verena, Carlos, Vero, Nerio, Javi, Camilo, Cris, etc. muchísimas gracias a todos por formar parte de estos maravillosos años.

A mis amigos, que siempre han tenido una palabra de ánimo y siempre están ahí cuando los necesito. Gracias a Samuel, a Rocío, a Lorena M., a Lorena G., a Catalina, a María, a Esther, a todos os quiero muchísimo! Me hacéis sentir una persona muy afortunada. Gracias por todas las experiencias vividas y por todas las que nos quedan por vivir.

A todas aquellas personas que han estado presentes en mi camino y que me han escuchado, me han enseñado y me han guiado.

Finalmente, y con el amor más especial a mi familia: a mis padres, a mi madriña y a mi hermano, por estar siempre e incondicionalmente a mi lado, por no dejar que dudara ni un solo instante de que **querer es poder.** Gracias por los

valores inculcados, por enseñarme que el trabajo duro finalmente tiene recompensa, por animarme, por quererme, por cuidarme, por enseñarme tanto día a día. Gracias a vosotros soy quién soy. En resumen, gracias por hacer que mi vida sea plena.

A todos muchas gracias.